



UNIVERSIDADE D
COIMBRA

João Pedro Teixeira Marques

**NUMERICAL AND EXPERIMENTAL
EVALUATION OF A NOVEL ROLLER SKATE
PLATFORM**

**Dissertação no âmbito do Mestrado em Engenharia Mecânica, na área de
Produção e Projeção orientada pela Professora Doutora Ana Paula Betencourt
Martins Amaro e Professor Vítor Manuel Maranhã Lopes e apresentada ao
Departamento de Engenharia Mecânica da Faculdade de Ciências e Tecnologia da
Universidade de Coimbra**

Junho de 2023

1 2



9 0

FACULDADE DE
CIÊNCIAS E TECNOLOGIA
UNIVERSIDADE DE
COIMBRA

Numerical and experimental evaluation of a novel roller skate platform

A dissertation submitted in partial fulfilment of the requirements for the degree of Master in Mechanical Engineering in the speciality of Manufacturing and Design

Avaliação numérica e experimental de uma nova geometria da plataforma de um patim

Author

João Pedro Teixeira Marques

Advisors

Professora Doutora Ana Paula Betencourt Martins Amaro

Engenheiro Vítor Manuel Maranhã Lopes

Jury

Chair Professora Doutora Beatriz Branquinho Gomes
 Professora Auxiliar da Universidade de Coimbra

Vowel Professora Doutora Maria Augusta Neto
 Professora Auxiliar da Universidade de Coimbra

Advisor Engenheiro Vítor Manuel Maranhã Lopes
 Assistente Convidado da Universidade de Coimbra

Coimbra, junho, 2023

“Sempre chegamos ao sítio aonde nos esperam”

José Saramago, em *A viagem do elefante*

ACKNOWLEDGEMENTS

I would like to express my utmost gratitude to everyone who was part of this endeavour.

Firstly, my advisors were extremely helpful and patient all along. I would very much like to thank them for everything they have taught me and the valuable input throughout this work.

Special thanks to ISEC for the assistance during the experimental process.

A very warm thank you to my girlfriend Ivone who supported me all the way.

Last, but not least, I want to express my profound gratitude to my parents. Nothing that I am or have achieved would be possible without them.

Abstract

The main objective of this work is the development of an innovative concept of a roller skate platform, intended for the practice of the sport of roller hockey.

Compared to other existing models, the platform that was developed using additive manufacturing techniques, is lighter and also able to support various load scenarios. In order to appeal to existing and new users of the sport, the structure was designed to be more cost-effective.

In the process of creating the platform, a Computer Aided Design (CAD) tool was used to model the innovative structure. This platform proposal was validated through the use of the finite element method (FEM), by simulating some tests described in the standard EN 13899:2003. This new platform structure was created in conformity with an existing roller skate platform, being the remaining components disassembled from the latter and, subsequently, assembled on the new platform and used in the experimental tests.

Therefore, the resulting prototype was manufactured and experimentally tested. The results were acquired using a strain gauge and were recorded, and used, to compare and validate the numerical models. The prototype failed during one of the experimental tests, but enough data was collected to produce several conclusions.

The final platform model requires some changes. However, this concept showed a great potential and could work properly after the suggested modifications.

Keywords: Roller skate, Additive manufacturing, Computer Assisted Design, Finite Element Analysis, Data Acquisition

Resumo

O objetivo principal deste trabalho consiste no desenvolvimento de um conceito inovador de uma plataforma de patins, destinada à prática da modalidade de hóquei em patins.

Comparativamente a outros modelos já existentes, a plataforma que se desenvolveu com recurso a técnicas de fabrico aditivo, é mais leve sendo igualmente apta de suportar diversos cenários de carga. De modo a apelar à sua utilização, por parte dos já existentes e novos praticantes deste desporto, a estrutura foi concebida para ter um custo mais baixo.

No processo de criação da plataforma, utilizou-se uma ferramenta de Desenho Assistido por Computador (CAD) para modelar a estrutura inovadora. Tal proposta de plataforma foi validada através do recurso ao método dos elementos finitos (MEF), pela simulação de alguns ensaios descritos na norma EN 13899:2003. Esta nova estrutura de plataforma criou-se em conformidade com uma plataforma de patins já existente, sendo os restantes componentes desmontados desta e, posteriormente, montados na nova plataforma e utilizados nos testes experimentais.

Além disso, foi fabricado e ensaiado experimentalmente o protótipo resultante do referido desenvolvimento. Os resultados, foram adquiridos com recurso a um extensómetro, registados e utilizados para comparar, e validar, os modelos numéricos. O protótipo falhou durante um dos testes experimentais, mas foram recolhidos dados suficientes para produzir diversas conclusões.

O modelo de plataforma final carece de algumas alterações. No entanto, este conceito revelou bastante potencial e poderia funcionar corretamente após as modificações sugeridas.

Palavras-chave: Patins, Fabricação Aditiva, Desenho Assistido por Computador, Método de elementos finitos, Aquisição de Dados

Contents

| | |
|--|------|
| LIST OF FIGURES | ix |
| LIST OF TABLES | xiii |
| LIST OF SIMBOLS AND ABBREVIATIONS | xv |
| List of Symbols..... | xv |
| Acronyms/Abbreviations..... | xv |
| 1. INTRODUCTION | 1 |
| 1.1. The roller skate | 2 |
| 1.2. Influence on athlete performance..... | 3 |
| 1.3. General requisites | 3 |
| 1.4. Objectives | 3 |
| 1.5. Dissertation organization | 4 |
| 2. BACKGROUND | 5 |
| 3. DESIGN OF THE NEW PLATFORM | 9 |
| 3.1. Methodology | 9 |
| 3.2. First phase of development | 10 |
| 3.2.1. The base..... | 11 |
| 3.2.2. The centre area..... | 13 |
| 3.2.3. The brake area | 15 |
| 3.2.4. Reinforcements..... | 16 |
| 3.3. Second phase of development..... | 21 |
| 3.3.1. Model MD1.2 | 21 |
| 3.3.2. Numerical analysis | 23 |
| 3.4. Third phase of development | 25 |
| 3.4.1. Model MD1.3 | 25 |
| 3.5. Fourth phase of development..... | 28 |
| 3.5.1. Model MD1.4 | 28 |
| 3.6. Model in Aluminium | 29 |
| 4. NUMERICAL ANALYSIS..... | 33 |
| 4.1. Weight..... | 34 |
| 4.2. Attachment..... | 38 |
| 4.3. Frontal Impact on the truck (FIT)..... | 43 |
| 4.4. Frontal Impact on the brake (FIB) | 48 |
| 5. EXPERIMENTAL TESTING | 53 |
| 5.1. Prototype..... | 53 |
| 5.2. Placement of the strain gauge | 55 |
| 5.3. Testing | 58 |
| 5.3.1. Weight test..... | 59 |
| 5.3.2. Frontal impact on the brake..... | 60 |
| 5.3.3. Frontal impact on the truck..... | 65 |
| 6. RESULTS DISCUSSION | 67 |

7. CONCLUSIONS 71

REFERENCES 73

APPENDIX A 75

APPENDIX B 91

APPENDIX C 99

APPENDIX D 101

LIST OF FIGURES

| | |
|---|----|
| Figure 1.1. Portugal national team during a match. (Journal O Jogo, 2023)..... | 1 |
| Figure 1.2. Exploded view of the roller skate. The platform (model MD.1.4), in the centre in white, which was developed further in chapter 3..... | 2 |
| Figure 2.1. Traditional Manufacturing vs Additive Manufacturing. (Conner et al., 2014)... | 5 |
| Figure 3.1. The base of MD1..... | 11 |
| Figure 3.2. Equivalent von Mises stress (left) and resultant displacement deformed (right) plot; Simplified weight static numerical study; 2000 N..... | 11 |
| Figure 3.3. Concentration points of the load exerted by the foot. (Olmi, 2015). | 12 |
| Figure 3.4. Model MD4. | 13 |
| Figure 3.5. Centre of the model MD1.1. | 14 |
| Figure 3.6. Simplified weight static numerical testing with 2000 N: Equivalent von Mises stress (left) and resultant displacements (right)..... | 14 |
| Figure 3.7. Cross-section of the brake zone (left). Tensile, compression and torsional loads exerted on the brake zone (right)..... | 15 |
| Figure 3.8. Equivalent von Mises stress (top right) and resultant displacement (top left) of frontal impact on the brake; Equivalent von Mises stress (bottom right) and resultant displacement (bottom left) of weight on the brake; 1000 N..... | 16 |
| Figure 3.9. Trucks area conception with biding elements area identified. | 16 |
| Figure 3.10. Simplified weight static numerical study with 2000 N: Equivalent von Mises stress plot (left) and resultant displacement (right). | 17 |
| Figure 3.11. Reinforcements made in the frontend of the platform. | 18 |
| Figure 3.12. Reinforcements made in the backend of the platform. | 18 |
| Figure 3.13. Simplified weight static numerical study: Equivalent von Mises stress plot (top) and resultant displacement plot (bottom) of final MD1.1. | 19 |
| Figure 3.14. Simplified weight static numerical study: Equivalent von Mises stress plot (left) and resultant displacement plot (right) of MD2.1. | 20 |
| Figure 3.15. Brake zone of MD1.2. | 21 |
| Figure 3.16. Close-up of reinforcement under study (top left); Equivalent von Mises stress plot of simplified weight static numerical test: Depiction of concentrated stress on thin walls before (bottom right) and after reinforcements (bottom left) and MD1.1 before creating the hole of the M10 screw hole (top right)..... | 22 |
| Figure 3.17. Configuration of weight numerical study for MD1.2. | 24 |
| Figure 3.18. First assembly coarse static numerical study of the athlete's weight: Equivalent von Mises stress (left) and resultant displacement (right) plot; MD1.2. | 25 |

| | |
|---|----|
| Figure 3.19. Weight numerical study; Equivalent von Mises stress plots (left) and resultant displacements (right): with reinforcements (top) and without reinforcements (bottom); MD1.3. | 26 |
| Figure 3.20. Final brake zone: side cut view..... | 28 |
| Figure 3.21. Highlighted zones where material was added, near the M10 screw holes. | 29 |
| Figure 3.22. Model MD3.2; Section ISO View. | 30 |
| Figure 3.23. Simplified weight static numerical test: Equivalent von Mises stress (left) and resultant displacement (right) plot; MD3.2..... | 31 |
| Figure 4.1. Final weight numerical study configuration; MD1.4..... | 35 |
| Figure 4.2. Weight static numerical study: Equivalent von Mises Stress (left) and resultant displacements (right) plot; ABS..... | 36 |
| Figure 4.3. Weight static numerical study: Equivalent von Mises Stress (left) and resultant displacements (right) plot; CFRP..... | 37 |
| Figure 4.4. Weight static numerical study: Equivalent von Mises Stress (left) and resultant displacements (right) plot; eSun Resin. | 37 |
| Figure 4.5. Weight static numerical study: Strain plot; top close view with elements strain values; eSun resin..... | 38 |
| Figure 4.6. Exemplification of the attachment test from the standard 13899:2003. | 39 |
| Figure 4.7. Constrains of the top cap applied on the surface in blue..... | 40 |
| Figure 4.8. Final attachment numerical study configuration; MD1.4..... | 40 |
| Figure 4.9. Attachment static numerical study: Equivalent von Mises Stress (left) plot and full assembly resultant displacement plot (right); ABS. | 41 |
| Figure 4.10. Attachment static numerical study: Equivalent von Mises Stress (left) plot and resultant displacement plot (right); CFRP. | 41 |
| Figure 4.11. Full assembly resultant displacement plot; CFRP. | 42 |
| Figure 4.12. Attachment static numerical study: Equivalent von Mises Stress (left) plot and resultant displacement plot (right); eSun Resin. | 42 |
| Figure 4.13. Exemplification of the FIT test from the standard 13899:2003..... | 43 |
| Figure 4.14. Axle static numerical study to infer how the software applies the force on the model..... | 45 |
| Figure 4.15. Final FIT numerical study configuration; MD1.4. | 45 |
| Figure 4.16. FIT static numerical study: Equivalent von Mises stress (left) and resultant displacement (right) plot; ABS. | 46 |
| Figure 4.17. FIT static numerical study: Equivalent von Mises stress (left) and resultant displacement (right) plot; CFRP. | 47 |
| Figure 4.18. FIT static numerical study: Equivalent von Mises stress (left) and resultant displacement (right) plot; eSun Resin. | 47 |
| Figure 4.19. Exemplification of the FIB test from the standard 13899:2003. | 48 |

| | |
|--|-----|
| Figure 4.20. The constrain applied in the FIB configuration which later proved to be wrong..... | 49 |
| Figure 4.21. Final FIB numerical study configuration: Wrong on the left and corrected on the right; MD1.4..... | 49 |
| Figure 4.22. FIB corrected static numerical study: Resultant displacement plot; ABS..... | 50 |
| Figure 4.23. FIB (corrected) static numerical study; Equivalent von Mises stress plot; ABS..... | 51 |
| Figure 4.24. FIB (corrected) static numerical study: Equivalent von Mises stress (left) and resultant displacement (right) plot; CFRP..... | 51 |
| Figure 4.25. FIB (corrected) static numerical study: Equivalent von Mises stress (left) and resultant displacement (right) plot; eSun Resin..... | 52 |
| Figure 5.1. CAD of metal inserts: Trucks casket on the left and brake casket on the right. | 54 |
| Figure 5.2. Place of choice for the strain gauge..... | 56 |
| Figure 5.3. Strain gauge assembled with the cabling..... | 57 |
| Figure 5.4. Testing platform with all cables and module connected. Final setup minus the PC..... | 57 |
| Figure 5.5. Final testing setup on the athlete; Roller skate platform without the braking device..... | 58 |
| Figure 5.6. Roller skate after failure and the removal of the boot by the athlete..... | 66 |
| Figure C.1. Wrong FIB static numerical study: Equivalent von Mises Stress plot (left) and resultant displacement (right); ABS..... | 99 |
| Figure C.2. Wrong FIB static numerical study: Equivalent strain plot; eSun Resin..... | 99 |
| Figure D.1. Front Panel of LabVIEW program for weight testing..... | 101 |
| Figure D.2. Block diagram of LabVIEW program for weight testing..... | 101 |
| Figure D.3. Front Panel of LabVIEW program for FIT and FIB testing..... | 102 |
| Figure D.4. Block diagram of LabVIEW program for FIT and FIB testing..... | 102 |
| Figure D.5. Graphs of weight testing test runs: first (top left), second (top right), third (middle left), fourth (middle right), fifth (bottom centre)..... | 103 |

LIST OF TABLES

| | |
|--|----|
| Table 2.1. Evaluation of the materials adequacy to this work. (Ashby & Jones, 1996; Farah et al., 2016). | 6 |
| Table 2.2. Material properties from the 3 materials chosen. (ESUN LCD Water Washable Resin 0.5KG – ESUN Official Store, n.d.; INNOVATEFIL PA CF, n.d.; ABS from the <i>Solidworks</i> ® material library). | 7 |
| Table 3.1. Mesh parameters of the simplified weight static numerical study of the base of MD1.1. | 12 |
| Table 3.2. Mesh parameters of the weight static numerical study of MD1.2. | 23 |
| Table 3.3. Mesh parameters of the weight numerical study with and without the reinforcements; MD1.3. | 26 |
| Table 3.4. Material properties of aluminium 7075-T6. (Source: <i>Solidworks</i> ® material library). | 30 |
| Table 4.1. Material properties of the suspension elastomer-made bodies. (Sousa, 2012). | 33 |
| Table 5.1. Cost of one MD1.4 platform in ABS and CFRP. (Evolt Fiberlogy ABS, n.d.; INNOVATEFIL PA CF, n.d.; Price KWh EDP, June 2023, n.d.). | 55 |
| Table 5.2. Weight average and standard deviation of micro-strain for each test run. | 59 |
| Table 5.3. Experimental and numerical results obtained and expected strain. | 60 |
| Table 5.4. Time recorded during testing and velocities, acceleration, and force of impact calculated values. | 62 |
| Table 5.5. Comparison between the force and strain obtained experimentally (with or without the residual strain) and numerically estimation for FIB. | 63 |
| Table 5.6. Estimated experimental micro-strain values from forces calculated from the numerical relation. | 64 |
| Table A.1. Study and mesh properties for all static numerical studies. | 75 |
| Table A.2. Fixtures; Weight static numerical study. | 76 |
| Table A.3. Loads; Weight static numerical study. | 77 |
| Table A.4. Rigid Connectors for weight, attachment, and FIT static numerical studies. | 78 |
| Table A.5. Bolt connectors for weight, attachment, and FIT static numerical studies. | 78 |
| Table A.6. Contact information for weight, attachment and FIT static numerical studies. | 80 |
| Table A.7. Fixtures; Attachment static numerical study. | 83 |
| Table A.8. Loads; Attachment static numerical study. | 85 |
| Table A.9. Fixtures; FIT static numerical study. | 85 |
| Table A.10. Loads; FIT static numerical study. | 87 |

Table A.11. Fixtures; FIB static numerical study. 87

Table A.12. Loads; FIB static numerical study..... 88

Table A.13. Contact information; FIB static numerical study. 88

Table B.1. Mesh convergence for all the numerical studies done for model MD1.4. 91

Table B.2. Continuation of mesh convergence for all the numerical studies done for model MD1.4. 92

Table B.3. Continuation of mesh convergence for all the numerical studies done for model MD1.4. 93

Table B.4. Continuation of mesh convergence for all the numerical studies done for model MD1.4. 94

Table B.5. Mesh convergence for all the numerical studies done for model MD1.3. 95

Table B.6. Continuation of mesh convergence for all the numerical studies done for model MD1.3. 96

Table B.7. Continuation of mesh convergence for all the numerical studies done for model MD1.3. 97

Table C.1. Numerical results from the wrong FIB static studies for the 3 different materials. 99

LIST OF SIMBOLS AND ABBREVIATIONS

List of Symbols

E – Modulus of Elasticity

kg – kilograms

Acronyms/Abbreviations

CAD – Computer Assisted Design

DEM – Departamento de Engenharia Mecânica

FCTUC – Faculdade de Ciências e Tecnologia da Universidade de Coimbra

FDM – Fused Deposition Modelling

FEA – Finite Element Analysis

FIB – Frontal Impact on the Brake

FIT – Frontal Impact on the Trucks

SLA – Stereolithography

1. INTRODUCTION

The present dissertation describes the development of a new and improved roller skate platform. These are used in many sports, such as hockey and figure skating. However, the focus is on quad hockey. It is referred to as the type of hockey where the athletes use roller skates with four wheels and two axles instead of inline and ice skates (used in inline and ice hockey, respectively). It is the most popular type of hockey in Europe. The sport also gained much traction in Portugal due to the Portuguese national team's success over the years.

During a match, the athletes are at all times equipped with the roller skates as it is observable in Figure 1.1.



Figure 1.1. Portugal national team during a match. (Journal O Jogo, 2023).

The improvement of a roller skate platform came about after observing the struggle of children playing quad hockey. The weight of the roller skates noticeably influenced how the children moved, as it is considerable for their size and strength. Adult players would also benefit from the reduction of weight.

The price of roller skates is a significant consideration for those wanting to get into the sport for the first time. Therefore, various materials and fabrication processes will be considered to lower the price. However, the focus will be on additive manufacturing (AM).

1.1. The roller skate

As shown in Figure 1.2, the roller skate comprises various parts which will be developed further. The platform is attached to the sole of the boot using four screws, which are not represented in the figure below.

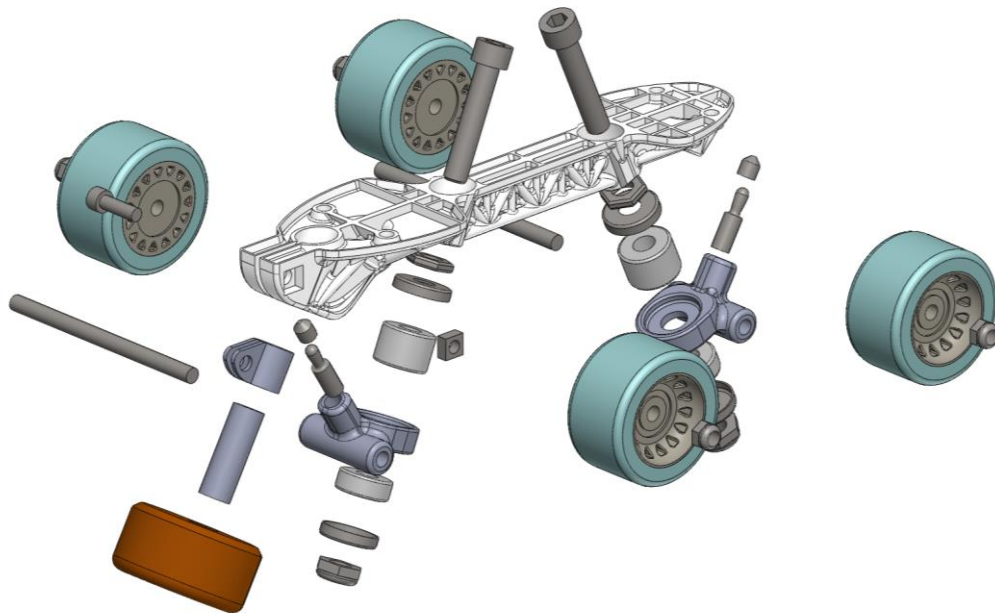


Figure 1.2. Exploded view of the roller skate. The platform (model MD.1.4), in the centre in white, which was developed further in chapter 3.

The platform (or chassis) of the roller skate is the component under study in this dissertation. It is typically made from steel, aluminium, or titanium, depending on the price range. The goal is to decrease the mass of the platform. Some companies fabricated them from polymers to create more light and affordable platforms. The polymer-made roller skates' mass in existence do not differ significantly from those made from aluminium and titanium, and they are considerably cheaper.

According to Fuentes (2018), the mass of one of the most popular roller skates, the Boiani STAR RK 16, is about 410,400 g. This one is made from aluminium 6061-T6.

On the other hand, the TVD platform, made from Zytel®, was evaluated at only 151,880 g (measured in laboratory in a precision scale with a sensibility of around $\pm 0,010$ g). This was the roller skate to be used as a base comparison as is one very common model.

1.2. Influence on athlete performance

Lightweight roller skates have always been the preference for those who play the sport. A hockey athlete must carry the roller skates as well as the stick and protections during the game. The weight of all that gear adds to the athlete's physical effort when moving. In this work, only the roller skate platform is the subject of improvement.

A diminished mass of the platform contributes to better manoeuvrability and does not lead to as much fatigue during long sessions of skating. In addition, the lower the platform's mass, the lower the centre of mass of the roller skate since most of the weight becomes from the axles and wheels, when using a lighter platform. Thus, it improves stability.

If athletes can move more freely, efficiently and become less fatigued, it is safe to assume that it will result in fewer injuries.

Moreover, for children who practice quad hockey, it will be less of an effort to move. The weight of the roller skates has a more preminent impact on how they move rather than in adults. A lighter platform would enable the children to focus more on the game and make it easier for them to enjoy the sport.

1.3. General requisites

The roller skate must follow the standard EN 13899:2003 (Roller skate equipment – Roller skates – Safety requirements and test methods). The former describes the critical aspects of the roller skate and testing scenarios. There is also a standard for the elastomers from which the trucks (sub-assembly which contains axle, wheels, and suspension) are composed. That norm will not be used since the trucks are out of scope.

The standard EN 13899:2003 addresses different aspects of many components of the roller skate. However, only those regarding the roller skate platform will be scrutinized in this work.

1.4. Objectives

This dissertation aims to create a new and improved platform with reduced mass. The remaining components which constitute the roller skate are out of scope.

In addition, certain measurements such as main dimensions and angles of the trucks must be like those of the TVD roller skate provided by Faculty of Sport Sciences and Physical Education of University of Coimbra (FCDEFUC). This, because the remaining parts constituent of this roller skate will be mounted on a prototype to test it experimentally.

The roller skate platform is to be designed and validated through FEA. In the standard EN 13899:2003, various tests are described to ensure the roller skate is safe. It will be made several approximations of those tests in the FEA to ensure the new design complies with the regulations.

The platform will then be tested experimentally according to this standard and compared with the numerical results.

Children are the main targets when conceiving the structure, therefore, it must be light and low price for an easier entry in the sport. However, the roller skates are going to be designed as it was to withstand with an adult. This way it can not only ensure it will be safe for children, as it can also be beneficial for adults, maximizing performance.

The models are to be designed leveraging the possibilities that additive manufacturing provides. There will be one final model which will be regarded for polymer additive manufacture, and another concept for metal additive manufacturing which will not be fabricated and tested due to the high price of manufacture. The former will be a proof of concept for a future where metal additive manufacturing is affordable.

To sum up, the goal is to make low-price, light-working prototypes complying with the standard and continue to ensure the safety of athletes.

1.5. Dissertation organization

This dissertation consists of 7 chapters. **Chapter 1** introduces the scope of this dissertation along with the aim and requirements of this work. **Chapter 2** contains a preliminary review of the area of research. **Chapter 3** includes the design process of the novel structure. **Chapter 4** comprises the numerical analysis done on the structure. **Chapter 5** contains the details of the experimental procedures done to attest to the numerical analysis. **Chapter 6** is the discussion of the results and **chapter 7** concludes the findings of this dissertation.

2. BACKGROUND

Roller skates are made from many different materials, mainly steel and aluminium in more demanding sporting conditions, as well as polymeric materials, for more recreational and relaxed purposes. This is because of the superior performance of the metallic platforms over the existing polymer platforms, despite the increase in mass.

The metallic platforms are usually made through machining. This does not only increase the fabrication price as it has limitations regarding the platform geometry. For this reason, additive manufacturing was chosen as the preferred manufacturing method. This will allow for more freedom of design and to create novel geometries otherwise deemed impossible to manufacture through subtractive manufacturing processes. However, it is certainly less profitable than injection moulding for large production (for polymer-made platforms), but that manufacturing process has its design limitations.

Furthermore, additive manufacturing is getting cheaper with time. Depending on the number of units to be fabricated, it can be more affordable than injection moulding if it is a smaller production. An essential factor to be considered is that the price of a part to be produced by injection moulding increases exponentially with the complexity of the part (Conner et al., 2014). Therefore, additive manufacturing could be the most profitable choice because of the high complexity of the parts to be created (Figure 2.1).

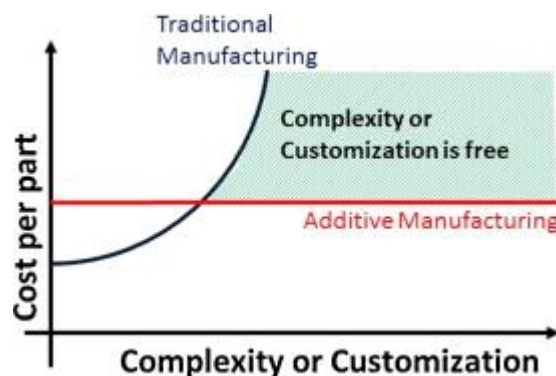


Figure 2.1. Traditional Manufacturing vs Additive Manufacturing. (Conner et al., 2014).

The FDM (Fused Deposition Modelling) and SLA (Stereolithography) manufacturing technologies were chosen since it is the most widely spread additive manufacturing processes, making it inexpensive and accessible.

High stiffness and impact resistance are critical, as stated before. Therefore, thermoplastics with a high elastic modulus were the focus. Also, the higher the yield stress, the better it can support higher loads.

For the FDM process, there were some materials considered like ABS (Acrylonitrile Butadiene Styrene), Nylon (Polyamide), PLA (Polylactic acid) and PP (Polypropylene). One of the most common thermoplastic polymers with high stiffness is ABS. This material is cheap and highly accessible. Another material considered was Nylon. However, even though it has a higher yield stress, it has a lower elastic modulus. If the stress in the structure is maintained below the yield stress value of the ABS, there would be no need for a material with a higher yield stress like Nylon. In addition, Nylon has a lower elastic modulus resulting in bigger unwanted displacements. For these reasons, Nylon was discarded. Although Nylon alone was not good enough for the application, it would significantly improve the modulus of elasticity and yield strength if reinforced with carbon fibre. This would be a much sturdier option, yet more expensive. Other thermoplastics, such as PLA and PP, were considered, but none had the specified requirements. That said, ABS and Carbon Fibre Reinforced Polyamide (CFRP) were the materials considered.

Table 2.1, evidences the different materials considered and their effectiveness **in the context of this work**.

Table 2.1. Evaluation of the materials adequacy to this work. (Ashby & Jones, 1996; Farah et al., 2016).

| | Tensile strength | Stiffness | Price |
|-------|------------------|-----------|-----------|
| ABS | Good | Good | Excellent |
| Nylon | Good | Good | Good |
| PP | Good | Medium | Excellent |
| PLA | Good | Medium | Excellent |
| CFRP | Excellent | Excellent | Poor |
| Resin | Good | Good | Excellent |

Resin 3D printing (SLA) was also taken into account. Some ABS-like resins could provide the exact requirements. Also, it would have a better finish and resolution. Therefore, the final prototype will be made with resin. This is because the fabrication process is less

prone to irregularities. A controlled environment was necessary for ABS and CFRP to print it perfectly. This will help to eliminate a tremendous amount of error due to the fabrication process.

The material properties of the 3 materials chosen are found in the Table 2.2.

Table 2.2. Material properties from the 3 materials chosen. (ESUN LCD Water Washable Resin 0.5KG – ESUN Official Store, n.d.; INNOVATEFIL PA CF, n.d.; ABS from the *Solidworks*® material library).

| | ABS - from <i>Solidworks</i> ® | CFRP - INNOVATEFIL PA CF | Resin - eSun Water washable Resin |
|--|-----------------------------------|-----------------------------|--------------------------------------|
| Modulus of elasticity (MPa) | 2000.000 | 1400.000 | 15000.000 |
| Poisson's ratio | 0.394 | 0.300 | 0.300 |
| Mass density (kg/m³) | 1020.000 | 1250.000 | 1250.000 |
| Tensile strength (MPa) | 42.000 | 68.000 | 170.000 |

When designing the new platform, there are various factors to consider. First, since the new platform will be mounted on the boot of the provided roller skate with the respective trucks, it must have specific dimensions like the provided roller skate. Stiffness is vital, so material must be added to specific areas to increase it. The same has to be done to maintain structural integrity. Finally, the platform must endure the skater's weight, and all impacts inherent to this sport. All of this must be achieved while keeping the platform structure light.

The platform must be tested to check if it complies with the standard EN 13899:2003 requirements. Therefore, the different concepts will be simulated through static numerical studies (FEA) during the design process. Although various tests described in the standard are not static, they will be simplified to equivalent static numerical studies to make it easier and faster to obtain results and understand how the structure behaves.

This standard refers to 2 classes of roller skates. Class A roller skates are intended for athletes from 60.000 *kg* to 100.000 *kg*. Class B is for athletes with a mass up to 60.000 *kg*. Since **class A is the most demanding one**, all tests will have in mind the maximum mass for this class, despite the objective consumer being children. This way, it can be used by an adult and maximise safety for children.

The standard also mentions that class B roller skates must have straps to attach the roller skate to the child's boot and need to be of expandable size either. It was opted to go for the class A roller skate not only because of those reasons mentioned above but also because the price of these novel roller skate platforms should be significantly lower and faster to fabricate. This would make buying another roller skate platform easier as the child grows and provide the young athlete with more safety and performance.

There were many tests in the standard but many regarding the wheels, trucks, or straps. There was also a fatigue test which is not to be considered in this work. The scope of this dissertation is only the platform, therefore, only the tests specified further in this work are of interest.

The experimental tests should be performed in a hockey arena with an athlete to verify real-life scenarios and adequately compare with the numerical results.

3. DESIGN OF THE NEW PLATFORM

This chapter will describe how the new roller skate platform was developed and all the criteria that led to the final model. All models and concepts created were named accordingly. More specifically, all models from now onwards shall be identified with the specific model number (e.g., MD1 – Model 1), and subsequent iterations of those models will be identified with a suffix number following a single dot (e.g., MD1.3, MD2.1).

All considerations throughout the development focused on making the roller skate out of ABS. As stated before, more robust materials will be considered, but the structure was conceived with the weakest material in mind. Therefore, the structure should perform with stronger materials, but also making it possible to produce low-price and accessible platforms using ABS.

3.1. Methodology

First, an existing roller skate must be acquired to provide exact measurements (TVD model). This will be the starting point. Meanwhile, different concepts are to be considered and analysed with simplified static numerical studies, which will be relevant to identify critical areas while designing. Then, in a second phase, the chosen models will be developed more rigorously according to the provided roller skate measurements.

All models are designed using CAD software and numerically tested using FEA software. The tool used for both applications is *Solidworks*®.

Once achieved a satisfying design, this must be more rigorously tested. The remaining parts constituent of the roller skate will be designed, and an assembly created. Static numerical studies will be created to try and replicate with the most accuracy the different testing scenarios described in the standard EN 13899:2003. The structure will be analysed and modified as needed. Mesh convergence will be done at this stage in order to make results more accurate.

After all numerically validated models, the next step is manufacturing. Additive manufacturing is used since it can provide, in this instance, low prices, rapid prototyping, as well as final products. A prototype must be made first to confirm that all measurements are

correct. If not, these will be corrected, and a new prototype will be made to check measurements again. Also, if the geometry is slightly altered, new mesh convergence studies need to be made to ensure accurate results comparable to the experimental ones. The final CAD model will be put through more thorough numerical studies, discussed in chapter 4.

3.2. First phase of development

Throughout this development phase, numerical studies were carried out which do not correspond to the final ones. These were made using a very coarse mesh and an extremely simple approach to the model configuration to accelerate the process. All further described forces were applied to the platform structure. Only in a further phase of development will proper numerical studies be carried with all the components constituent of the roller skate. This will allow a full understanding of the platform's behaviour under stress.

In this early stage, static numerical studies were done to identify the maximum stress and displacements. The first studies conducted consisted of applying 2000.000 *N* (Newton) on the top surface of the platform which would contact the boot. The force was applied as if it was the weight of the athlete. In this instance, the standard only describes that it must endure 100.000 *kg* (approximately 1000.000 *N*). However, it was opted for doubling that with safety as a priority. The direction of this force was perpendicular to the surface where it was applied. The platform was fixed (simply supported, which restrains all translational degrees of freedom to zero) in the 8 surfaces (walls and bottom) constituent of the holes of the trucks.

Also, another two important static numerical studies were done in this phase. It had to be considered the efforts made in the brake area since it is highly affected by impact. Moreover, athletes often put their entire weight on the brakes, using them for standing still and impulse. In these numerical studies, a 1000.000 *N* force was applied on the cylindrical wall of the brake hole, parallel to the centreline of the hole, to simulate the athlete supporting all the weight on the brake. A second numerical study of the brake was similar to the previous one but with the force being parallel to the top surface of the platform, pointing to the back of the platform, mimicking a frontal impact. In both these studies the top surface of the platform was fixed (simply supported).

3.2.1. The base

Firstly, the new platform needed to be lighter but still extremely rigid since it affects how the skater transfers his energy to the ground. The stiffer it is, the more efficient. It also had to endure heavy loads for its size. Trusses were immediately considered due to their capability to carry significant loads while maintaining a rigid and light configuration.

Moreover, the roller skates must have four holes where the trucks are attached, another for mounting the brake and four holes to attach the platform to the boot. The designing was commenced by drawing a base and the extrudes where the trucks and brake device were to be assembled, as in Figure 3.1.

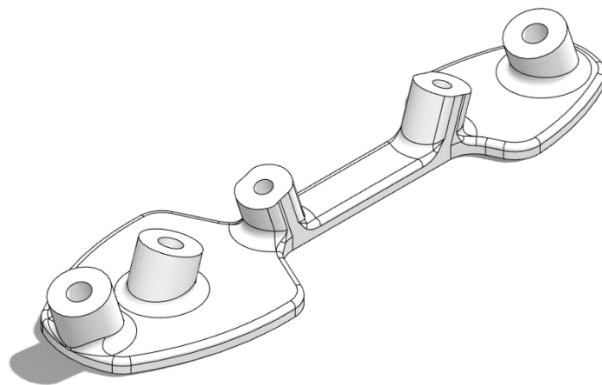


Figure 3.1. The base of MD1.

When drawing the base, some measurements from the TVD roller skate had to be considered as this is to be a replacer of that. A different shape was idealised to improve manoeuvrability. Figure 3.2 gives some insight into how the base behaves under load.

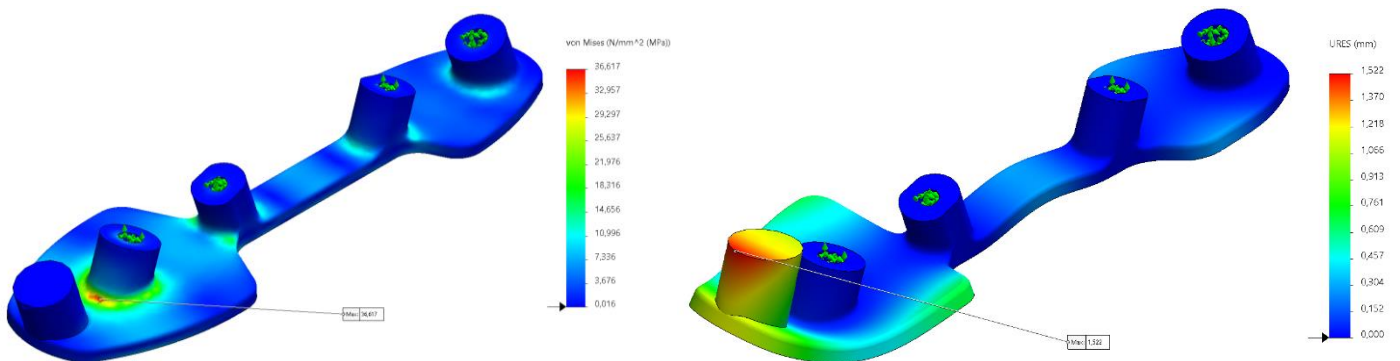


Figure 3.2. Equivalent von Mises stress (left) and resultant displacement deformed (right) plot; Simplified weight static numerical study; 2000 N.

The study was configured according with the above stated. It was created a **solid curvature-based mesh** with **high-quality tetrahedral elements** as for all numerical studies conducted in this work. The high-quality elements are of higher order and have more nodes than the draft elements. This way the elements of higher order can better accommodate the curvature of the body. At this stage, it was just to understand where material was needed.

Table 3.1. Mesh parameters of the simplified weight static numerical study of the base of MD1.1.

| | |
|--------------------------|------------|
| Max. element size | 7.90429 mm |
| Min. element size | 1.58086 mm |
| Total nodes | 34076 |
| Total elements | 20118 |

From the plot in Figure 3.2, it can be noted the brake zone is where the maximum resultant displacement is, probably because it is not supported in any way. Also, the zones further away from the trucks exhibit some of the larger displacements as well. This structure is only a starting point but immediately shows where reinforcements are needed to increase stiffness.

The brake zone must be properly supported. Moreover, the centre and side edges must also be reinforced to decrease displacements and improve manoeuvrability. The equivalent von Mises stress plot too indicates material is needed in those zones to reduce stress.

According to Olmi (2015), the main forces applied by the skater’s foot are in points A, B and C in Figure 3.3. So, it is crucial that the base adequately addresses the forces on those points to improve reaction.

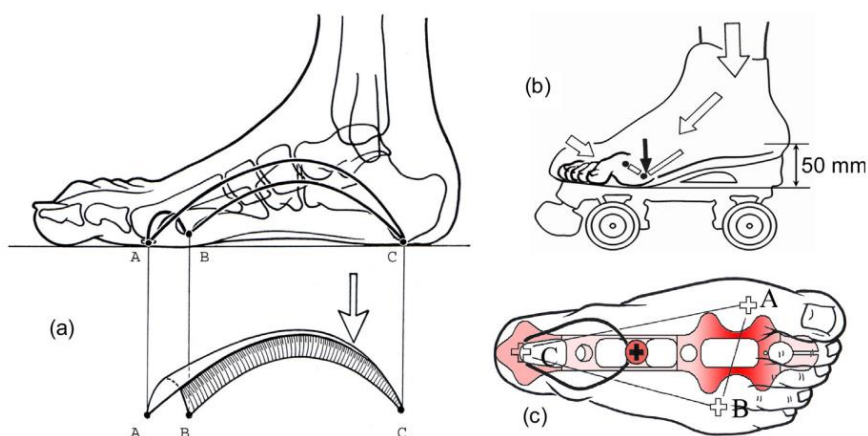


Figure 3.3. Concentration points of the load exerted by the foot. (Olmi, 2015).

Also, as we can observe in Figure 3.3 (c), the platform does not support directly under the loading points A and B. With the new design, there was an attempt to resolve that to improve handling. This will be further elaborated on in this chapter. However, for these reasons, the base was designed wider and with a different shape from the TVD roller skate. In addition, it was conceived with a more conic shape to imitate the shape of the foot.

Regarding the extrudes where the trucks and brake are to be mounted, they had to have specific angles to be compatible with the trucks available for the experimental testing. Although, it must be considered that these are older trucks. There are more recent models with different angles that contribute immensely to perfect manoeuvrability. However, in this dissertation, the angles had to be exact to those of the TVD roller skate, as stated before.

Plenty of features still needed to be added to make it usable and more rigid. Therefore, the work proceeded to reinforce the centre of the platform.

3.2.2. The centre area

The roller skate structure behaves similarly to a beam. Consequently, the centre is expected to exhibit substantial displacement, in a real-world scenario, if not reinforced. There were various attempts to increase the platform's rigidity.

One of the initial ideas was to design a structure like the one below (model MD4, Figure 3.4).

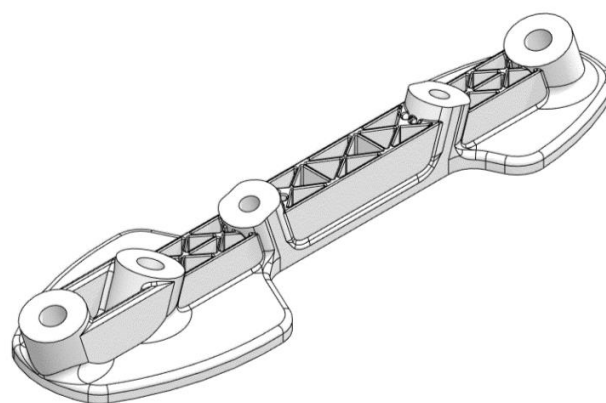


Figure 3.4. Model MD4.

It would result in a stiff structure, but it is still being determined how would deal with the various scenarios of loading that happen during skating. Also, it is similar to existing

platforms. Moreover, the various missing features in this concept would further increase the platform's mass. Therefore, this concept was abandoned.

A second, more promising concept was one inspired in trusses. These are made of a collection of straight, slender members and allow us to build robust and efficient structures. This resulted in the centre of model 1 (MD1.1) in Figure 3.5.

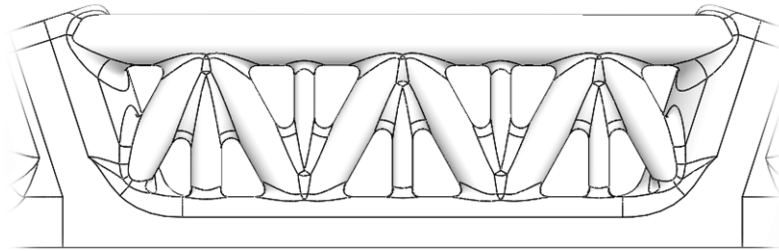


Figure 3.5. Centre of the model MD1.1.

The simplified static numerical study representing the skater's weight revealed low resultant displacements and equivalent von Mises stress in the centre area, as seen in Figure 3.6. Since the results revealed a significant decrease in displacement and stress with this design philosophy, it was decided to proceed with this method. It is noticeable the brake zone is where the maximum stress and displacement occurs thus, making it a focal point to reinforce as approached *infra*.

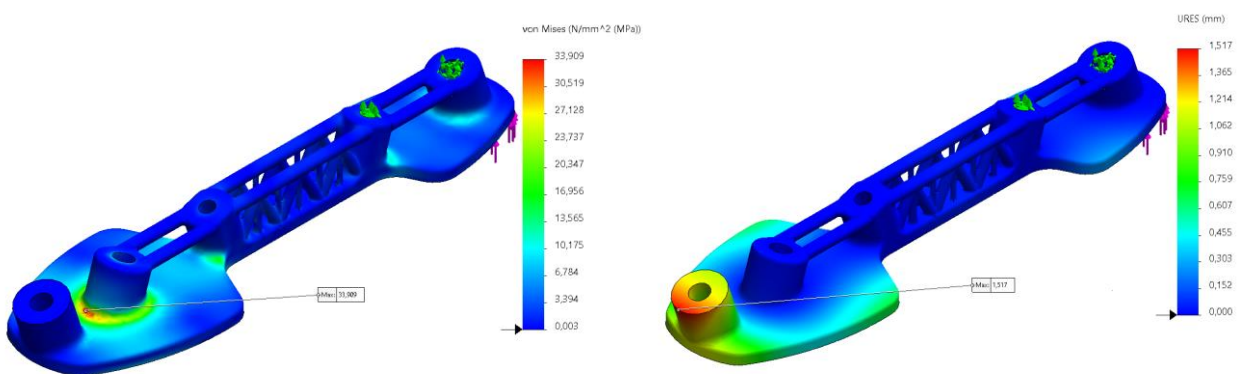


Figure 3.6. Simplified weight static numerical testing with 2000 N: Equivalent von Mises stress (left) and resultant displacements (right).

A third concept consisted of making a lattice structure using 3D printing capabilities. This idea was not followed because it would make it challenging to analyse the structure

numerically, experimentally and overcomplicate the manufacturing process. This is due to the AM processes and materials chosen in this work (Tao & Leu, 2016). The intricacies of such structure would make it more difficult to assess it and diminish fabrication defects. The design for manufacturing is out of scope and does not comprise the objectives, but it was considered to future-proof the concepts developed. Furthermore, being safety a top priority, this option was disregarded for now.

3.2.3. The brake area

Another critical area, as mentioned previously, is the brake. This zone has to be reinforced appropriately due to the loads it has to withstand. The brake is a protuberant component in front of the skate. Therefore, it is highly susceptible to impact. Moreover, as stated before, the athletes often fully support their weight on the brakes.

It was decided to build an I-beam-like profile. The top surface has that shape to handle all the different loads it is subjected to. These are exemplified in Figure 3.7. If narrower, it would be less effective with any lateral load. This way, it is possible to absorb frontal impacts better and diminish displacements, as perceived in Figure 3.8.

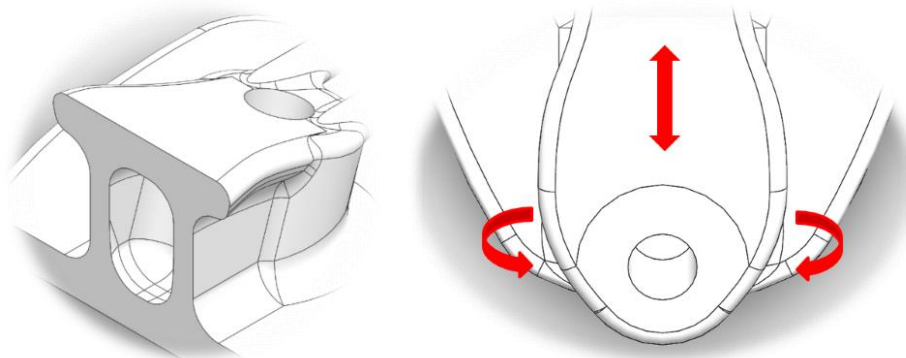


Figure 3.7. Cross-section of the brake zone (left). Tensile, compression and torsional loads exerted on the brake zone (right).

The plots in Figure 3.8 exhibit two static studies representing a frontal impact and the athlete's weight supported on the brake, as described in the beginning of this chapter (3.2). The mesh was a **fine high-quality, curvature-based solid mesh** (no mesh convergence made at this stage).

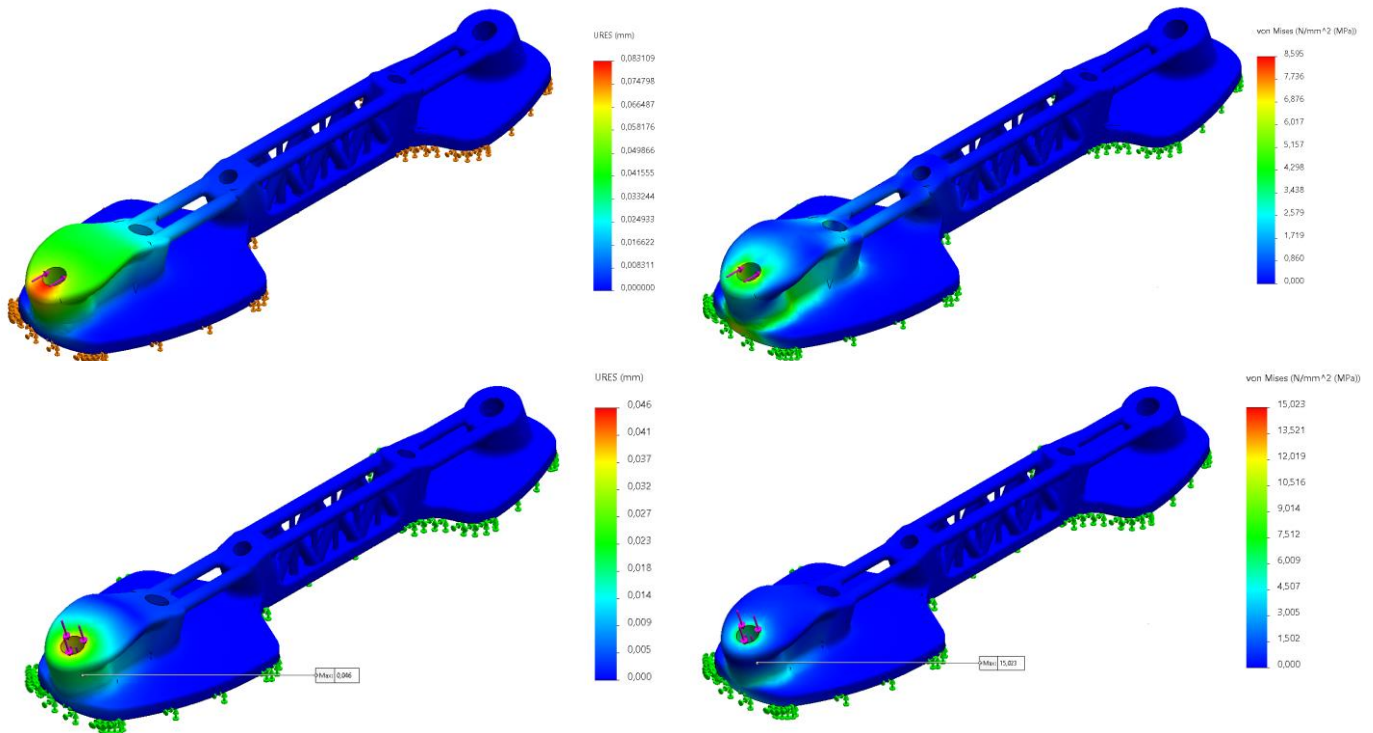


Figure 3.8. Equivalent von Mises stress (top right) and resultant displacement (top left) of frontal impact on the brake; Equivalent von Mises stress (bottom right) and resultant displacement (bottom left) of weight on the brake; 1000 N.

The results indicated this model had an extremely low resultant displacement for both load cases. Furthermore, the maximum equivalent von Mises stress in both instances is far below the yield stress of ABS. Therefore, the design path taken for the brake was deemed satisfactory.

3.2.4. Reinforcements

The structure still needed more support in the binding elements (trucks) area, since there was large stress values around the trucks extrudes (Figure 3.6). A truss-like structure was made in those areas resulting in the model below (Figure 3.9). Thicker cylinders were made since it is a high-stress zone because it is the area which connects directly to the trucks.

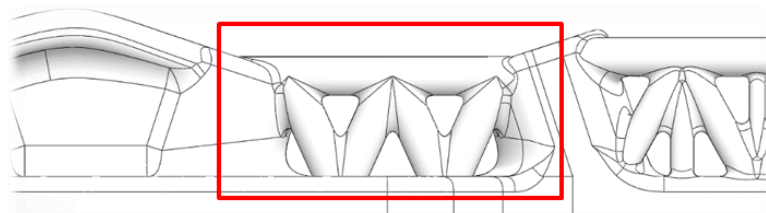


Figure 3.9. Trucks area conception with biding elements area identified.

The platform was subjected to the weight numerical test once more to verify the effect of these alterations. When comparing with the results from Figure 3.6 with the ones in Figure 3.10, both the maximum equivalent von Mises stress and resultant displacement decreased. The most pronounced change is the decrease of the maximum resultant displacement to less than half. The brake reinforcements also contribute to this decrease. However, this area is still of high importance, and these were made to ensure safety.

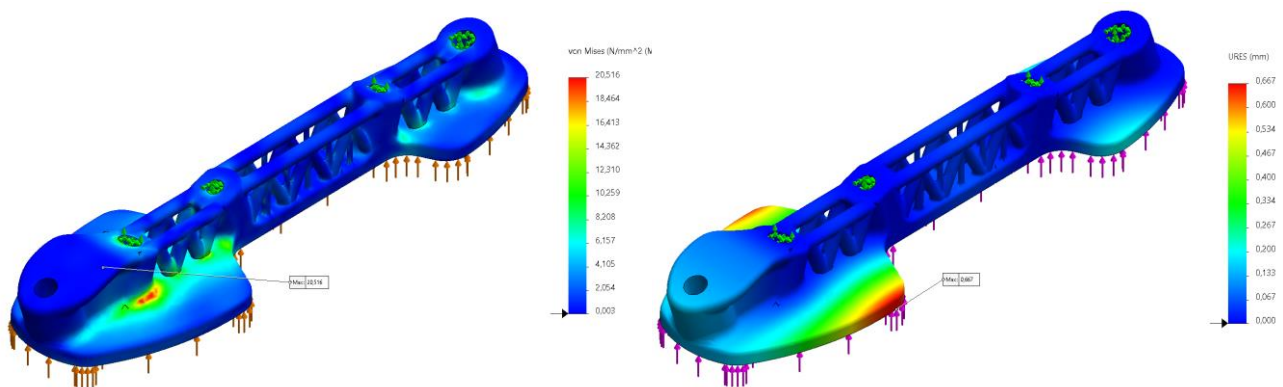


Figure 3.10. Simplified weight static numerical study with 2000 N: Equivalent von Mises stress plot (left) and resultant displacement (right).

The equivalent von Mises stress around the trucks extrudes decreased substantially where the brake and trucks reinforcements were made. Still, on the sides of the front trucks extrudes the maximum equivalent von Mises stress was still overly high. Therefore, some reinforcements in the side areas had to be made to make it safer there and rigid as well (displacements also too high).

Although they serve other purposes, all these side reinforcements aim to make the structure stiffer and improve manoeuvrability. The two cylinders identified by the number 1 in Figure 3.11 not only help decrease the displacements in the place where it was highest, but they also absorb any lateral forces caused by the trucks when turning or being impacted from the sides. Therefore, the cylinders are made to endure different loads from different directions depending on the situation. The point where the two cylinders intersect is also close to point B in Figure 3.3, where much of the force made by the foot acts. This makes for better manoeuvrability.

The cylinder identified with the number 2, despite not being in any of the main points where the foot supports the athlete's weight, also diminishes displacement on the base and absorbs lateral impacts.

Cylinder 3 serves the purpose of absorbing frontal impacts and aiding cylinders 1 and 2 to decrease the displacements and stress on the platform. However, cylinder 4 was created with the aim of supporting the critical brake zone. This helps with impact and resolves any torsion problem resulting from the athlete moving while supporting himself on the brakes.

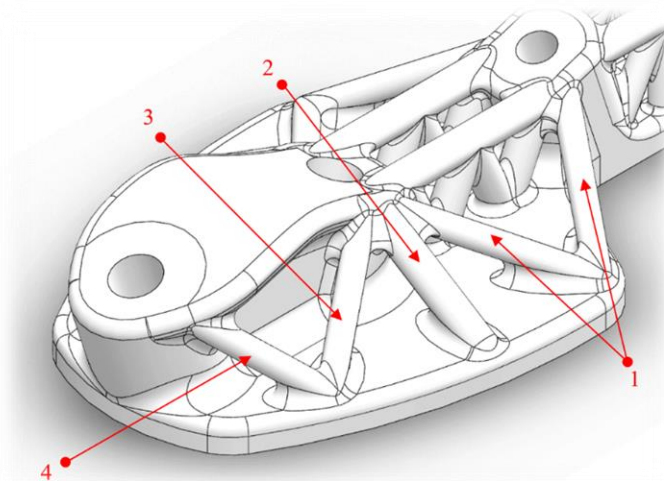


Figure 3.11. Reinforcements made in the frontend of the platform.

The number 5 cylinder (in Figure 3.12) absorbs eventual lateral impacts and helps to support the backend trucks since it has less material than on the frontend. As for the cylinders identified with the number 6, these have the same function as the ones identified with the number 1.

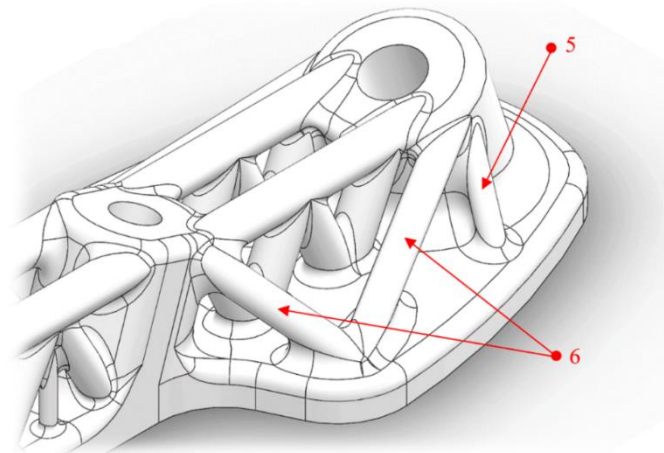


Figure 3.12. Reinforcements made in the backend of the platform.

These reinforcements (Figure 3.13), compared to Figure 3.10, exhibited a diminishing of the displacement by 4.3 times when subjected to the athlete's weight.

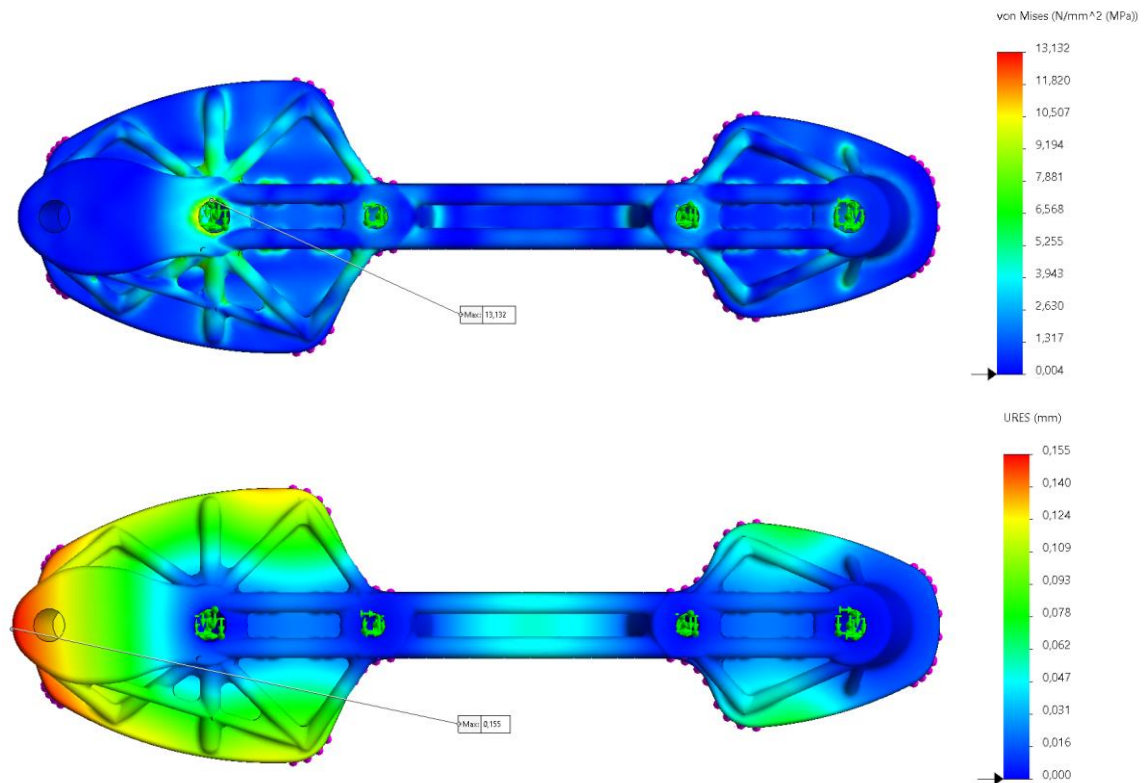


Figure 3.13. Simplified weight static numerical study: Equivalent von Mises stress plot (top) and resultant displacement plot (bottom) of final MD1.1.

In the study presented in Figure 3.13, the maximum stress on the overall structure was lowered to around 10.000 MPa , which is about half of the observed in Figure 3.10. Although it displays a maximum value of 13.132 MPa , this value is due to concentrated stress in the fixed fixture originating a singularity.

It can also be observed that there is another cylinder created in the front side area on the bottom side. This was added to improve the response on the brake zone. However, it was contemplated that it generates unwanted stress close to the brake. Also, the simplified frontal impact static numerical studies showed an undesirable effect on the brake zone. It does not have much of a positive effect, hence deciding to remove it and preserve a lower mass.

Other approaches were attempted (like the model MD2), but ultimately the one in Figure 3.11 and Figure 3.12 (MD1) was the chosen to proceed. The model MD2 was

developed until version MD2.2 (Figure 3.14), and then it was decided not to proceed with this model.

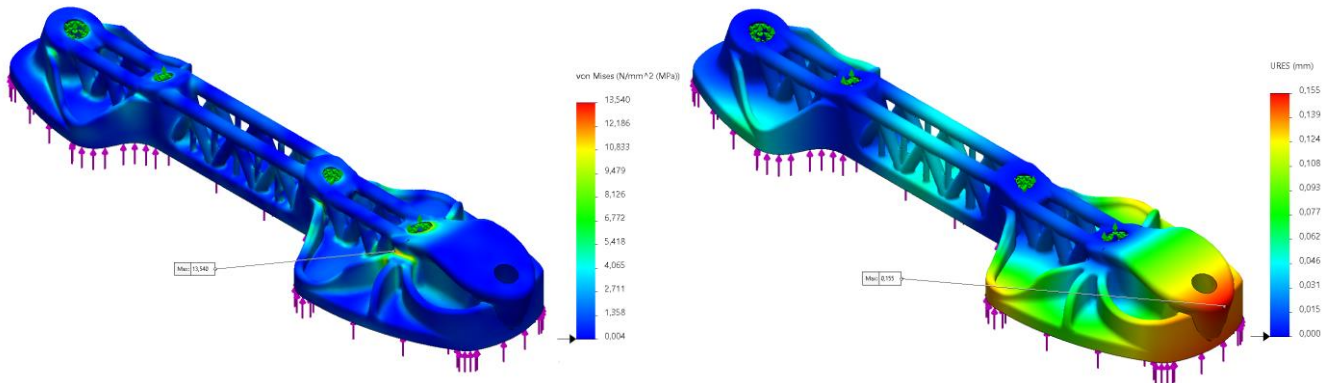


Figure 3.14. Simplified weight static numerical study: Equivalent von Mises stress plot (left) and resultant displacement plot (right) of MD2.1.

Models MD1.1 and MD2.1 had the same basic structure with a different approach only to the reinforcements made on the base. As stated before, the priority is mass reduction and the rigidity of the structure. When analysing the two approaches, despite this model being easier to print since it demands less supports, it also requires more material thus, increasing mass.

Furthermore, the numerical results exhibited similar results of displacement, but the overall stress was a little higher for MD2.1 (13.500 MPa). Despite the maximum equivalent von Mises stress being about the same as in MD1.1, the overall stress was around 10.000 MPa (Figure 3.13). In this model that value represented a singularity due to a fixture. As for the MD2.1, the maximum stress was in a reinforcement. Therefore, at this stage it was opted to proceed with only one model and the MD1.1 was the most promising.

The model MD1.1 is just a concept, but it proved to be functional. However, it had to be refined and dimensioned adequately according to the TVD roller skate to be tested appropriately.

3.3. Second phase of development

3.3.1. Model MD1.2

Model MD1 started with the concept MD1.1 shown previously in Figure 3.11 and Figure 3.12. However, this concept did not have the correct measurements because earlier concepts were idealized before having access to the TVD roller skate for reference. It was not fit to conduct proper static numerical studies. Therefore, several changes were made to turn the previous concept into an operational structure. In addition, several features were added so the remaining components could be assembled.

Firstly, in the brake area, there was a need to make an extrude where it would be possible to fit a screw (Figure 3.15). According to the referred standard EN 13899:2003 (point 4.3.5), the braking device shall not be unscrewed when subjected to a torque of 8.000 N.m . Therefore, it was opted for a similar design to other proved roller skates in the market.

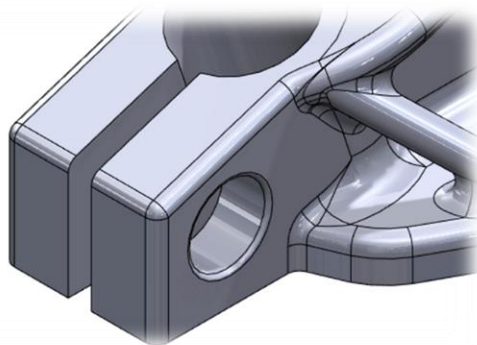


Figure 3.15. Brake zone of MD1.2.

Second, 4 holes in the base had to be made to attach the platform to the boot. These are optimally made right about where the axles are, so it improves responsiveness. However, since the platform was to be tested in the same boot as the TVD roller skate, the holes were made in the same place despite the TVD model being outdated.

Third, regarding the holes that lodge the M10 screw, as seen in Figure 3.16, some reinforcements in that area had to be made. This is because the walls became too thin (0.500 mm) after creating the holes like the TVD model. It resulted in an increase in stress in those walls, as can be observed on the two images, on the right, in Figure 3.16.

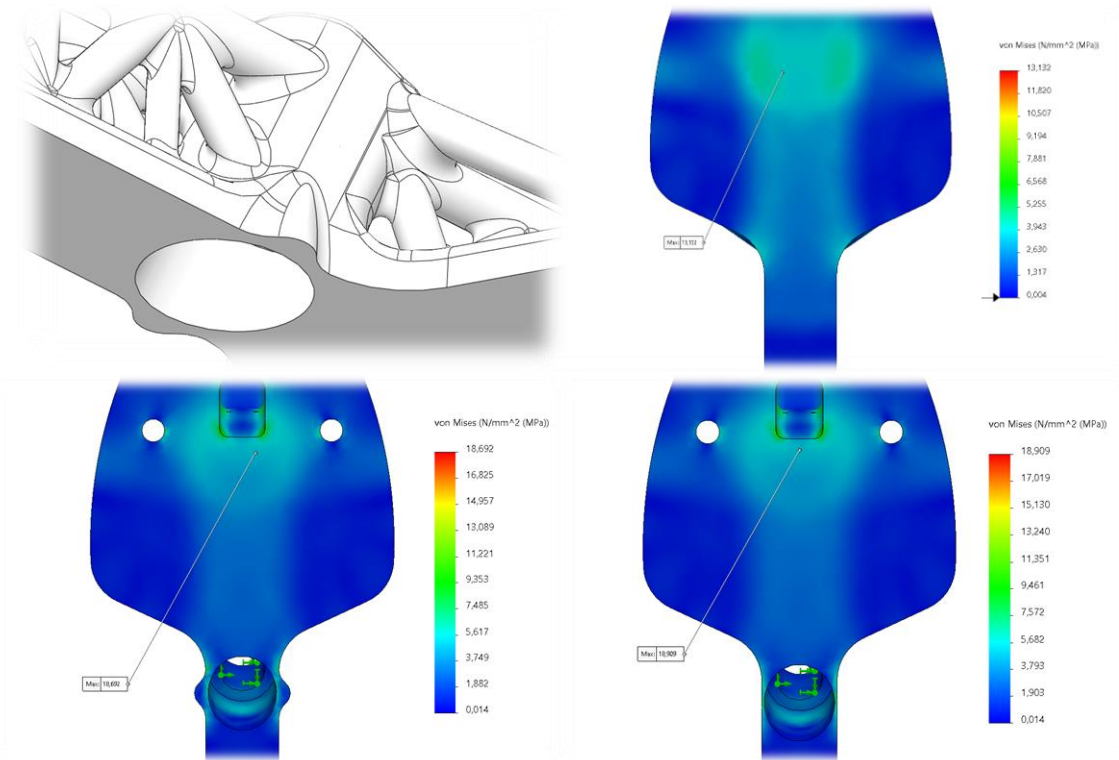


Figure 3.16. Close-up of reinforcement under study (top left); Equivalent von Mises stress plot of simplified weight static numerical test: Depiction of concentrated stress on thin walls before (bottom right) and after reinforcements (bottom left) and MD1.1 before creating the hole of the M10 screw hole (top right).

To resolve this and decrease the stress on those critical areas, reinforcements were added, which can be noted in the Figure 3.16. There was a slight decrease and redistribution of stress. This was thought to be a possible zone of crack initiation hence the reinforcement. The numerical results presented in chapter 4, which depicts this zone as one of the highest stress, later attests for the suspicion.

This alteration was preferred to simply increase the width of the platform. The latter would result in a more significant increase of the mass, which was undesirable. This alteration also affects the manufacturability of the platform.

Lastly, there were several more measurements to be corrected. To make the holes of the attachment screws in the same place as the TVD model, the heel base width had to increase from 50.000 mm to 60.000 mm . In addition, the overall length of the roller skate had to be increased to allow a distance of 160.000 mm between axes. The angles of the trucks were also altered to make it possible to mount the other components from the TVD model.

3.3.2. Numerical analysis

The developed model was complete and ready to undergo a more complete numerical evaluation. The studies conducted in this phase were to try and mimic real scenarios described in the standard EN 13899:2003. To accomplish this, all the other components constituent of the roller skate were considered. Also, it had to be created some representation of the boot's sole since it is how the athlete transfers his energy to the platform. This will be further described in more detail in chapter 4. In this phase, the studies were made with a **tetrahedron element, high-quality, curvature-based mesh** to understand how the structure behaved. It was chosen a **fine** mesh for the assembly to provide more accurate results with the parameters in Table 3.2.

Table 3.2. Mesh parameters of the weight static numerical study of MD1.2.

| | |
|--------------------------|---|
| Mesh type | Mixed mesh (Solid mesh for all bodies except for the two representing the sole which were rigid bodies) |
| Max. element size | 6.80578 mm |
| Min. element size | 1.36116 mm |
| Total nodes | 484257 |
| Total elements | 302392 |
| Solver | Intel Direct Sparse |

In this static numerical study (weight), a fixed support (simply supported) was applied where the wheels were supposed to be. According to Olmi (2015), the forces were applied in points A (22.3%), B (44.3%) and C (33.3%) (Figure 3.3 (c)). However, to simplify and maintaining symmetry in the results, the forces regarding each sole were applied on the two top surfaces of the boot instead of specific points. Therefore, the weight of the athlete was assumed to be $2/3$ (the sum of points A and B) on the front part of the sole and $1/3$ (point C) on the heel. The loads were applied perpendicular to the boot's surface, directed to the platform, as seen in Figure 3.17. Furthermore, 100.000 kg is approximately 1000.000 N (Newton). Regarding each surface, the front and heel loads were $2/3$ of 1000.000 N , which is 666.000 N , and $1/3$ is 333.000 N , respectively.

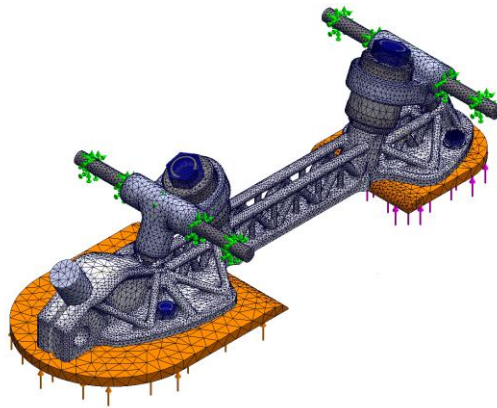


Figure 3.17. Configuration of weight numerical study for MD1.2.

The material was ABS (Table 2.2) for the platform and a standard steel like the AISI 1020, from the *Solidworks*® material library, for the metal components. The elastomers from which the suspension is made were from material properties established according to Sousa (2012). The contacts and interactions are the same as in the final numerical studies, described in Appendix A.

No mesh convergence was done at this stage since it was only to check if the platform could be further improved.

As observed in Figure 3.18, the maximum equivalent von Mises stress on the platform does not exceed the yield strength which is 42 MPa . Moreover, the higher stress is located where there is less material, like around the M10 screw holes. Also, the backend trucks zone is where the maximum equivalent von Mises stress is and could be an area to reinforce. The remainder of the structure has far lower equivalent von Mises stress values. Therefore, it is feasible to remove more material and making the structure lighter. The stress in other components other than the platform is irrelevant because those components are out of scope.

The maximum resultant displacement is in the centre of the structure focused more on the backend of the platform centre area. It occurs where expected since the platform behaves like a beam.

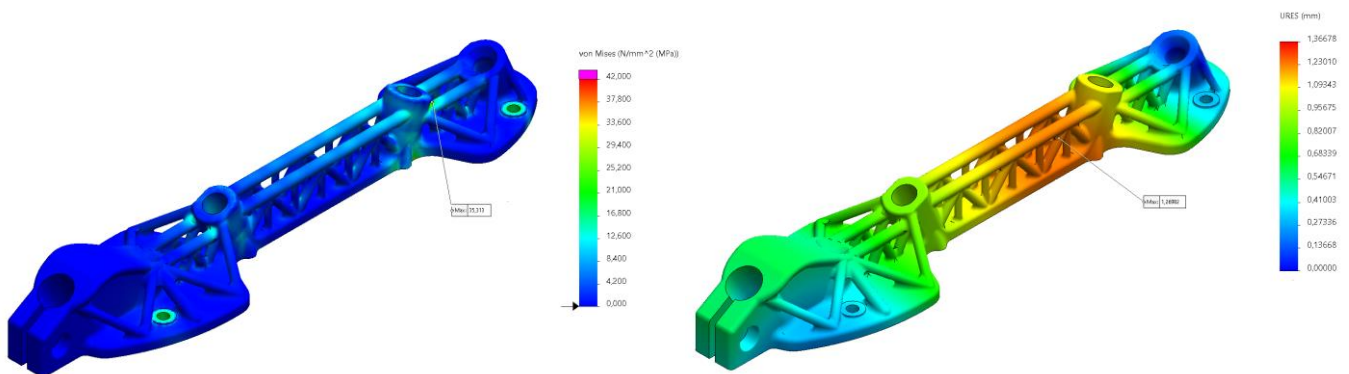


Figure 3.18. First assembly coarse static numerical study of the athlete's weight: Equivalent von Mises stress (left) and resultant displacement (right) plot; MD1.2.

The model MD1.2 had a mass of 87.89 g. This value was calculated by *Solidworks*® using the mass density of ABS (Table 2.2). This roller skate platform had a 42.13% decrease in mass compared to the TVD model. At this point, the structure was very sturdy, but after a careful evaluation, it was decided to attempt to lower the mass even more.

3.4. Third phase of development

This model came to fruition after considering removing more material from specific areas and verify if it could be further improved. The approach in this phase was distinct. It was carried out a process of hollowing the structure to decrease the mass of the platform.

3.4.1. Model MD1.3

In this model, after hollowing the structure, several changes had to be made to mitigate the impact of the material removal.

Making the roller skate hollow decreased the mass to 52.23 g. However, considering the significant removal of material, some unwanted stress and displacement emerged.

Naturally, some regions had to be reinforced. For example, beam-like extrudes were added to decrease displacements and stress in critical areas such as the screw holes (Figure 3.19). Also, from front to back, it was reinforced with longitudinal extrudes since the entire roller skate structure behaves similarly to a beam subjected to flexural stress. It dramatically reduced the maximum resultant displacement. Also, all of the equivalent von Mises stress that exceeded the yield value was eliminated.

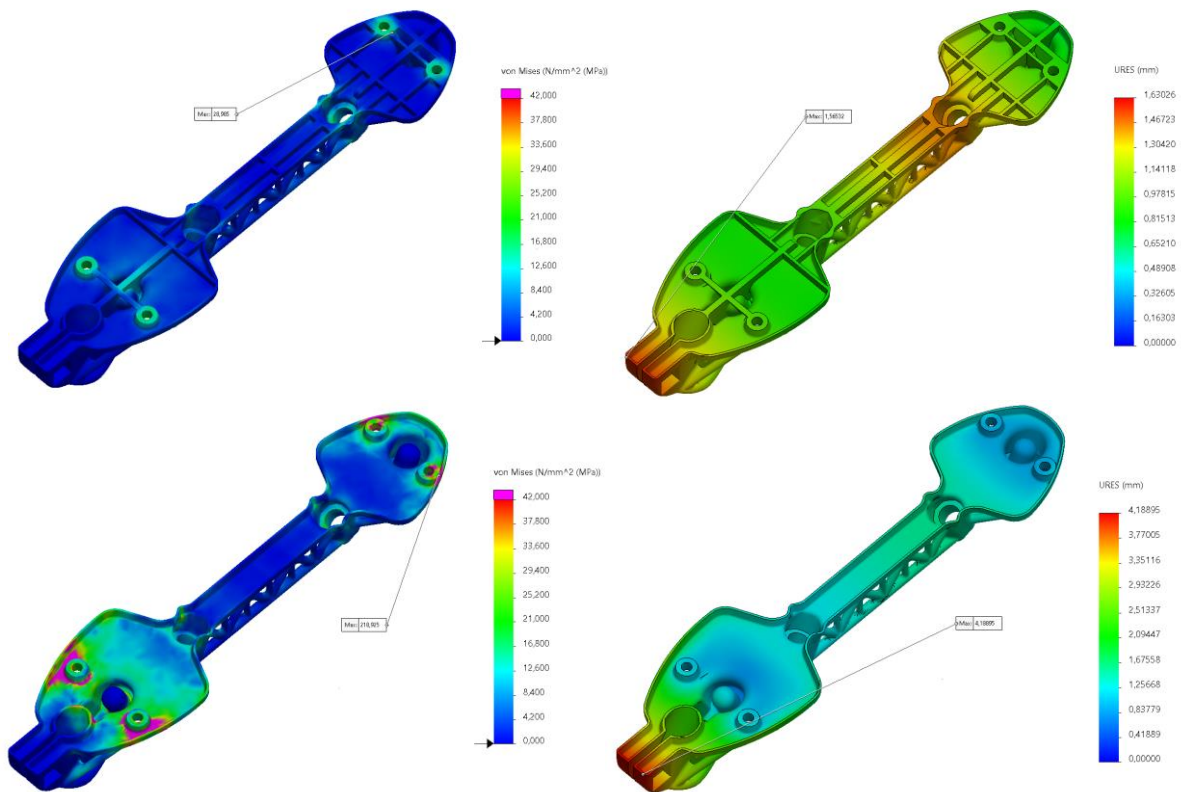


Figure 3.19. Weight numerical study; Equivalent von Mises stress plots (left) and resultant displacements (right): with reinforcements (top) and without reinforcements (bottom); MD1.3.

The results also attest for the statement in chapter 3.3.1, which states the reinforcements in Figure 3.16 are in some of the higher stress zones. The study was done with a **high-quality, curvature-based mesh**. It was used **tetrahedron elements**. The mesh had the parameters described in Table 3.3.

Table 3.3. Mesh parameters of the weight numerical study with and without the reinforcements; MD1.3.

| | With reinforcements | Without reinforcements |
|--------------------------|---|------------------------|
| Mesh type | Mixed mesh (the two sole bodies are rigid, and all others are solid bodies) | |
| Max. element size | 24.71880 mm | |
| Min. element size | 4.94375 mm | |
| Total nodes | 94121 | 82201 |
| Total elements | 52031 | 44266 |
| Solver | Large Problem Direct Sparse | |

It was used large elements which makes for a coarser mesh. While designing, this study was only to evaluate where the higher stresses were in order to address them.

Around the four attachment screw holes, large deformations and stress were detected, especially on the backend. This explains being added more material there than was in the front. In addition, the areas close to the M10 screw (where the trucks are fixed) got especially reinforced due to being a fragile zone where the cross-section gets significantly diminished. Therefore, it was expected to be a stress concentration zone, thus needing more material.

The brake extrusion, where the screw that prevents the brake from getting loose is located, got rounded to remove unnecessary material.

The model was ready to undergo the **final** numerical tests to check if it could go to the next phase, which is prototyping.

This model was put through all numerical testing with both ABS and CFRP and proceeded to prototyping to check the measurements and possible defects. The numerical tests in this phase were conducted as it was for the final model, described in the next chapter. The mesh convergence and results of the MD1.3 are in Appendix B.

A prototype was made from PLA, using the FDM method, due to availability and ease of manufacturing. It is none of the materials studied, but it does not require a controlled environment like ABS and is cheaper than CFRP. And since it was only to check if all components were assembled perfectly, it did not have to be usable to skate.

The prototype revealed wrong diameter measurements in all screw holes, and the angles of the trucks were unsuitable, making it impossible to assemble the remaining components. The diameters were correct in the CAD file, but it was not taken into account the filament dilation during printing. Therefore, a tolerance had to be given in all holes and the angles adjusted.

Also, in a visual inspection, two zones noticeably needed to be readjusted. It was on the walls of the M10 screw holes. The walls were still too thin on the sides, where the previous reinforcements (Figure 3.16) did not reach. This produced an incorrect geometry in the M10 walls above the reinforcements made precisely for that reason. Those reinforcements had to reach higher.

Because this model had to be corrected, retested, and fabricated once more, in this chapter, there was no need to dive into the numerical studies done. This is because these studies are **equal** to those the corrected model will undergo. Therefore, in chapter 4, all numerical studies carried out in models **MD1.3 and MD1.4 will be detailed through the final model (MD1.4)**.

3.5. Fourth phase of development

In this fourth and last phase of the platform development, there were some minor changes made. The aim was to correct the structure to make it possible to fully assemble the remaining components of the roller skate. This, because the prototype from MD1.3 did not have the correct measurements. The alterations were mainly for **fixing all the wrong dimensions and defects in the previous model**, observed in the prototype.

3.5.1. Model MD1.4

The diameter of the holes for the M10 screws had to be increased slightly to compensate for the contraction during printing. However, this could only be accomplished by making the walls even thinner. To solve this problem, the base of the roller skate was made wider. This way, both the wall thickness and the diameter of the M10 screw holes were increased. The reinforcements in Figure 3.16 were also made to reach higher on the walls to increase support of the thin walls.

Furthermore, the height of the trucks extrudes were reduced for the trucks to fit perfectly without dramatically changing the rest of the structure. Also, a slight change in the angles of the trucks extrudes was done.

On the bottom, the hole depth, where the M10 screws were to be placed, was increased so the screw no longer protruded from the platform and did not interfere with the boot's sole.

Moreover, material was slightly removed from the brake zone to fit the brake insert, as seen in the Figure 3.20. The brake zone was widened to maintain structural integrity.

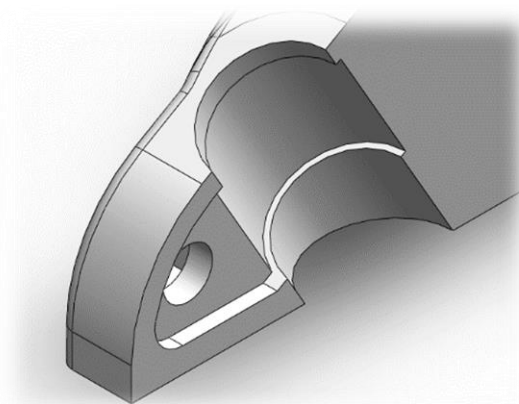


Figure 3.20. Final brake zone: side cut view.

The reinforcements near the holes of the attachment screws (cylinders 2 and 3 in Figure 3.11) had to be repositioned away from the attachment screw holes by 2.000 mm. The prototype of model MD1.3 made it impossible to tighten the attachment screws to the boot because the tools would interfere with the reinforcements.

Lastly, the highlighted zones in the next figure are some of the highest stress as seen in Figure 3.18. This aspect was worthy of improvement. It could become problematic therefore, material was added.

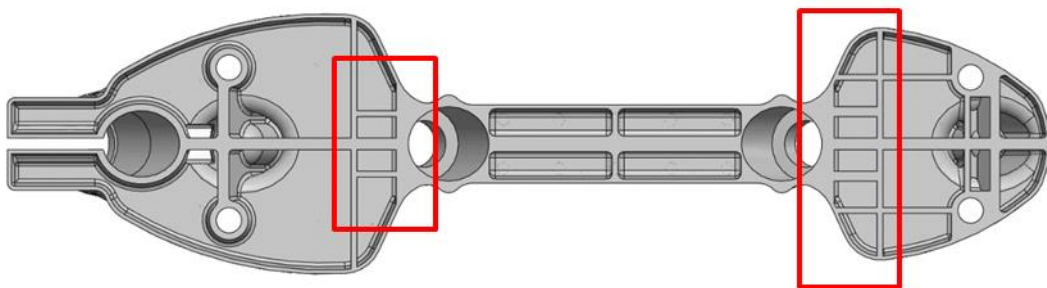


Figure 3.21. Highlighted zones where material was added, near the M10 screw holes.

After all the changes were made, the MD1.4 was put through the static numerical studies described in chapter 4, as was the previous model. After numerical validation of the model MD1.4, it was then manufactured another prototype in PLA to check for measurements. The model was verified to fit all parts perfectly. The final prototype could now be fabricated to conduct the experimental tests.

The final mass of the model **MD1.4 in ABS**, according to *Solidworks*®, was 67,23 g. It represents approximately a decrease in mass of 23,51% when comparing to model MD1.3.

3.6. Model in Aluminium

Before advancing into the numerical testing of the polymer model in chapter 4, there is one more model to consider. This specific model was not expected to go further from a concept. Instead, it only exemplifies what could have been achieved through metal additive manufacturing if this option was financially viable.

The chosen material was **Aluminium 7075-T6** from the *Solidworks*® material library (Table 3.4). It was chosen an aluminium of higher grade than the Boiani model (aluminium

6061-T6) (Fuentes, 2018). This was due to the better properties, allowing to remove more material with less compromising.

Table 3.4. Material properties of aluminium 7075-T6. (Source: *Solidworks*® material library).

| Aluminium 7075-T6 - from <i>Solidworks</i>® | |
|--|-----------|
| Modulus of elasticity (MPa) | 72000.000 |
| Poisson's ratio | 0.330 |
| Mass density (kg/m³) | 2810.000 |
| Yield strength (MPa) | 505.000 |
| Tensile strength (MPa) | 570.000 |

This material has a greatly larger modulus of elasticity and yield strength than the polymers considered previously. Therefore, more material could be removed in this model than in the polymer ones. However, the density of aluminium 7075-T6 is also higher than the considered polymers density. This could result in a heavier structure than the polymer models despite having less material.

A model based on MD1 was created (MD3) and evolved until its second version. Since aluminium has a much higher yield strength than the polymers considered, it was possible to make the structure almost entirely hollow, as observable in Figure 3.22.



Figure 3.22. Model MD3.2; Section ISO View.

This resulted in the model MD3.2 having a mass of only 115.27 g, according to *Solidworks*®. It is an improvement of **24.10%** over the TVD model without the compromises the latter has.

A weight numerical test was done as in the first phase of development of the polymer models. It consisted of only applying a 2000.000 N force on top of the platform and fixing the holes where it would contact the trucks. The mesh was a **coarse, solid, curvature-based mesh** with **tetrahedron** elements.

Figure 3.23 shows that the maximum equivalent von Mises stress was minor considering the yield strength of the material. It demonstrates the far superior properties of aluminium in this instance. Furthermore, with such a low maximum equivalent von Mises stress there is plenty of margin to try to reduce the mass even more.

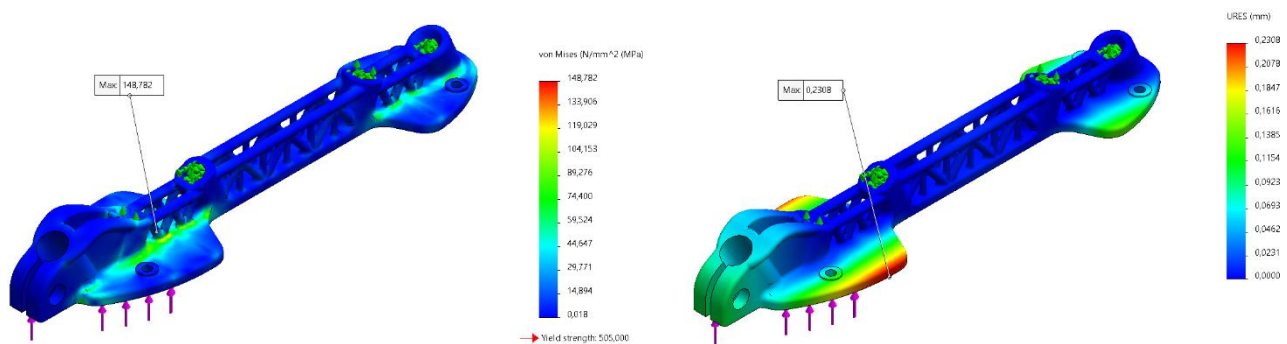


Figure 3.23. Simplified weight static numerical test: Equivalent von Mises stress (left) and resultant displacement (right) plot; MD3.2.

The maximum resultant displacement is even lower than the MD1.1 (Figure 3.10) despite this one being hollow. Plus, if reinforcements were made like the polymer models the results could be vastly improved. The maximum value of displacement could be diminished on the outer edges of the platform to outperform the polymer models established in this work.

Comparing with the TVD model, the difference in mass of the MD3.2 is not as significant to the athlete like the polymer models though, the behaviour of the roller skate would be. This, because the structure would be much **stiffer**. This would result in improved manoeuvrability and better energy transfer from the athlete's foot to the ground while still being slightly lighter than the TVD model.

This model would offer a lightweight roller skate while maintaining, or even surpass, the performance of already existing models in the market made from aluminium and steel. The problem resides in the price and scalability of production. Still, with the continuous

technological improvements throughout the years, metal additive manufacturing could become affordable, and this model could become a possibility in the future.

This structure was not further improved for the reasons previously stated but has immense potential. It represents what the optimal performance roller skate could be with the design freedom of AM.

4. NUMERICAL ANALYSIS

According to the standard EN 13899:2003 and in the scope of this dissertation, there were **four** tests the roller skate had to pass to comply. Therefore, four different static numerical studies were created to mimic as reliably as possible those tests. However, two of them, regarding impact tests, were dynamic tests. Therefore, there was an attempt to create static studies equivalent to the dynamic ones.

These numerical analysis were carried out in phases three and four of development. In this chapter, only the final model (MD1.4) will be addressed since it is the model to be experimentally tested, and the numerical tests are the same for both models (MD1.3 and MD1.4). This, because MD1.3 was thought to be the final model however, the prototype of this model had incorrect dimensions. It had to be corrected as described in chapter 3.5. Therefore, this analysis was done for MD1.3 before prototyping, and then had to be repeated for MD1.4.

All studies for MD1.4 were carried out with the roller skate platform being made from ABS, carbon fibre reinforced polyamide (CFRP), and with the eSun water-washable resin (SLA 3D printing). The latter is the material in which the final prototype will be fabricated and experimentally tested.

There were 3 more materials to be defined for the remaining components of the roller skate. All metallic components were considered to be a standard steel (AISI 1020) from the *Solidworks*® material library. The polymer component of the trucks seemed made out of generic plastic-moulded polyamide. Therefore, it was assumed to be made from Nylon 101, also from the *Solidworks*® material library.

Lastly, there were the four components made of vulcanized rubber which act as absorbers (suspension). According to Sousa (2012), the rubber mechanical properties were the following (Table 4.1):

Table 4.1. Material properties of the suspension elastomer-made bodies. (Sousa, 2012).

| Density (kg/m ³) | Modulus of Elasticity (MPa) | Poisson's ratio |
|------------------------------|-----------------------------|-----------------|
| 1270.000 | 16.000 | 0.400 |

Two bodies, mentioned before, were also created with approximate measurements of the sole of the boot. This was to mimic more precisely how the load is applied on the structure. Because the material from the sole is unknown, the bodies were considered to be rigid. It implies that the bodies do not deform, nor *Solidworks*® requires elastic material properties. This way there is no need to define the material for the *software* to proceed with the calculations. In a real-world scenario the sole would deform as well and that would decrease the stress in the zones of contact. However, by making these bodies rigid, and making the sole incapable of deforming, the numerical results will represent the most demanding scenario thus, being on the side of safety.

These tests were simplifications to make possible to establish numerical studies which would be like real testing conditions. This would make possible to design and develop a roller skate platform accordingly with these studies without the need of prototyping and experimental testing. Only invest to test a final prototype reducing waste and costs while saving time as well.

Whenever simplifications and compromises had to be made, the most demanding scenario was always the chosen one.

The contacts and connections were made for the whole assembly. When any part was excluded, it automatically excluded the corresponding connections and contacts. There were some exceptions as explained further. Mesh convergence values are in Appendix B and due to the extensiveness of the information, there are further details regarding the connectors, interactions, fixtures, and mesh parameters in Appendix A. The information is regarding both MD1.3 and MD1.4 models.

4.1. Weight

The first static numerical study was to check if the platform could withstand the weight of the athlete. This is the same study conducted in chapter 3.3.2 to verify if changes needed to be made.

All components constituent of the roller skate, with exception of the wheels, were considered in this numerical study to be as exact as possible. The elastomer-made component of the brake was excluded from analysis. The body which represents the screw was kept avoiding excessive deformation on the brake zone of the platform.

The wheels were not necessary since any load or restraint could be applied on the axes. Four lesser bodies diminish calculations, time, and complexity. The bolt and nut which locks the brake screw were also excluded from the analysis. The remainder of the screws were replaced by virtual screws.

The forces acting as the athlete's weight were applied to the two surfaces representing the sole. In this study, a 666.000 N force was applied on the front sole and a 333.000 N force on the back sole (heel). This was explained in chapter 3.3.2. The model was fixed on both axes, which impedes any translation in selected finite elements, considering the athlete was standing still on one foot. In a real scenario, it was expected the wheels would move slightly apart from each other. It is believed it would not affect much the roller skate platform though, it might contribute to a small increase in the error of experimental results. However, that displacement would be minor and deemed neglectable in this instance.

The study configuration was the following in Figure 4.1. More details in Appendix A.

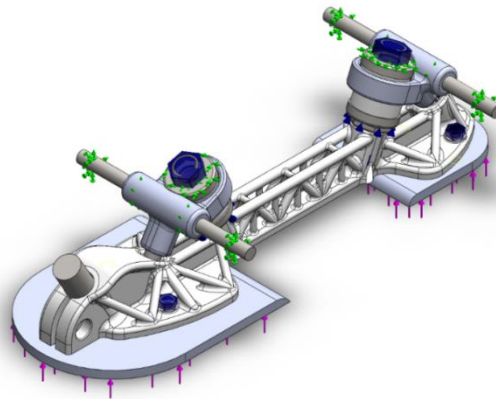


Figure 4.1. Final weight numerical study configuration; MD1.4.

Since the roller skate platform is the scope of this work, in the following results only the platform is displayed.

Model MD1.4 had a maximum equivalent von Mises stress lower than the yield stress of all 3 materials as seen in the following results.

The maximum equivalent von Mises stress in the ABS structure is below 30.000 MPa normally. The maximum value in Figure 4.2 is a concentrated value resulting from the virtual bolts. Nonetheless, on the backend, where the front of the heel presses against the platform, it is evident that it is where the higher stress is located, apart from the bolted connections. The sole being considered a rigid body might have exacerbated the phenomena. In a real-

world scenario the maximum equivalent von Mises stress would be slightly less. However, this makes for the most demanding situation. Conversely, the suspicion that led to the reinforcements in Figure 3.21 was proved correct. Still, it is safe to presume it would only occur elastic deformation on this structure since the values are under 42.000 MPa .

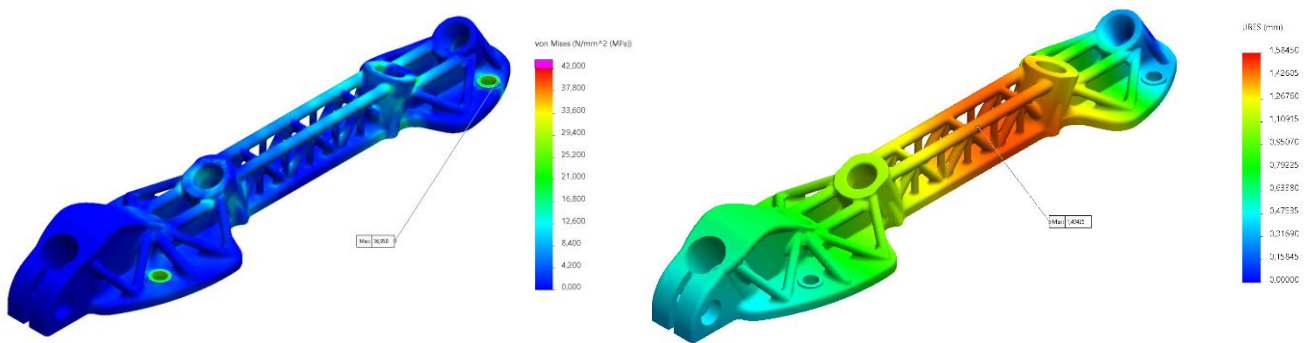


Figure 4.2. Weight static numerical study: Equivalent von Mises Stress (left) and resultant displacements (right) plot; ABS.

The assembly had a maximum resultant displacement of 1.585 mm and the platform structure had a lower maximum resultant displacement of 1.494 mm . The displacement of the assembly is higher because of the higher deformation of the suspension. Regarding the platform's maximum resultant displacement, it was in the middle as expected. Moreover, it was a low value, considered almost imperceptible by the athlete, which checks for the stiffness criteria.

The ABS model is only intended as a less expensive option for young athletes (class B). Therefore, if it can withstand the weight of an adult (class A), it can safely be assumed the roller skate platform is suitable for children.

The same model made from CFRP is an option for a more robust platform. The maximum equivalent von Mises stress on the platform is less than half of what it can withstand (170.000 MPa) thus being suitable for an adult to use it safely (Figure 4.3).

Apart from the bolted connections, the highest equivalent von Mises stress values are also in the zone of contact with the heel of the boot, for the same reasons as for the ABS model since the geometry and study configuration is the same.

This model differs in the increase in rigidity. This is due to the 49.46% decrease in the platform's maximum resultant displacement. Overall, this material offers a sturdier platform despite the increase in price of the CFRP.

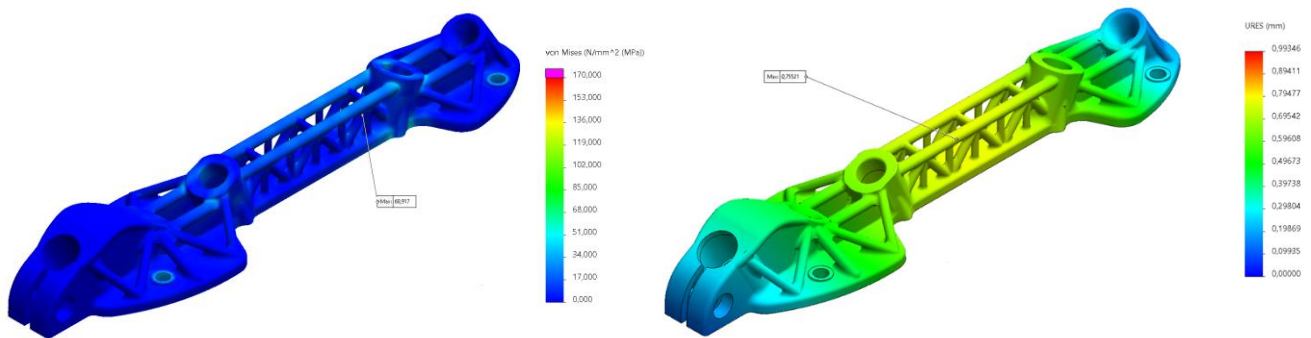


Figure 4.3. Weight static numerical study: Equivalent von Mises Stress (left) and resultant displacements (right) plot; CFRP.

Lastly, the same model made from eSun water-washable resin is tested for the weight requirements (Figure 4.4). The maximum equivalent von Mises stress is almost half of the maximum tensile strength (68.000 MPa). Stress distribution is similar to the other two models as stated before. The maximum resultant displacement on the roller skate platform is 1.612 mm which results in a rigid platform. Nevertheless, the value is not much higher than the ABS model. It is important to denote, this model is only for testing and not intended for final production as indicated in chapter 2.

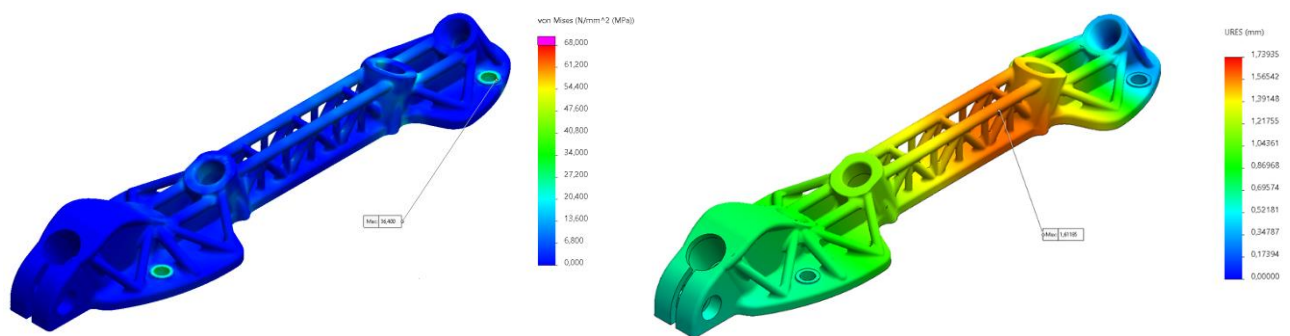


Figure 4.4. Weight static numerical study: Equivalent von Mises Stress (left) and resultant displacements (right) plot; eSun Resin.

In this model is relevant to display the equivalent strain plot because this is to be compared with the experimental results. As expected, there is more strain around the attachment screws as well as the zone of the M10 bolt hole on the backend of the platform. This zone is a focal point of stress.

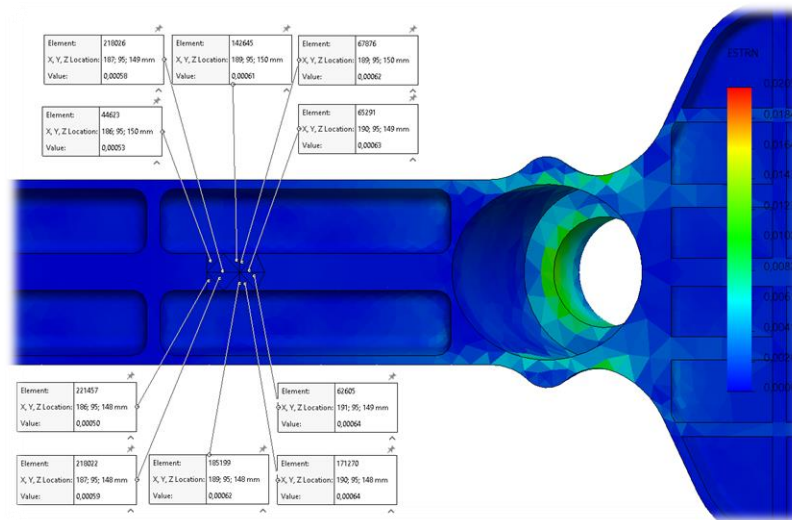


Figure 4.5. Weight static numerical study: Strain plot; top close view with elements strain values; eSun resin.

An average equivalent strain of all the elements of where the strain gauge is to be placed (depicted in Figure 4.5), is calculated. The average is $600.000 \mu\epsilon$ (micro-strain). This placement of the strain gauge is further described in chapter 5 where the experimental process will be detailed.

4.2. Attachment

This study was idealized accordingly with paragraph 5.3.7.2 of the standard EN 13899:2003. This test is to ensure the roller skate platform is properly secured to the boot. This study is within the scope of this work because the platform is under a lot of stress when the binding elements are being pulled on. More specifically, the zones around the M10 screw holes as well as the four attachment screw holes, are expected to be under significant stress.

Furthermore, paragraph 5.3.7.2 states the platform must not detach from the boot. This is secured by the attachment screws. In experimental testing, these will be the same as the already proven TVD model screws. Only the platform is within the scope of this work, and only the stress those connections cause on the platform is of interest.

In this test a roller skate is mounted along the whole length of its chassis in a universal test machine. Then, a force is applied on both axes by a support as shown in the Figure 4.6.

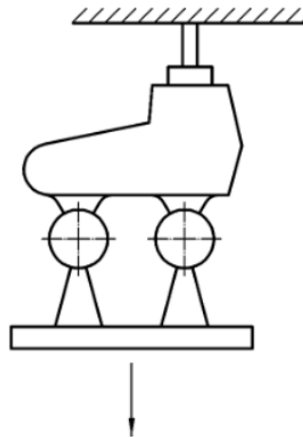


Figure 4.6. Exemplification of the attachment test from the standard 13899:2003.

The force is a **quasi-static** tensile force and is applied at a speed of $< 20 \text{ mm/min}$ up to a tensile force of 1000.000 N . To simplify, and having into account the force is quasi-static, in the numerical study the structure was considered to be under a static tensile force of 1000.000 N . This force was applied on both axes thus, *Solidworks*® automatically divides it by the two axles ($500.000 \text{ N} + 500.000 \text{ N}$). It does not depict **exactly** what is in Figure 4.6 but it provides a close approximation. The forces being applied directly on the axle is a more unfavourable scenario thus having safety as a priority.

The numerical model used for this study was **similar** to the model regarding the weight numerical testing. All the same components were included in this study with the same materials, including the 3 different platform materials considered in this dissertation.

However, it was created one more fixture than in the weight configuration. Due to the force being tensile as opposed to compressive as in the weight scenario, the top cap of the trucks was behaving inconsistently. In order to preserve the most characteristics as possible from the weight configuration, only this one fixture was added. This was done so both tests were almost equal, so this numerical test can be deemed correct by only conducting experimentally the weight test.

The top cap was constrained of all translations on the x and y axis, being the plane made by these two axes, parallel to the top surface of the cap, as we can observe in Figure 4.7 (in blue).

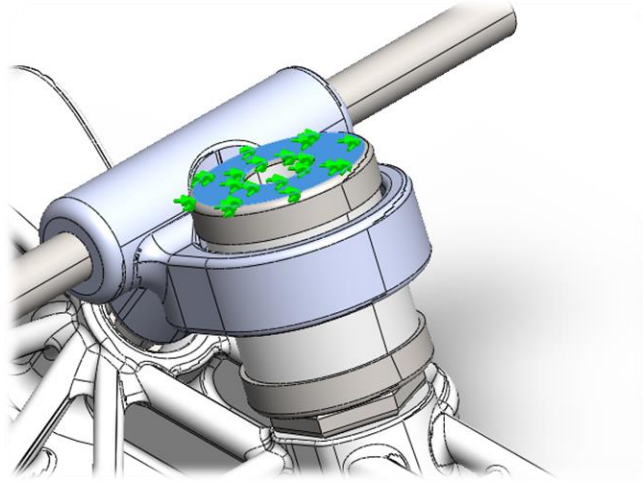


Figure 4.7. Constrain of the top cap applied on the surface in blue.

This fixture only permits the cap to have a perpendicular movement relative to the surface highlighted in blue in Figure 4.7. This is not exactly true but was a **minor** simplification. More extensive information of the configuration (Figure 4.8) on Appendix A.

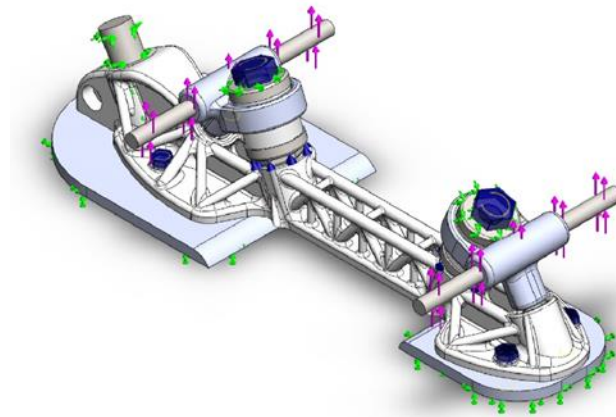


Figure 4.8. Final attachment numerical study configuration; MD1.4.

Conversely, the maximum equivalent von Mises stress is above the tolerable by the material. However, there is only a few finite elements which are above that value. Moreover, they are all located on the four attachment screw holes. This may indicate it is contact derived stress from the virtual bolted connections. Considering the ductility of ABS, it could result

in slight plastic deformation but not failure. The remaining of the structure is below the required values.

It can be verified, in Figure 4.9, the expected high stress zones are precisely around the M10 screw holes and the four attachment screw holes.

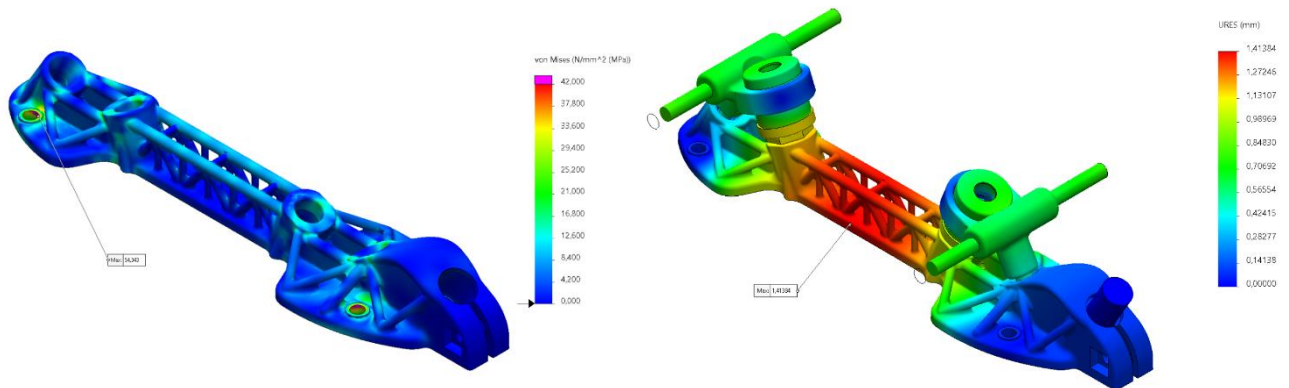


Figure 4.9. Attachment static numerical study: Equivalent von Mises Stress (left) plot and full assembly resultant displacement plot (right); ABS.

Regarding the resultant displacement, the maximum occurs on the platform itself. It occurs in the middle of the structure and is symmetric relative to the mid axes plane, which was expected.

For CFRP (Figure 4.10), the maximum equivalent von Mises stress is way below the maximum tensile strength. This model once more proves to be the right choice for adults due to its robustness.

Additionally, in the resultant displacement plot of the CFRP model, the maximum value is 0.213 mm, which attests for the higher rigidity required for higher performance.

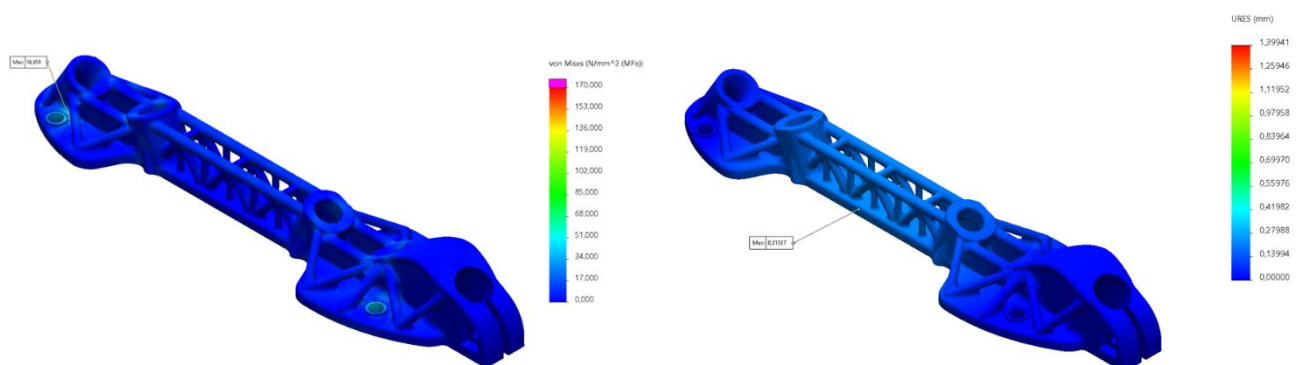


Figure 4.10. Attachment static numerical study: Equivalent von Mises Stress (left) plot and resultant displacement plot (right); CFRP.

Notably, the maximum displacement in the assembly of the CFRP model (in the top caps of the suspension) differs more from the maximum displacement on the platform (Figure 4.11) than the model in ABS (Figure 4.9). This occurs due to the smaller displacement of the structure. Since the structure will not budge as much as in the ABS model the suspension must, hence the bigger displacement of the caps.

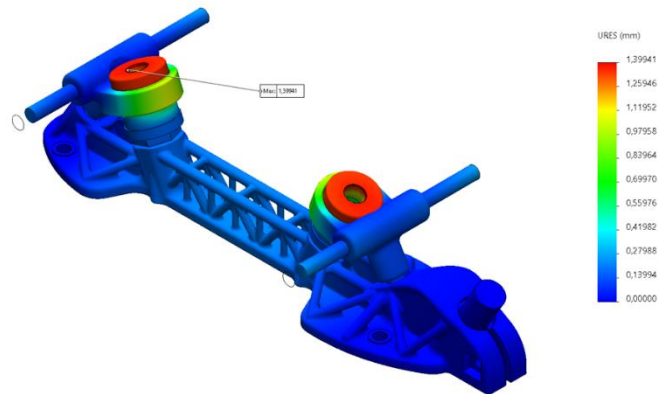


Figure 4.11. Full assembly resultant displacement plot; CFRP.

Lastly, the resin model results (Figure 4.12) were more like the ABS model. Importantly, the maximum equivalent von Mises stress on the platform, as with the other two materials, is in an attachment screw hole. Regarding the displacement, the behaviour is also similar to the ABS model, but the value is larger. This was expected since the modulus of elasticity is slightly smaller.

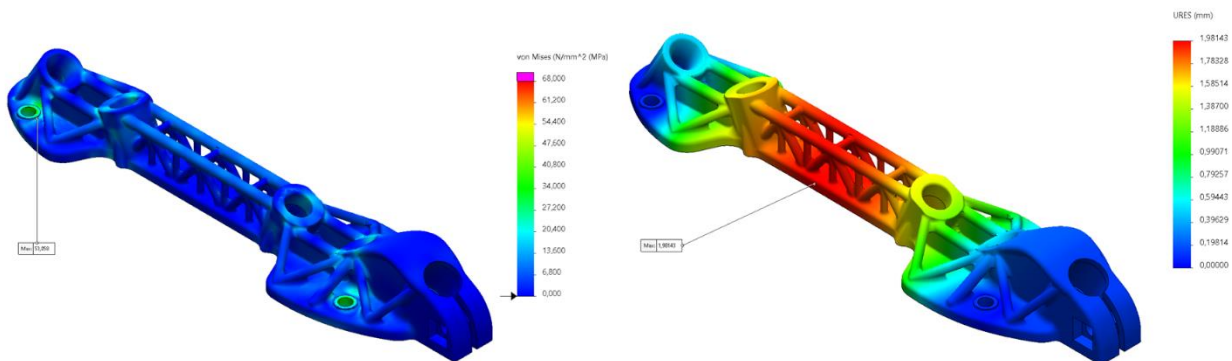


Figure 4.12. Attachment static numerical study: Equivalent von Mises Stress (left) plot and resultant displacement plot (right); eSun Resin.

In this instance the maximum displacement is on the structure. The top caps of the suspension had a smaller displacement as expected since the resin is even more giving than the ABS thus, the suspension had to contract less.

The strain values in the zone where the strain gauge is to be placed, is relevant for the comparison that will be made with the experimental results. It was used the same strategy as in chapter 4.1 (Weight). The average value of equivalent micro-strain in the strain gauge area is $1498000.000 \mu\epsilon$.

According with the numerical results displayed above, the structure was deemed to be compliant with paragraph 5.3.7.2 of the standard EN 13899:2003.

4.3. Frontal Impact on the truck (FIT)

This study was made accordingly to paragraph 5.3.8 of the standard EN 13899:2003. This paragraph indicates the roller skate must endure a frontal impact on the front wheels for instances where is not being used a braking device. The impact must be against a kerb held rigidly in position, with an equal height to the diameter of the wheels. The roller skate goes against the kerb as illustrated in Figure 4.13.

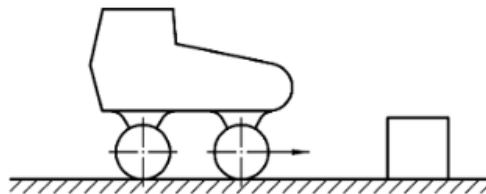


Figure 4.13. Exemplification of the FIT test from the standard 13899:2003.

Moreover, in the standard EN 13899:2003 there are energy and impact velocity parameters stipulated for each class of roller skate. As stated before, all studies will be conducted for the most demanding conditions which are the conditions of class A. These stipulate the impact must be carried out with an energy of $90.000 J$ (Joules) and an impact velocity of $3.500 \pm 0.400 m/s$.

Nevertheless, there was an attempt to recreate an equivalent static numerical study to mimic the stress in the instant of impact. The standard provided the energy and velocity

value. In this instance, the potential energy is null therefore, the total mechanical energy is only comprised of kinetic energy. The latter is calculated through the equation (4.1):

$$K = \frac{1}{2} \times m \times v^2, \quad (4.1)$$

where, K is the kinetic energy, m is the mass of the moving body and v is the velocity of the body.

Assuming the roller skate is static, and another body collides with the roller skate, it is possible to obtain similar results as if it was the roller skate to go against a kerb (Newton's third law). However, the force which the collision occurs must be deduced. Therefore, with the values provided by the standard it is possible to obtain a value of mass in kg through:

$$90.000 = \frac{1}{2} \times m \times 3.900^2, \quad (4.2)$$

Which would be,

$$m = 11.834 \text{ kg}. \quad (4.3)$$

According to Newton's second law, this mass when multiplied by the gravitational acceleration (g), considered approximate to 10.000 m/s^2 , gives the force (F).

$$F = m \times g. \quad (4.4)$$

$$F = 11.830 \times 10.000 = 118.300 \text{ N}. \quad (4.5)$$

This value of force can be introduced in *Solidworks*® in a static numerical study.

Notably, the approximation to 10 m/s^2 increases the value of the force which slightly increases the force exerted on the platform, which contributes to increasing the safety factor.

According to standard EN 13899:2003, the impact occurs on the front wheels. However, there was no need to compute the results adding the two front wheels which would overcomplicate the study unnecessarily. Therefore, the force was applied directly on the front axle. This also contributes to an increase in the safety factor since the wheels would absorb part of the impact. This is especially due to the exterior of the wheels being made from an elastomer. However, it had to be assessed if the restrains were being applied on the surface of the axle or in the mid axis that goes through the centre of the front axle. To check this, the force previously calculated was applied on the axle alone (Figure 4.14). The axle was fixed on both ends. In *Solidworks*®, it was activated the option to calculate the reactions on the body. On the next figure, it can be observed that the reactions on both ends are the same and are half of the total force applied. Also, the force is entirely in the x direction which

is the desirable one. There are some minor values of force on the axis y and z but are extremely small compared to the value of the axis x thus, neglectable.

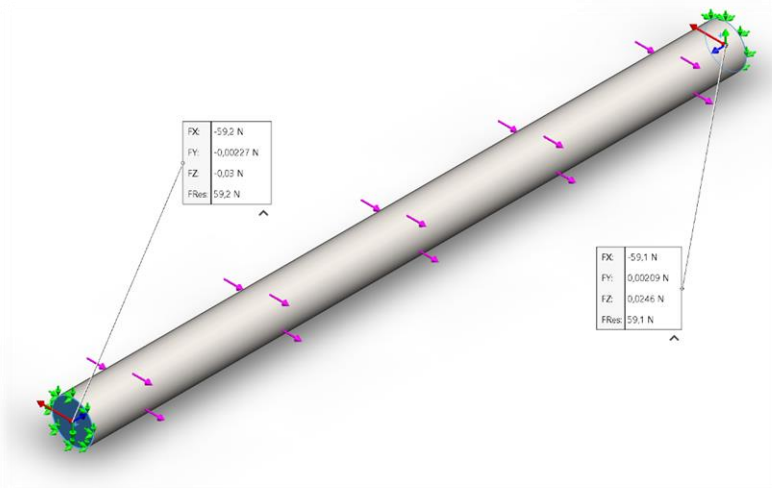


Figure 4.14. Axle static numerical study to infer how the software applies the force on the model.

Having calculated the force value and confirmed that it can be applied on the front axle, the remainder of the model for this study had to be configured. The materials of all components remain the same as in the previous numerical studies conducted. The connections and fixtures are also similar to the ones encountered in the weight numerical study. More detailed information about all of these can be read in Appendix A. The final configuration of this study was the following in Figure 4.15.

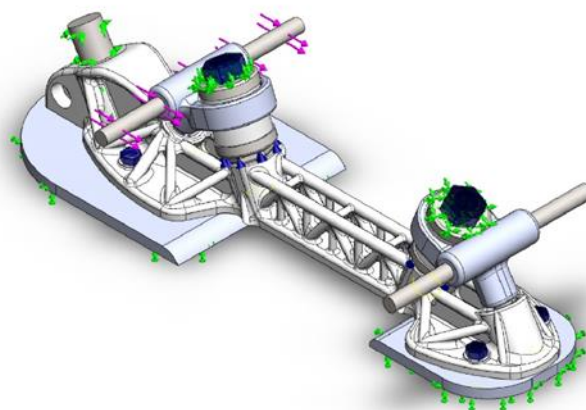


Figure 4.15. Final FIT numerical study configuration; MD1.4.

All components included in the two previous studies were also included in this one. Since the impact is on the frontend trucks, it could have a big influence in the middle of the structure and the backend trucks could have a role to play in the results as well. Therefore, it was opted to keep the backend trucks.

The assembly was fixed (simply supported) on the sole of the boot. This way it is considered the obstacle goes against the roller skate and not the contrary. Nevertheless, according to Newton's third law of motion, the results should be the same.

Regarding the concentrated stress on the attachment screw holes (Figure 4.16), **at this stage**, it was believed it would result in plastic deformation but not in failure of the part. It could also be due to contact derived stress from the bolted connections. Everywhere else in the platform structure, the equivalent von Mises stress does not go over the yield stress of ABS.

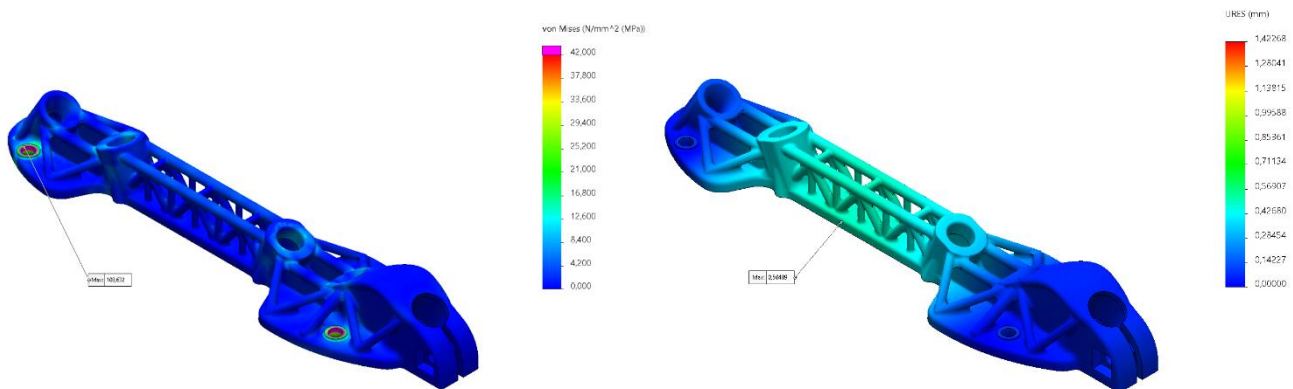


Figure 4.16. FIT static numerical study: Equivalent von Mises stress (left) and resultant displacement (right) plot; ABS.

As can be observed, the highest resultant displacement occurs in the middle of the platform structure as expected. This attests for the prior decisions made relatively to include the backend trucks in the numerical study. The resultant displacement plot indicates the back-suspension elements (backend trucks) most definitely had an influence on the results.

The model in CFRP had the same concentrated stress problem as the ABS model. However, even though the concentrated stress is high, the tensile strength of the material is even higher. In the resultant displacement plot of the CFRP model, it is observable an expected behaviour as well. The displacement on the platform has diminished and, on the trucks, it is higher to compensate for the lower displacement on the platform (Figure 4.17).

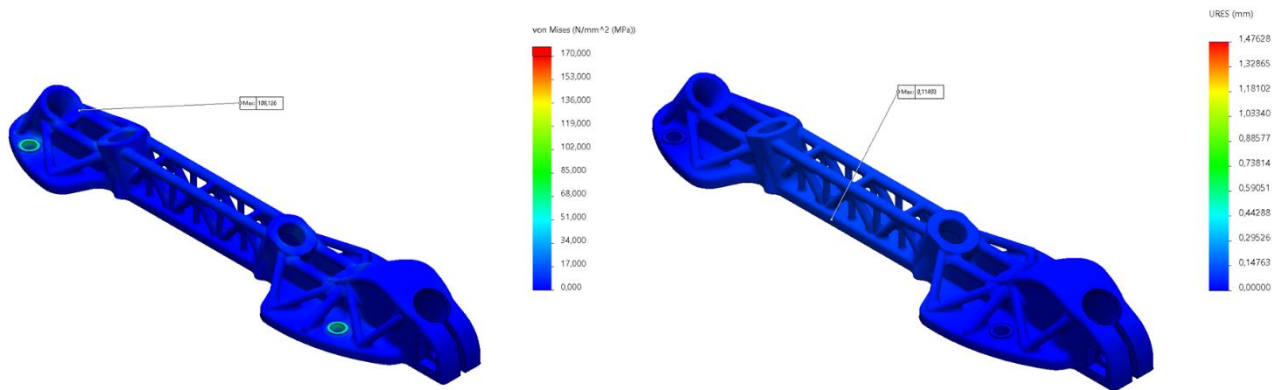


Figure 4.17. FIT static numerical study: Equivalent von Mises stress (left) and resultant displacement (right) plot; CFRP.

Lastly, the resin model encounters the same problem as the ABS one despite the slightly higher tensile strength (Figure 4.18). It was also thought it would result in plastic deformation. In the experimental testing it will be verified that was not the case. The displacement is according to expected. Higher than the ABS model due to the lower modulus of elasticity.

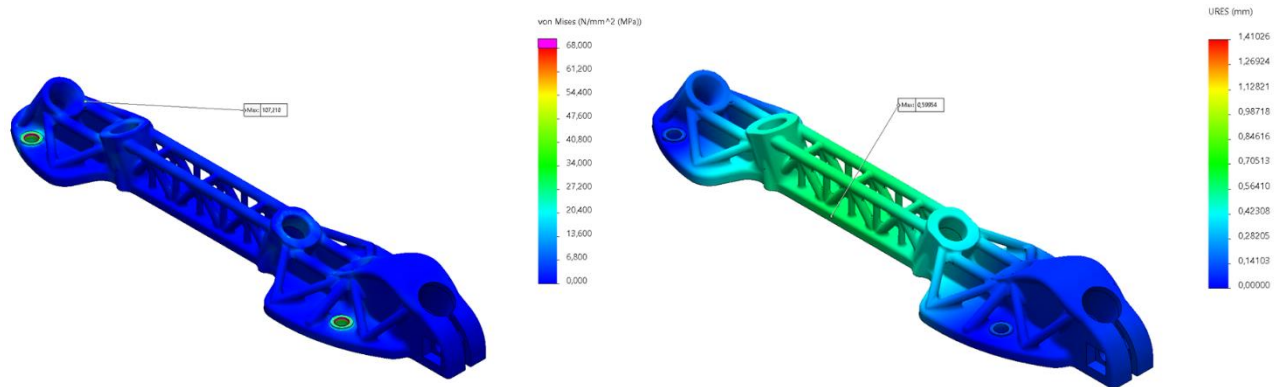


Figure 4.18. FIT static numerical study: Equivalent von Mises stress (left) and resultant displacement (right) plot; eSun Resin.

The average value of equivalent micro-strain in the strain gauge zone is $296.900 \mu\epsilon$. This value was obtained accordingly with the strategy previously used.

Finally, all the results mentioned in this chapter were deemed sufficient to proceed with the experimental testing.

4.4. Frontal Impact on the brake (FIB)

This study was made accordingly to paragraph 5.3.9 of the standard EN 13899:2003. This test is like the previous test but, this one is with the braking device assembled. There must be no damage to the roller skate. It is also to test the sturdiness of the platform's braking zone. This is a zone of high stress, as stated previously, and the standard accounts for that.

The test proceeds with the roller skate going straight ahead against a kerb with a greater height than the one of the braking devices, which is held in a rigid position (Figure 4.19).

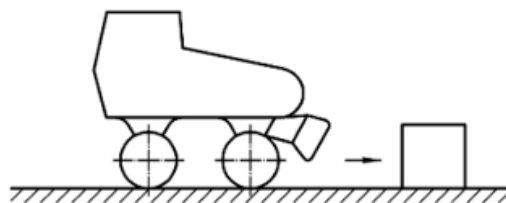


Figure 4.19. Exemplification of the FIB test from the standard 13899:2003.

The standard stipulates the impact should be carried out with an energy of $90 J$ and an impact velocity of $3.5 \pm 0.4 m/s$ for class A roller skates. The maximum velocity is then $3.9 m/s$ in class A. Therefore, this will be the test to be carried out since it is the most demanding scenario.

Since the energy and velocity demands of this study are the same as in the frontal impact on the trucks, the final value of the force is the same as in equation (4.5). It only changes where the force is applied. In this instance, it was opted to exclude the elastomer constituent of the braking device and apply the force on the top surface of the brake screw. The elastomer on the braking device eliminates part of the impact force. Additionally, the material of this elastomer was unknown hence not being possible to conduct the numerical studies with it anyway.

At this stage, the following consideration, which later revealed to be wrong, is the steel tip of the frontend trucks as well as the correspondent casket were included in this study. This because it could influence deformation on that zone. This was to account for the deformation that could occur in the hole where the tip fits into. However, it could not be left “loose”. The tip was fixed on the surfaces where it would contact the remainder of the trucks sub-assembly.

This inference was wrong since the steel tip would constrain the movement of the brake screw. However, this consideration was thought to be correct at the time of the numerical testing. Only in the experimental testing was reevaluated and considered a flawed interpretation.

Furthermore, it was created a **fixture on the cylindrical surface of the brake screw** (surface in blue in Figure 4.20). This was added to stabilize the model. The connection between the brake screw and the brake casket was of contact between the touching surfaces. Because of this, the model was not stabilized, and the brake screw body would have excessive displacement. To combat that, the surface in blue in the figure below was restrained of axial, radial and circumferential translation as well as circumferential rotation. This was an assumption that later revealed to be **flawed**. This diminishes all displacement around the brake screw where it was not supposed.

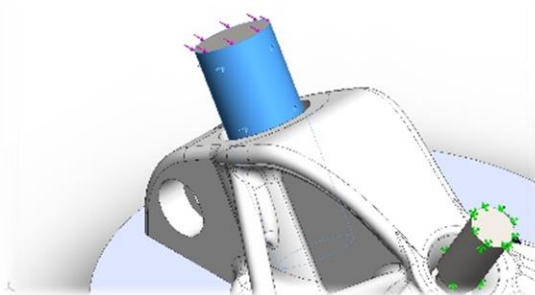


Figure 4.20. The constrain applied in the FIB configuration which later proved to be wrong.

The numerical study was deemed to suffice all criteria. Only after analysing the experimental data and comparing with the numerical data, were these flaws encountered.

The Figure 4.21 depicts the study configuration before and after the corrections.

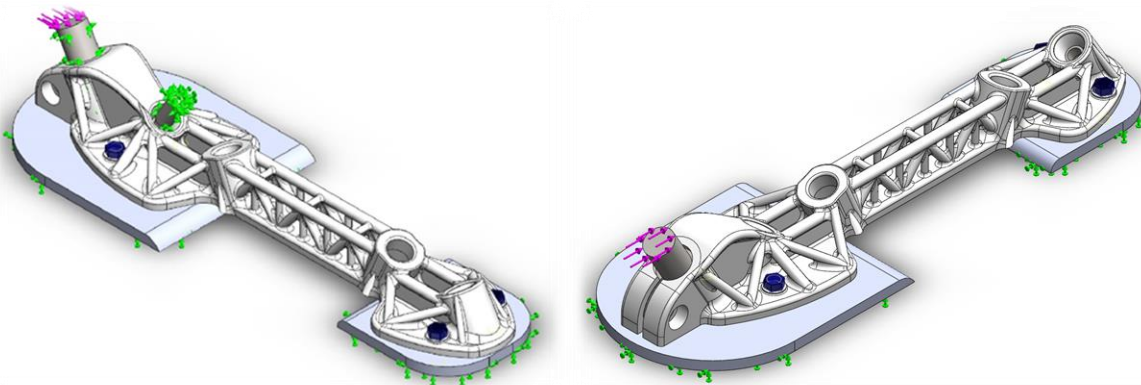


Figure 4.21. Final FIB numerical study configuration: Wrong on the left and corrected on the right; MD1.4.

The **correct** configuration would not include that fixture exemplified in Figure 4.20. Instead, it being a screw and tightened so it is secure, it could be assumed it is **bonded** to the casket. This, considering the touching surfaces are expected to have zero relative displacement to one another. This would make for a correct depiction of reality and would stabilize the numerical model.

The brake screw is a plain cylinder and not a proper screw to simplify calculations. There could be applied a small tightening virtual screw to restrain the brake screw. However, the brake insert (casket) is made of AISI 1020. This fits perfectly within the platform and was considered to hold the brake screw in place. The results proved there was no need for the additional screw.

More details of contacts, fixtures, interactions, and mesh are showcased in Appendix A. Mesh convergence details are in Appendix B.

The following results are the **corrected** ones for comparison with the experimental results. The results that were **flawed** and deemed fit to proceed to the experimental phase are in Appendix C for consulting.

The expected results for displacement coincide with the results obtained in the corrected study (Figure 4.22). The highest resultant displacements are in the brake area, and it bends backwards as it should. Because of the front attachment screws constraining the rest of the structure, the displacements are lower from there to the back.



Figure 4.22. FIB corrected static numerical study: Resultant displacement plot; ABS.

Once more, the contact stress around the virtual attachment screws were considered neglectable for reasons previously stated. The remainder of the platform had extremely low equivalent von Mises stress (Figure 4.23) with the attachment screws as an exception. The maximum stress in these holes does exceed the yield point of ABS but it was thought to

result in plastic deformation at most (contact resultant stress). The zone of the front attachment screws had the most pronounced stress, but still very low.

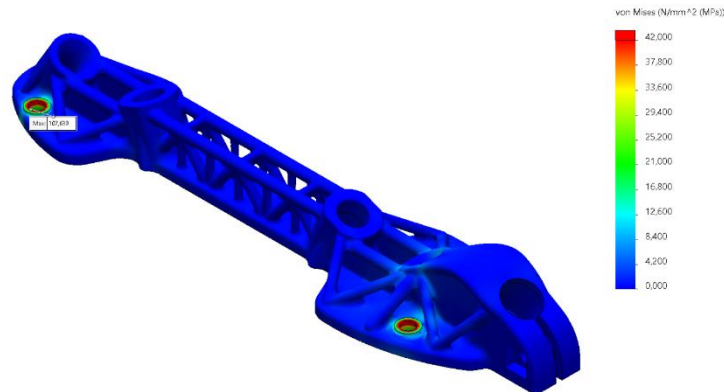


Figure 4.23. FIB (corrected) static numerical study; Equivalent von Mises stress plot; ABS.

The resultant displacement plot (Figure 4.24) attests once more for the improved rigidity the CFRP provides relatively to the other two materials, cementing this model as the performance one. The displacements distribution is symmetric. Regarding the equivalent von Mises stress, it is exceptionally low all over the structure except in the attachment screw holes due to contact stress. However, the maximum value does not exceed the 170 MPa.

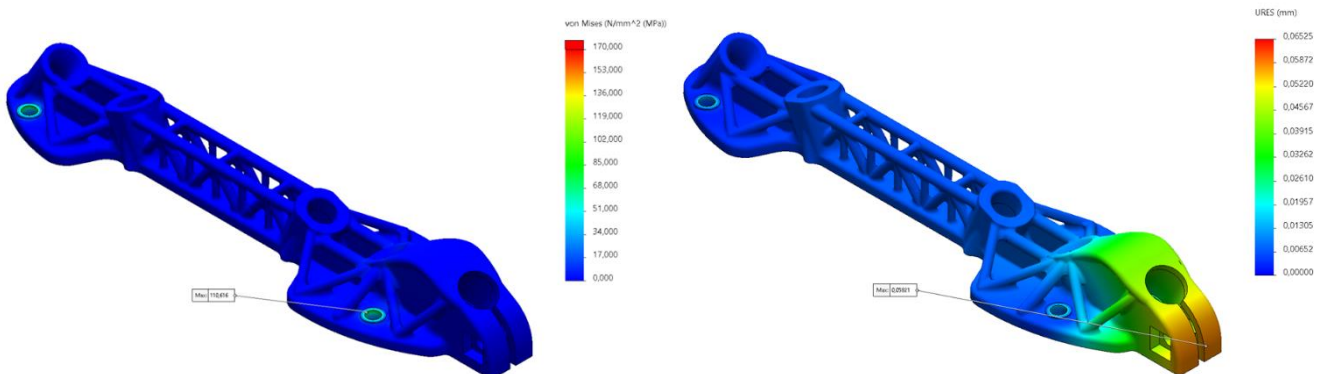


Figure 4.24. FIB (corrected) static numerical study: Equivalent von Mises stress (left) and resultant displacement (right) plot; CFRP.

Finally, the eSun resin option demonstrated results similar to ABS as anticipated. The maximum equivalent von Mises stress plot is like the ABS one (Figure 4.25). The stress around the attachment screw holes was also higher than the yield stress but it was disregarded for the same reasons as the ABS model.

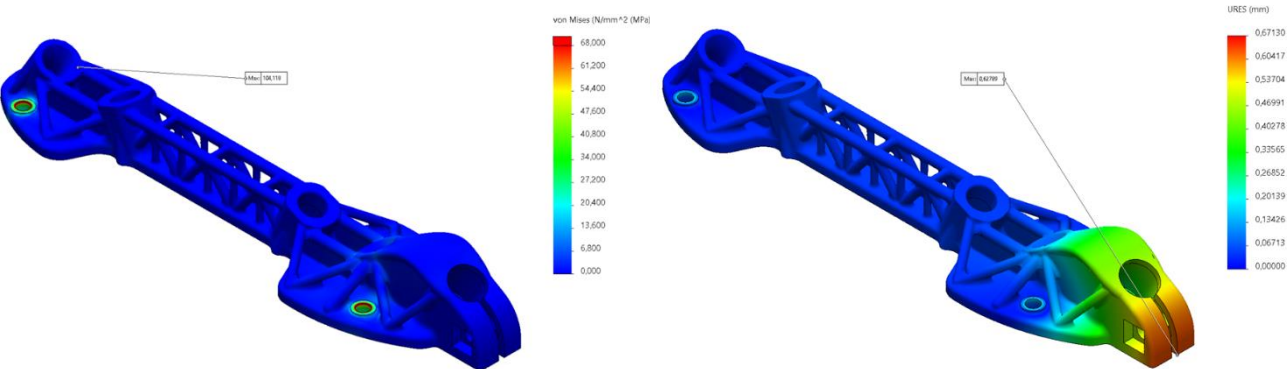


Figure 4.25. FIB (corrected) static numerical study: Equivalent von Mises stress (left) and resultant displacement (right) plot; eSun Resin.

The average value of equivalent micro-strain in the strain gauge area, calculated as for the previous studies, is 193.000 $\mu\epsilon$ (micro-strain).

Lastly, a final prototype had to be produced to confirm experimentally all results exposed in this chapter.

5. EXPERIMENTAL TESTING

The final model had all the correct dimensions. It underwent all numerical studies described in chapter 4 and the structure demonstrated to be capable of enduring all the loading scenarios contemplated. The platform now had to undergo experimental tests to check the accuracy of the numerical studies and how the structure behaves in a real-world scenario.

The experimental studies were done using a strain gauge. This strain gauge measures deformation and sends that signal to a computer which automatically logs the values of strain. The collection of the data was done using the LabVIEW software.

5.1. Prototype

The final prototype was made through SLA from the eSun water-soluble resin which was described *supra*. The prototype, in *Solidworks*®, without the metal inserts, had a **mass of 82.38 g. After fabrication**, the prototype had a mass of **82.79 g**.

In all numerical studies conducted the material was considered isotropic and homogeneous. Both FDM and SLA processes, very simply, make components by binding layers to each other. This might result in an anisotropic behaviour of the structure. Other factors such as humidity (which highly affects polyamide), temperature of filament or room, among others all influence the behaviour of the structure in the different materials considered. Having considered that, the prototype was fabricated through SLA for the reasons stipulated in chapter 2.

The metal inserts had likewise to be manufactured to be inserted into the platform. For polymer made roller skates on the market, the manufacturers put metal inserts in the trucks and brake zones since the platform must withstand severe impact there. These were designed and included in the numerical studies as well as fabricated for the experimental testing.

In Figure 5.1 there is a CAD representation of the inserts fabricated. Two trucks caskets were needed to absorb the impact from the trucks (front and back). The brake casket insert that was supposed to be threaded (M16 fine pitch) on the inside. It does not show in the CAD file but for experimental testing the casket was indeed threaded.

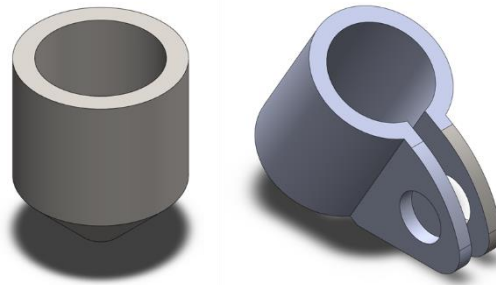


Figure 5.1. CAD of metal inserts: Trucks casket on the left and brake casket on the right.

The inserts were made from stainless steel, but this material was not the most suitable. There could have been developed other inserts with other materials and fabrication processes. However, the focus of this dissertation is only the platform. The material was chosen due to availability at the time and safety concerns. However, these inserts were only to test the platform despite increasing the mass of the roller skate. It exists better caskets with lighter materials that almost do not alter the mass of the roller skate. Those could be used in the future in a commercially ready platform.

Lastly, one of the main objectives was to make the roller skates affordable. Primarily, for children, for which the ABS model is the most suitable.

Considering that in the fabrication:

- It is used Fiberlogy ABS (850 g spool) which is 16.72€ (*Evolt Fiberlogy ABS*, n.d.), or INNOVATEFIL PA CF (500 g spool)(*INNOVATEFIL PA CF*, n.d.) that costs 40.38€.
- It is printed in a Prusa i3 MK3 printer (120 W).
- And the average price per kilowatt hour is 0.13640€ in Portugal in 2023 (*Price KWh EDP, June 2023*, n.d.).

The MD1.4 cost could be deduced as in the following Table 5.1.

Table 5.1. Cost of one MD1.4 platform in ABS and CFRP. (*Evolt Fiberlogy ABS, n.d.; INNOVATEFIL PA CF, n.d.; Price KWh EDP, June 2023, n.d.*)

| | Fiberlogy® ABS (850 g Spool) | INNOVATEFIL PA CF (CFRP) (500 g Spool) |
|---|------------------------------|--|
| Filament price | 16.72€ | 40.38€ |
| Used filament (including supports) according to PrusaSlicer (g) | 416.56 | |
| € per gram | 0.02€ | 0.08€ |
| Full filament price per platform | 8.16€ | 33.64€ |
| Average energy consumption of printer | 120.000 W | |
| Time of print | 15h41m | |
| kWh spent in printing | 7.65 | |
| kWh price in Portugal | 0.14 | |
| Price of printer energy consumption | 1.04€ | |
| Total | 9.21€ | 34.69€ |

It would only cost **9.21€** to fabricate one platform in ABS, without the metal inserts. Still, the metal inserts, if acquired in great quantity are relatively low price. Therefore, this platform would suffice the criteria for a low price. Other comparable roller skates on the market, like the TVD model, are sold with the remainder of the components and the price of those is unknown.

The CFRP price is notably higher, but it is still relatively low price for a performance roller skate platform.

5.2. Placement of the strain gauge

The placement of the strain gauge was of great importance. In all numerical studies, the strain plots were used to choose the place where the strain was stabilized. In other words, the place where the strain gauge is going to be placed must be a surface entirely in either tensile or compressive strain. This was to ensure the data was correct.

Furthermore, it had to be considered that the roller skate would be fully assembled when being tested. This means not all surfaces of the platform can be considered. The zones where the platform would contact the boot were considered impossible to place the strain gauge. If placed either on the front or back, the wires could also interfere with the wheels. Therefore, the middle section was considered ideal. The platform's design also does not allow for many solutions since there were very few flat surfaces to place the strain gauge.

The top of the middle section was selected as seen below and it would be preferably in the centre of the platform.

Though, the strain gauge had to be placed where the strain was stabilized. It had to be in either compression or tension, not in a transition region. Every strain plot (equivalent strain, x axis strain, y axis strain and z axis strain) of each of the four numerical studies were analysed to verify this.

Noticeably, the strain was better stabilized on the backend of the middle section, identified in Figure 5.2 with a red rectangle.

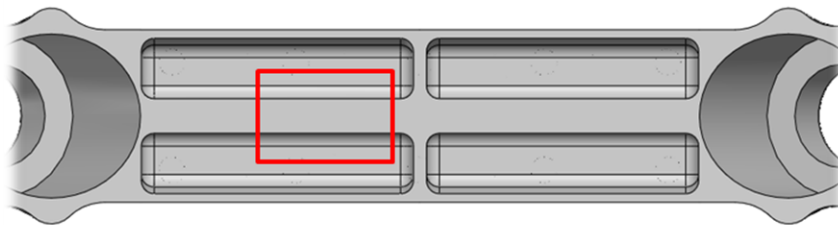


Figure 5.2. Place of choice for the strain gauge.

The strain gauge is unidirectional, but the structure is subjected to multiple direction forces. However, the strain gauge should register the total amount of strain in each area where is mounted, despite a slight loss in accuracy.

The strain gauge chosen was from HBM type 3/350 LY18. However, the strain gauge was wider than the surface selected. This implied there had to be a slight enlargement of that surface to accommodate the strain gauge.

Having the placement chosen and the prototype altered, it was possible to proceed to assembling the strain gauge. The values to be used further in the comparison are the ones from the **equivalent strain plots** from the previous chapter.

The strain gauge leads were not soldered directly to the cables as a precaution. The cables were wrapped around the structure to prevent accidental ripping of the wires, Figure 5.3.

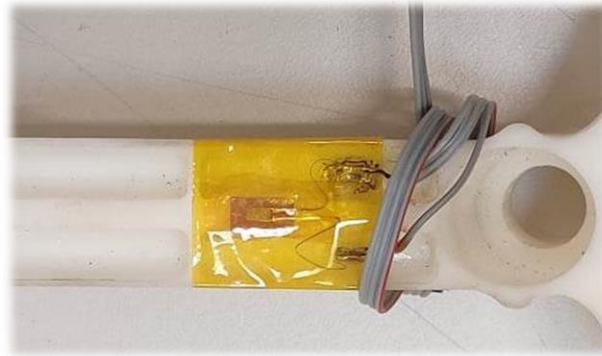


Figure 5.3. Strain gauge assembled with the cabling.

The strain gauge was configured as a **Wheatstone quarter-bridge type I** because only one of the four resistive elements in the bridge is a strain gauge. It measures axial and bending strain (*Types of Strain Gauges*, 2023).

Finally, the strain gauge was assembled and connected to the input module NI-9219 from National Instruments (Figure 5.4). This module is then connected to the computer.

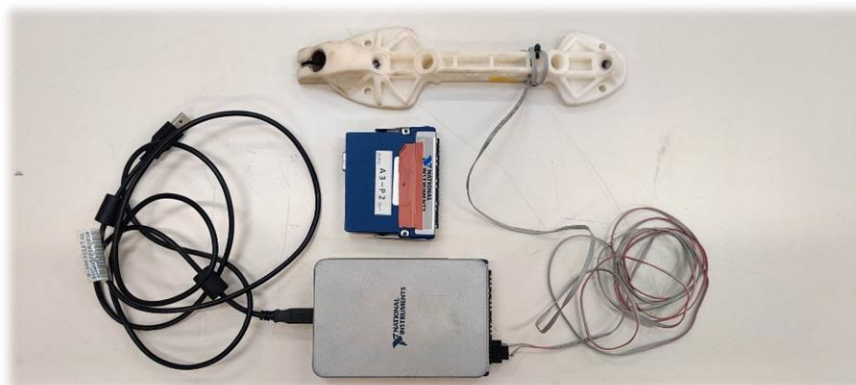


Figure 5.4. Testing platform with all cables and module connected. Final setup minus the PC.

The LabVIEW software was used to read and collect the data from the strain gauge. A program was created which reads the values of strain and records them in an Excel® file. The program is detailed in Appendix D.

All 4 numerical analysis were to be experimentally tested and the results compared to the numerical ones.

5.3. Testing

The experimental tests were conducted in an arena of quad hockey. The materials needed were an instrumented roller skate, numerous tools to adjust and assemble different components, an obstacle which will act as the kerb, tape for constricting the cables coming from the roller skate to the PC, a backpack for keeping the PC during testing, a chronometer, a scale for acquiring the mass of the athlete and a PC.

Firstly, the testing session began with the weighing of the athlete with no shoes. The athlete had a mass of 104.100 *kg*. Then, the athlete had to put on the roller skate which was already assembled. The cables had to be carefully handled and attached to the athlete's body using the tape. It was only necessary to put on one roller skate since he had to support all his weight on the single roller skate being evaluated. It also leaves the other foot free for the athlete to support himself in an emergency (Figure 5.5).

After preparing the athlete, the arena had to be prepared as well. The obstacle was placed against the barrier of the arena. Then, a mark with tape was made 5 meters away from the obstacle in a straight line. This mark was for the athlete to start in the frontal impact tests.

A test run was made before start recording data to check if everything was according to plan.



Figure 5.5. Final testing setup on the athlete; Roller skate platform without the braking device.

5.3.1. Weight test

The weight test consisted of the athlete standing still with all his weight on the roller skate, as explained previously.

Before initiating each of the tests the strain gauge was calibrated. Then, the program was initiated. This is done with the roller skate in the air. Only after starting the program and waiting 10 seconds will the athlete support his weight on the roller skate. That position must then be held for at least 15 seconds. The program is terminated, and the data is saved in an Excel® file. This protocol is repeated **5 times** to check for repeatability.

In the LabVIEW program the frequency chosen was 2 Hz and the number of samples was 10. It was used the *High-Resolution* mode of the module because it was a static test.

The 5 different graphs obtained of the 5 tests are in Appendix D for consultation.

The average was calculated in each test for the values of strain **when the athlete had the foot on the ground** (Table 5.2).

Table 5.2. Weight average and standard deviation of micro-strain for each test run.

| Test | Average ($\mu\epsilon$) | Standard deviation ($\mu\epsilon$) |
|------|---------------------------|--------------------------------------|
| 1 | 713.256 | 15.586 |
| 2 | 647.804 | 55.588 |
| 3 | 680.466 | 109.062 |
| 4 | 657.952 | 40.924 |
| 5 | 690.525 | 68.309 |

These values seemed consistent. An average of these 5 micro-strain values was then obtained: **$678.000\ \mu\epsilon$** . This is considered the average value of micro-strain in the zone of the strain gauge. Moreover, the standard deviation was $26.075\ \mu\epsilon$.

According to Newton's second law, when the weight is the only force, since the athlete is static, the force exerted on the roller skate is:

$$F = m \times g = 104.100 \times 10.000 = 1041.000\text{ N}. \quad (5.1)$$

In the numerical study, the force applied was **1000.000 N** and the strain obtained in the gauge placement was **$600.000\ \mu\epsilon$** . It is assumed the structure is within the limits of elasticity, therefore having a linear relation. So, it is possible to obtain the numerical value of strain for the force of **1041.000 N** .

The same applies to the experimental results. Knowing the strain value obtained from the gauge and the force exerted by the athlete we obtain a linear relation, also assuming the structure is within the limits of elasticity. From this relation it can be calculated the equivalent value of strain for 1000.000 *N*.

Table 5.3. Experimental and numerical results obtained and expected strain.

| Force (N) | Micro-Strain (Experimental) | Micro-Strain (Numerical) | Standard deviation ($\mu\epsilon$) |
|-----------|-----------------------------|--------------------------|--------------------------------------|
| 1000.000 | 663.912 | 600.000 | 45.192 |
| 1041.000 | 678.000 | 624.600 | 37.760 |

The error between the numerical and experimental values is:

$$\frac{\mu\epsilon_{experimental} - \mu\epsilon_{numerical}}{\mu\epsilon_{numerical}} = \frac{678.000 - 624.600}{624.600} = 8.550\%. \quad (5.2)$$

The error might be due to some simplifications made in the numerical studies such as the sole of the boot being infinitely rigid, the use of virtual screws, and the difference in the materials the actual manufacturer used for the remaining components of the roller skate. Additionally, the experimental results are higher than the numerical ones. However, given the error is approximately 8.550%, it is not so significant and can be accounted for in the future.

5.3.2. Frontal impact on the brake

These frontal impact experimental tests were conducted with the breaking device assembled. The test was repeated **3 times**. The strain gauge was calibrated with the roller skate suspended (not touching the ground). The program was then started, and the PC placed inside the backpack. The athlete had to go to the 5-meter mark mentioned before and, from a standing still position provide an impulse with the other foot, so it initiates a straight movement towards the barrier of the arena. The time the athlete took from standing still position to the instant of impact was noted with the assist of a chronometer.

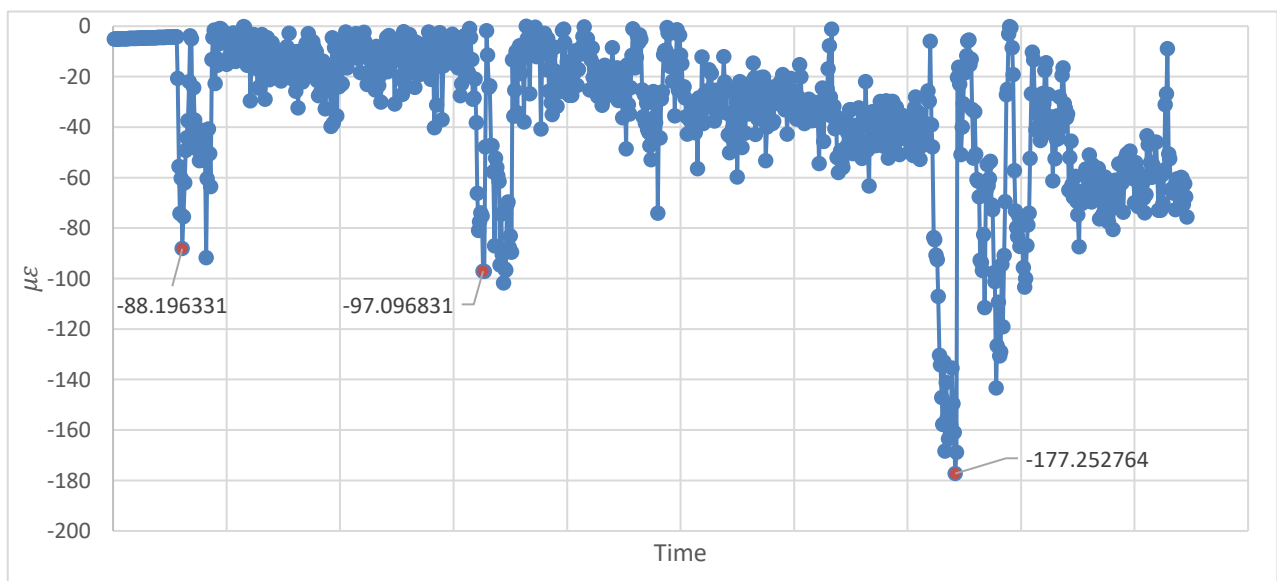
The PC was kept in the backpack for the 3 tests. This implies the gauge could provide more despair results. The value of strain could diverge further from zero, when the roller skate is suspended (zero position) after an impact. However, through the intervals given between tests, is possible to assess the average value of strain measured with the roller skate suspended and account for that difference, subtracting the average from the strain registered.

The tests were filmed so they could be more thoroughly inspected later.

For this test some alterations had to be made to the program used in the weight test. Because the moment of impact is instantaneous, a *High-speed* mode (60 Hz) was utilized. This, because the frequency had to be higher to detect the instant of impact. Moreover, the number of samples was altered to 480. More on the specifications of the program utilized in Appendix D.

In LabVIEW, a function to detect and register the minimum values of strain was added to the program. It was the minimum, not the maximum because after consulting the numerical strain results, the strain gauge should be under compression during the instant of impact (should provide negative values).

The following graph shows the data collected on the frontal impact on the brake. The results clearly indicate 3 moments where an abrupt deviation from zero occurs. Those represent the 3 repetitions. In every test it is observable there are multiple points where the impact supposedly happens. This is due to the “kerb” (in this case a wooden obstacle) not being adequately fixed since it was impossible to do so. Also, the athlete would move after impact, and more contact with the roller skate could have caused these points to appear. However, the first point of each test is considered the instant of impact. These are identified in red in the Graph 5.1.



Graph 5.1 Experimental values obtained from the strain gauge for the FIB test.

The **force of impact** was then calculated for each test. This was necessary to evaluate if the results were consistent. To obtain the force of impact, there were several assumptions made. First, it was assumed the athlete’s velocity in the first instant of each test was **zero**, and it would have a linear behaviour. Also, the acceleration is assumed to be constant. Since it is such a small period, this assumption can be made safely.

Therefore, the medium velocity (v_m) can be calculated since the time between start and impact (Δt) was recorded, and the distance was predefined ($\Delta x = 5\text{ m}$).

$$v_m = \frac{\Delta x}{\Delta t}. \tag{5.3}$$

Knowing the value of the medium velocity, it is possible to calculate the final velocity (v_f), which is the **velocity of impact**, if the initial velocity (v_i) is known as well. The initial velocity, as stated before, is equal to zero.

$$v_m = \frac{v_f - v_i}{2}. \tag{5.4}$$

At last, the **constant acceleration** can be calculated.

$$a = \frac{v_f - v_i}{\Delta t}. \tag{5.5}$$

Therefore, both velocity values (final and initial) are known, and the period was recorded during testing.

Finally, the force of impact can be obtained (Table 5.4) according to Newton’s second law ($F = m \times a$). The mass was the athlete’s, which was also recorded in the beginning.

Table 5.4. Time recorded during testing and velocities, acceleration, and force of impact calculated values.

| | Test 1 | Test 2 | Test 3 | Average | Standard deviation |
|----------------------------|--------|---------|---------|---------|--------------------|
| t (s) | 3.410 | 2.410 | 2.420 | 2.747 | 0.574 |
| v_m (m/s) | 1.466 | 2.075 | 2.066 | 1.869 | 0.349 |
| v_f (m/s) | 2.933 | 4.149 | 4.132 | 3.738 | 0.698 |
| a (m/s²) | 0.860 | 1.722 | 1.708 | 1.430 | 0.493 |
| F (N) | 89.525 | 179.232 | 177.754 | 148.837 | 51.371 |

The force of impact of each test can now be compared with the strain values from the experimental testing and with the strain values that had the residual strain subtracted (Table 5.5).

Table 5.5. Comparison between the force and strain obtained experimentally (with or without the residual strain) and numerically estimation for FIB.

| | Force (N) | Micro-strain (with residual strain) | Micro-strain (without residual strain) |
|---------------------------|-----------|-------------------------------------|--|
| Test 1 | 89.525 | -88.196 | -88.196 |
| Test 2 | 179.232 | -97.097 | -83.924 |
| Test 3 | 177.754 | -177.253 | -148.707 |
| Average | 148.837 | -120.849 | -106.942 |
| Standard deviation | 51.371 | 49.050 | 36.232 |
| Numerical | 118.300 | N.A. | -116.545 |

It is noticeable that the second test, despite having a force of impact closer to test 3, recorded an exceptionally low strain value for that force. The strain value for the second test should be higher than in test 3, but it is closer to the strain value of test 1. This is not consistent with the other two tests. It could be caused by the strain gauge not being calibrated before test 2 and 3, or from residual or permanent strain. Nevertheless, **test 2 was disregarded.**

Then, the expected value of strain, considering only the experimental results from tests 1 and 3, for the force applied in the numerical study, was calculated considering the structure is within the linear-elastic dominium (value also presented in the table above in the “Numerical” line).

The fact that the obstacle representing the kerb in both impact tests was not held rigidly could have had an influence. However, it is believed it did not have a significant effect. Nevertheless, it was considered the very first moment of impact as the result value to decrease its influence. Moreover, in the videos, it could be seen that the “kerb” did not move in that first moment of impact. However, it could have contributed to the inconsistent results, namely the second attempt at the FIB test, which was disregarded.

In the FIB test, at the instant of impact, the roller skate was subjected to the athlete’s weight plus the impact force. The numerical study did not account for the weight of the athlete. Ideally, the total strain should be the sum of the strain from the weight and the impact. The strain resulting from the athlete’s weight should be deducted from the total recorded strain so it could be obtained **only** the strain regarding the impact. However, after carefully analysing the video recordings, it could be inferred that such a deduction was

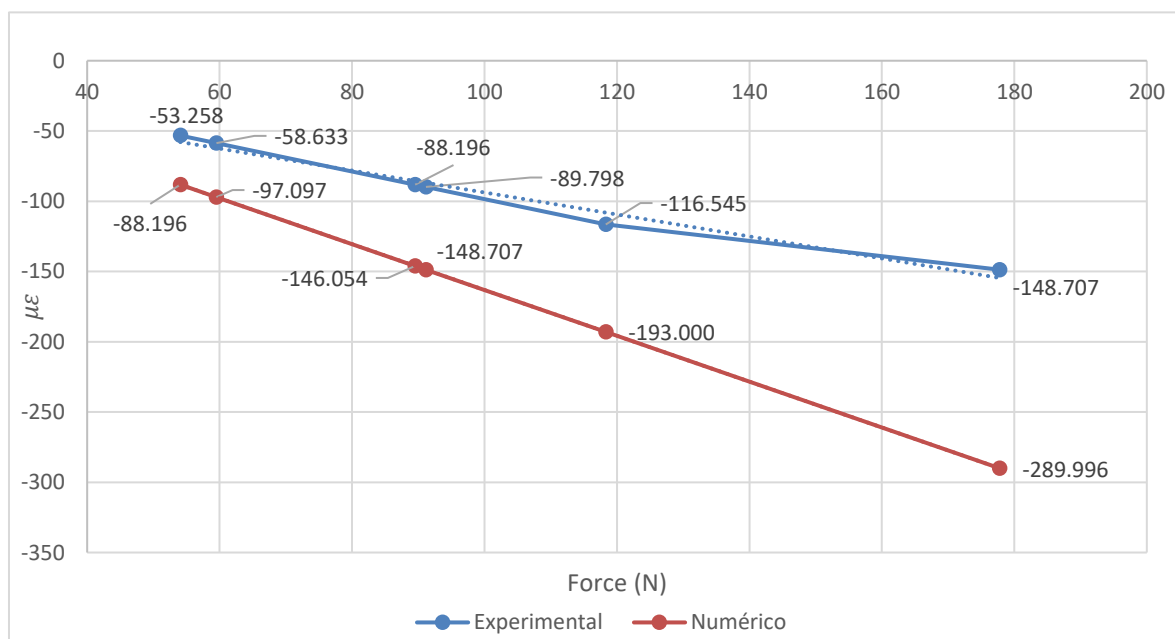
unnecessary and likely wrong. This is because the athlete unconsciously held on to the barriers just before impact to protect himself. This led to believe that the athlete, in an attempt to not get hurt, supported most of his weight on the barrier. Therefore, the results obtained experimentally are influenced by the frontal impact alone.

This test's static numerical study provided a strain value for the force applied on the brake screw (118.300 N). Considering the structure is within linear-elastic dominium, the strain and the force are linearly proportional. Therefore, the expected force values for the strains obtained experimentally can be calculated according to the numerical model.

Table 5.6. Estimated experimental micro-strain values from forces calculated from the numerical relation.

| | Force (N) | Micro-strain ($\mu\epsilon$) |
|---------------------------|-----------|--------------------------------|
| Test 1 | 54.004 | -53.258 |
| Test 2 | 59.454 | -58.633 |
| Test 3 | 91.150 | -89.798 |
| Average | 68.203 | -67.230 |
| Standard deviation | 20.059 | 19.729 |
| Numerical | 118.300 | -193.000 |

These values in Table 5.5 and Table 5.6 provide a basis for comparing the numerical results with the experimental ones, as exhibited in the Graph 5.2.



Graph 5.2 Graphical comparison between the experimental and numerical results of FIB test.

From the data in the Graph 5.2 it can be observed that, if the numerical results (red line) of this test indicate the model endures the impact, experimentally (blue line), the strain and stress values will be lower than the numerical ones and the prototype will also endure the impact. Thus, the numerical study proved conservative. The experimental results exhibited less strain than the numerical results indicated.

The error is more significant than in the previous study:

$$error = \left| \frac{\mu\varepsilon_{experimental} - \mu\varepsilon_{numerical}}{\mu\varepsilon_{numerical}} \right| = \left| \frac{-116.545 - (-193.000)}{-193.000} \right| = 39.614 \%. \quad (5.6)$$

This might be due to the various assumptions during calculations and the simplifications done on the numerical model. Such simplifications as applying the force directly on the brake screw also contribute to increase the error, but also, in this instance, to increase safety.

Moreover, the fact that the athlete held on to the barrier and the simplification of discarding the weight input might have influenced the error enormously.

5.3.3. Frontal impact on the truck

The frontal impact experimental tests, both on the brake and the trucks, were similar, only differing on one component of the roller skate. The impact against the brake was done with the braking device assembled, and the impact on the front truck was only possible with the removal of the braking device - the standard EN 13899:2003 accounts for sports where the braking device is not needed or used. Otherwise, the testing was set up precisely as the FIB testing and with the same LabVIEW program.

When preparing for the test initiation, after removing the braking device, the athlete made a trial run. It was verified that the obstacle used had to be taller (in Figure 5.5 it is noticeable that the trucks do not touch the obstacle). A taller obstacle, made from wood as well, was exchanged for this test.

When checking the obstacle, the athlete kicked the obstacle with the roller skate, and there was a slight cracking noise. However, the athlete immediately proceeded skating towards the 5-meter mark, and all seemed normal. Therefore, the noise was disregarded. Surprisingly, when the athlete was pressing the roller skate against the floor to gain impulse for the start of the first test run, the roller skate fractured. The resin from which the platform was fabricated revealed a **brittle** behaviour, scattering on the floor (Figure 5.6).



Figure 5.6. Roller skate after failure and the removal of the boot by the athlete.

Unfortunately, more tests could not be done, so the strain gauge data for the FIT test does not exist.

The roller skate platform did fracture during testing with regular use. The stress around the screw holes which attach the platform to the boot might have been the cause. In the equivalent von Mises stress plot in chapter 4.3, the maximum stress is around those holes, which was above the material's yield strength. However, it was considered neglectable because it could be due to the FEA method, or it could only cause plastic deformation. Nevertheless, the experimental results revealed that due to the **brittle** nature of the material used, the stress led to mechanical fracture.

The CFRP model had a higher yield strength, which would not represent a problem, and the ABS model is not as brittle as the eSun resin. Nonetheless, the concentrated stress around the attachment screw holes must be addressed.

There was insufficient data acquired to take any further inferences from the FIT experimental tests.

6. RESULTS DISCUSSION

The numerical results indicated that the platform design MD1.4 could endure all experimental tests.

Regarding the weight test, the MD1.4 model had a maximum equivalent von Mises stress lower than the yield strength of all 3 materials. Therefore, the numerical and experimental results attest to the platform's eligibility regarding the weight capabilities for class A.

The attachment test was to be performed after the tests in the arena. Although, since the platform incurred in failure, it was not feasible. This numerical model is similar to the weight numerical model. Also, according to the standard, the test is quasi-static. This leads to believe that the numerical results are correct. It would mean the resin and CFRP models would pass the test successfully. The ABS model has a slightly lower yield strength than the maximum equivalent von Mises stress on the plot (54.343 MPa). However, the difference is relatively small, and some plastic deformation could occur. This maximum value is also around the screw holes which attach to the sole of the boot. It was already believed there should be added material there to diminish the maximum stress, and it could address any doubt regarding the eligibility of the ABS model.

The FIT numerical testing revealed that the CFRP model could endure any impact due to its higher tensile strength. However, the resin and ABS models have a lower tensile strength than the maximum equivalent von Mises stress obtained. It was reasoned it would result in plastic deformation at most, but the experimental testing demonstrated that the resin model failed. This might not reflect in the ABS model, but still, the maximum stress had to be lowered. These stresses, once more, would only occur on the screw holes for the attachment of the platform to the sole of the boot.

At last, the FIB testing unrolled as expected. Therefore, the platform was thought to be capable of enduring these impacts, and the experimental results proved it. Interestingly, the maximum equivalent von Mises stress (from FIB numerical study) was also **higher** than the tensile strength for ABS and the eSun resin. As in the FIT numerical studies, these stresses were located around the 4 attachment screw holes. On the other hand, the roller skate performed 4 impact tests (1 test run and 3 serious runs), and the platform did **not** fracture.

This signifies that the assumptions previously made about the stress concentration on the screw holes were correct, at least concerning the FIB test.

The numerical and experimental results indicate an inconsistency in the attachment screw holes. The linear static analysis is not the most indicated for this issue. This type of analysis does not account, for instance, for stress distribution and the material behaviour after the yield stress point. A non-linear method would be more indicated to address this phenomena. The FIB numerical testing revealed a higher stress value than the yield value but did **not fail** experimentally. On the FIT testing, the numerical results indicated the same, but **it failed**.

It is important to denote that the athlete's feedback was taken seriously throughout the experimental testing. During the experimental weight testing, the athlete suggested the roller skate was very unstable. When trying to stand still, the foot would repeatedly wobble sideways. It demanded more effort from the toes to try to keep it still. During the transition from MD1.3 to MD1.4, the structure was hollowed, reducing the contact area with the boot's sole surface. Reinforcements, as described previously, were added, and contributed to increasing the platform's area of contact with the boot's sole. It helped to decrease the stress and displacements but, unintentionally, it also decreased stability. The removal of material in this process took away some functionality from other structure features created precisely to improve stability and control. The reinforcements in Figure 3.11 and Figure 3.12 were now not in contact with the boot's sole. Moreover, in the article from Olmi (2015), in the points where he considers the weight of the athlete is applied, there was material removed. This results in not enough contact established with the sole. The improvement in mass from MD1.3 to MD1.4 immensely affected the control over the roller skate.

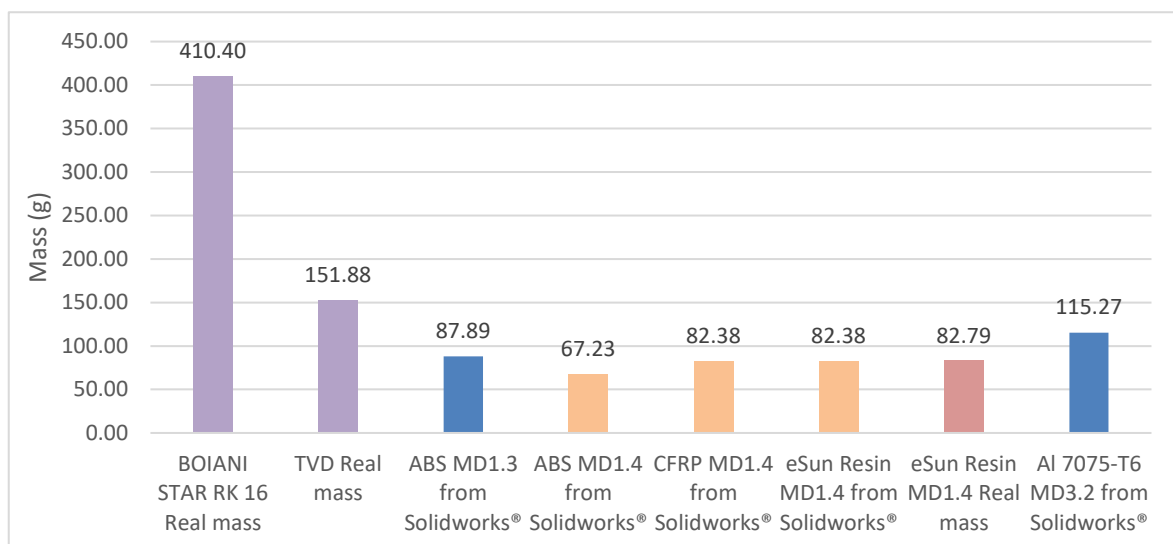
Additionally, there were some marks on the sole of the boot that was a result of concentrated forces on specific zones. All the zones where the sole had contact with the platform were slightly deformed after the experimental testing, which was quite a short amount of time compared to game time. This demonstrates the lack of surface contact between the platform and the sole due to the hollowing of the platform. It focused too much on some regions of the boot's sole.

Concentrated stress and balance problems could be addressed by creating a pattern on the bottom, with crossed beams, or adding material where the stress demanded it. These would result in a more even distribution of loads. It could also diminish the stress in the

attachment screw holes and eliminate the problem of brittle fracture encountered in the experimental testing. The points where the foot naturally applies the body's weight had to have material reintroduced. This would resolve the balance problem described by the athlete.

Model MD1.3 could possibly resolve all these problems. There is still a significant diminishing of mass relatively to the TVD model. This would be a more robust option as well as more manoeuvrable for the athlete. However, with an improvement of the MD1.4 there could be achieved an optimal solution in between. It could be a good compromise.

Ultimately, mass reduction was one of the main goals of this dissertation. In Graph 6.1, there is a mass comparison between the models in existence on the market and the developed ones in this work.



Graph 6.1. Mass of the different models studied.

It is to be considered that the eSun resin MD1.4 real mass does not include the mass of the metal inserts. This way it can be compared with the value calculated by *Solidworks*®. The difference between the two is minor. However, the metal inserts would increase the mass marginally. When compared with existing models on the market (in purple in Graph 6.1), mass reduction is still very pronounced. The MD1.4 in CFRP and resin benefited from the hollowing of the structure to reduce the mass, almost equalling the mass of ABS-made MD1.3 before the hollowing of the structure. This is due to their superior density compared to ABS.

Lastly, the aluminium model (MD3.2) had a far inferior mass than the Boiani model. It even had a lower mass than the TVD model.

7. CONCLUSIONS

The mass reduction was achieved successfully with a **reduction of 55.73%** of mass from the ABS MD1.4 model relative to the TVD model. Furthermore, the standard requirements within the scope of this dissertation were fulfilled. Despite the MD1.4 model not being fully functional, with some minor modifications described in the previous chapter, that could be achieved. Moreover, numerical configurations to test and develop other models in the future were established.

Contrary to the existing models on the market, the models conceived in this work are significantly cheaper to manufacture in the right conditions, in a low to medium volume.

Additionally, these models were primarily intended for children. Therefore, children can use a proper roller skate from the first contact with the sport without the need to have sizeable chunky roller skates with straps. It would make for a more enjoyable experience.

Children could use both the ABS and the CFRP models. However, the ABS one would have a lower price. Having the concentrated stress and the balance of the roller skate refined, it would make for an excellent option for beginners.

Despite being more expensive, the CFRP option would be more suitable for an adult where the product's lifespan is more extensive because the feet have stopped growing. This model was verified numerically in all studies conducted in this work. However, despite the only issue needing to be fixed is the balance of the roller skate, the concentrated stress could be addressed as in the ABS model to increase the safety factor.

These two remaining problems could be resolved with the changes described in the previous chapter.

Ultimately, the aluminium model showed immense promise with a lightweight structure while being significantly stiffer than its polymer counterparts. Its only downside is the price of metal additive manufacturing. However, it demonstrates the real benefits of additive manufacturing. The freedom AM gives when designing allows for a significant improvement in mass reduction while maintaining its capabilities. In a future where metal additive manufacturing is low-price, it would outperform every other option.

In the future, these concepts could be refined and retested. An impact analysis of when the athlete jumps in figure skating could also be considered for these structures. Furthermore, some other impact tests in the standard made with impact test machines could be carried out.

Finally, a fatigue analysis of the platform is worth considering thus, testing the longevity of the AM fabricated structures.

REFERENCES

- Ashby, M., & Jones, D. (1996), “Engineering Materials 1: An introduction to their properties & applications”, Second Edition ed., Volume 1.
- Conner, B. P., Manogharan, G. P., Martof, A. N., Rodomsky, L. M., Rodomsky, C. M., Jordan, D. C., & Limperos, J. W. (2014), “Making sense of 3-D printing: Creating a map of additive manufacturing products and services”, *Additive Manufacturing*, 1–4, 64–76, <https://doi.org/10.1016/J.ADDMA.2014.08.005>.
- EN 13899:2003 (2003). “Roller skate equipment – Roller skates – Safety requirements and test methods”, Slovenian standard. Slovenia.
- eSUN LCD Water Washable Resin 0.5KG – eSUN Official Store (n.d.), Retrieved 16 June 2023, from <https://esun3dstore.com/collections/water-washable-resin/products/esun-lcd-uv-405nm-water-washable-resin-rapid-3d-printer-resin-for-photon-curing-lcd-3d-printer-photopolymer-liquid-3d-resin-500g>.
- evolt Fiberlogy ABS. (n.d.), Retrieved 8 June 2023, from <https://evolt.pt/produto/abs-850g-beige-fiberlogy/>.
- Farah, S., Anderson, D., Langer, R. (2016), “Physical and mechanical properties of PLA, and their functions in widespread applications – A comprehensive review”, *Advanced Drug Delivery Reviews*, 107, 367-392, <https://doi.org/10.1016/J.ADDR.2016.06.012>.
- Fuentes, Aleix Sicília (2018), “Millora mecànica de la platina i l'eix d'uns patins d'hoquei”, Master's dissertation, Escola d'Enginyeria de Barcelona Est, Universitat Politècnica de Catalunya.
- INNOVATEFIL PA CF. (n.d.), Retrieved 1 June 2023, from <https://evolt.pt/produto/innovatefil-pa-cf-m-500g-nylon-fibras-de-carbono-preto-smart-materials-3d/>.
- Journal O Jogo (19/11/2021), “Hockey in European competitions”, Retrieved 2 June 2023, from <https://www.ojogo.pt/modalidades/hoqueiempatins/noticias/europeu-de-hoquei-em-patins-resultados-classificacao-e-proximas-jornadas-14324510.html>.
- Neto, M., Amaro, A., Roseiro, L., Cirne, J., & Leal, R. (2015), “Engineering Computation of Structures: The Finite Element Method”, Cham: Springer International Publishing.
- Olmi, G. (2015), “Failure of the chassis of roller skates for agonistic figure skating”, *Case Studies in Engineering Failure Analysis*, 3, 62–67, <https://doi.org/10.1016/J.CSEFA.2014.08.002>.
- Praveena, B., Lokesh, N., Buradi, A., Santhosh, N., Praveena, B., Vignesh, R. (2022), “A comprehensive review of emerging additive manufacturing (3D printing technology): Methods, materials, applications, challenges, trends and future potencial”, *Materials Today: Proceedings*, 52, 1309-1313, <https://doi.org/10.1016/J.MATPR.2021.11.059>.

- Price kWh EDP (2023), Retrieved 8 June 2023, from <https://lojaluz.com/fornecedores/edp/tarifas/preco-kwh>.
- Sousa, Emanuel S. (2012), “Validação Estrutural de um Novo Conceito de Base de Patim para Iniciação à Patinagem”, Master’s dissertation, Faculdade de Engenharia da Universidade do Porto, Universidade do Porto.
- Tao, W., & Leu, M. (2016), “Design of lattice structure for additive manufacturing”, 325–332, <https://doi.org/10.1109/ISFA.2016.7790182>.
- Types of strain gauges, Retrieved 18 June 2023, from <https://www.ni.com/pt-pt/shop/data-acquisition/sensor-fundamentals/measuring-strain-with-strain-gages.html>.

APPENDIX A

As a result of the extensiveness of the information, in the next tables there is information relating the connections, interactions and fixtures for each of the four different numerical studies. In the FIB numerical study there was an alteration to correct one of the fixtures. That change was described in chapter 4.4. In the following tables that change is not yet made. It was to show the numerical study carried prior to the experimental testing.

Table A.1. Study and mesh properties for all static numerical studies.

| | |
|---|---|
| Analysis type | Static |
| Mesh type | Mixed Mesh |
| Jacobian points for High quality mesh | 16 Points |
| Mesher Used: | Curvature-based mesh |
| Jacobian check for shell | On |
| Mesh Quality | High |
| Thermal Effect: | On |
| Thermal option | Include temperature loads |
| Zero strain temperature | 298 Kelvin |
| Include fluid pressure effects from SOLIDWORKS Flow Simulation | Off |
| Solver type | Large Problem Direct Sparse (weight and attachment) and Automatic (FIT and FIB) |
| Inplane Effect: | Off |
| Soft Spring: | Off |
| Inertial Relief: | Off |
| Incompatible bonding options | Automatic |
| Large displacement | Off |
| Compute free body forces | Off |
| Friction | Off |
| Use Adaptive Method: | Off |

Table A.2. Fixtures; Weight static numerical study.

| Fixture name | Fixture Image | Fixture Details |
|-------------------|---|---|
| Fixed-2 |  | Entities: 2 face(s) Type: Fixed Geometry |
| On Flat Faces-1 |  | Entities: 2 face(s) Type: On Flat Faces Translation: 0; 0; --- Rotation: ---; ---; --- Units: mm; rad |
| Virtual wall-2233 |  | Type: Virtual wall Entities: 1 face(s), 1 plane(s) Wall Type: Rigid |
| Virtual wall-2235 |  | Type: Virtual wall Entities: 1 face(s), 1 plane(s) Wall Type: Rigid |
| Virtual wall-2236 |  | Type: Virtual wall Entities: 1 face(s), 1 plane(s) Wall Type: Rigid |
| Virtual wall-2237 |  | Type: Virtual wall Entities: 1 face(s), 1 plane(s) Wall Type: Rigid |
| Virtual wall-2238 |  | Type: Virtual wall Entities: 1 face(s), 1 plane(s) Wall Type: Rigid |

| | | | |
|-------------------|---|----------------------------------|--|
| Virtual wall-2239 |  | Type: Entities: Wall Type: | Virtual wall 1 face(s), 1 plane(s) Rigid |
| Virtual wall-2242 |  | Type: Entities: Wall Type: | Virtual wall 1 face(s), 1 plane(s) Rigid |
| Virtual wall-2243 |  | Type: Entities: Wall Type: | Virtual wall 1 face(s), 1 plane(s) Rigid |
| Virtual wall-2244 |  | Type: Entities: Wall Type: | Virtual wall 1 face(s), 1 plane(s) Rigid |
| Virtual wall-2246 |  | Type: Entities: Wall Type: | Virtual wall 1 face(s), 1 plane(s) Rigid |

Table A.3. Loads; Weight static numerical study.

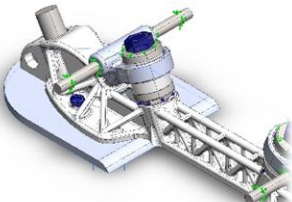
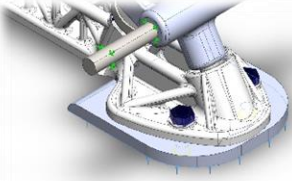
| Load name | Load Image | Load Details | |
|-----------|---|------------------------------|--|
| Force-1 |  | Entities: Type: Value: | 1 face(s) Apply normal force 666.000 N |
| Force-2 |  | Entities: Type: Value: | 1 face(s) Apply normal force 333.000 N |

Table A.4. Rigid Connectors for weight, attachment, and FIT static numerical studies.

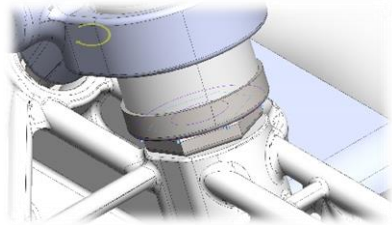
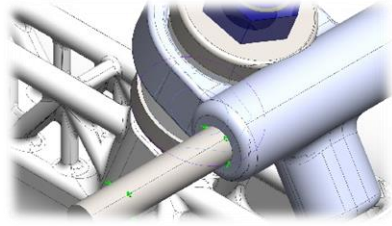
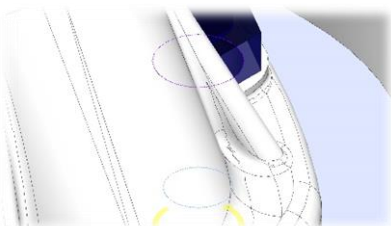
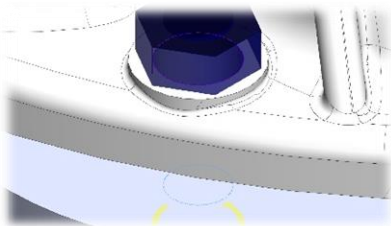
| Connector Name | Connector Details | Connector Image |
|-------------------|------------------------------------|---|
| Rigid Connector-1 | Entities: 2 face(s) Type: Rigid |  Rigid Connector-1 |
| Rigid Connector-2 | Entities: 2 face(s) Type: Rigid |  Rigid Connector-2 |

Table A.5. Bolt connectors for weight, attachment, and FIT static numerical studies.

| Model Reference | Connector Details |
|---|---|
|  Counterbore with Nut-1 | Entities: 2 edge(s) Type: Bolt (Head/Nut diameter) (Counterbore) Connection Type: Distributed Head diameter: 8.000 mm Nut diameter: 8.000 mm Nominal shank diameter: 5.000 mm Material name: Alloy Steel Young's modulus: 2.100e+11 N/m ² Poisson's ratio: 0.280 Preload (Torque): 1.000 N.m Friction Factor (K): 0.200 Tight Fit: No |
|  Counterbore with Nut-2 | Entities: 2 edge(s) Type: Bolt (Head/Nut diameter) (Counterbore) Connection Type: Distributed Head diameter: 8.000 mm Nut diameter: 8.000 mm Nominal shank diameter: 5.000 mm Material name: Alloy Steel Young's modulus: 2.100e+11 N/m ² Poisson's ratio: 0.280 Preload (Torque): 1.000 N.m Friction Factor (K): 0.200 Tight Fit: No |

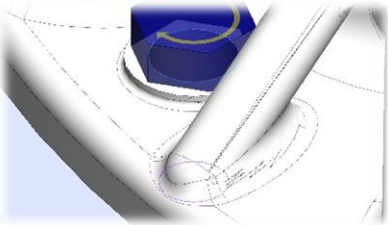
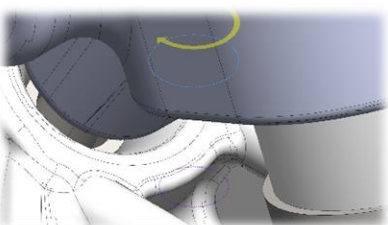
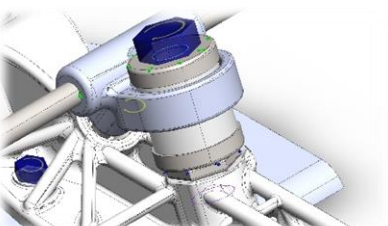
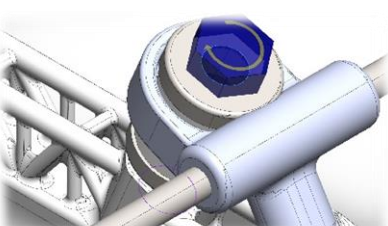

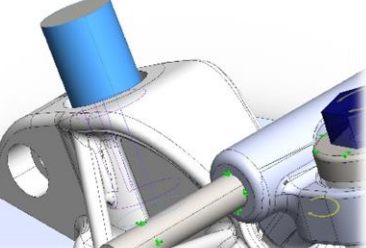
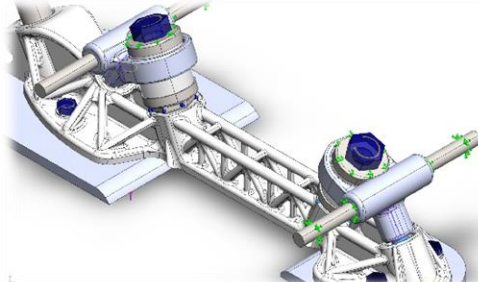
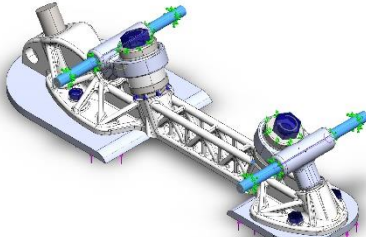
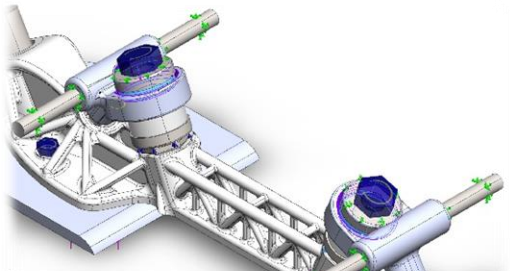
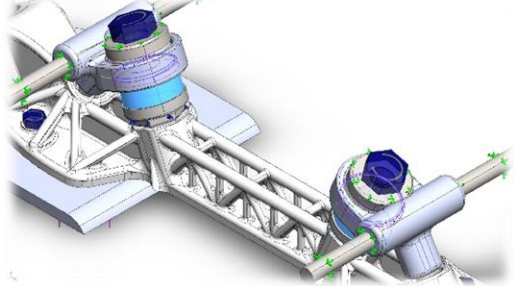
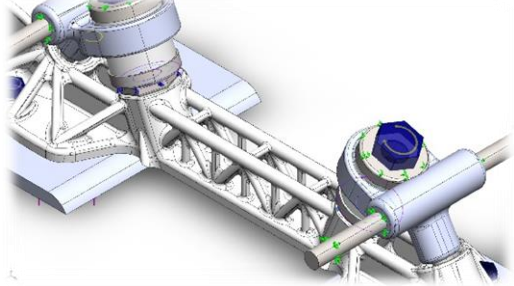
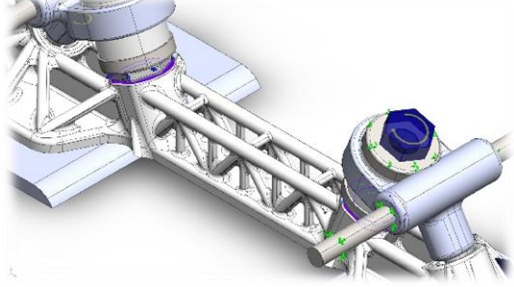
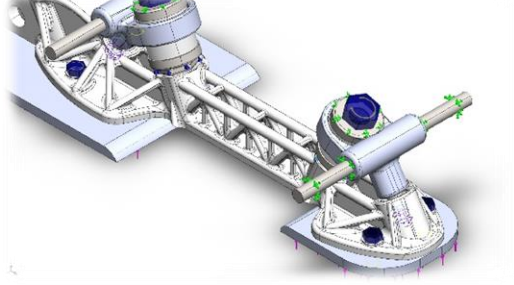
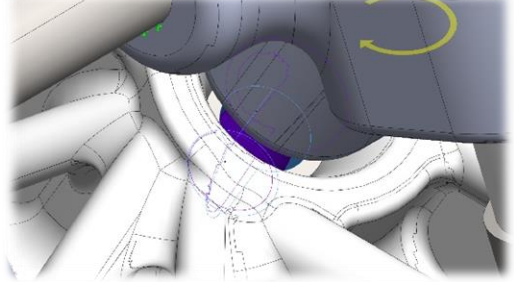
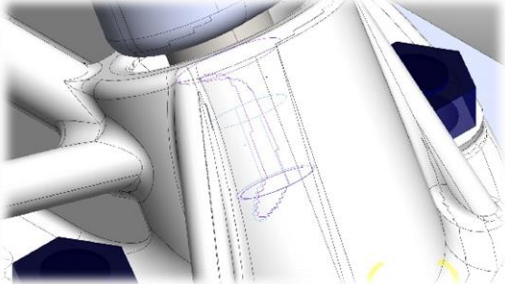
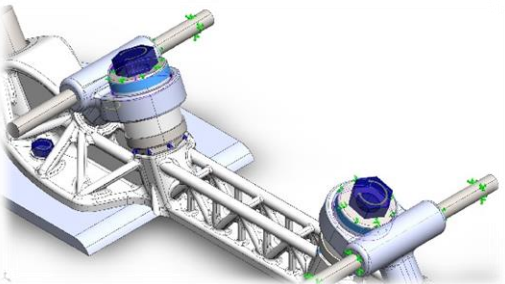
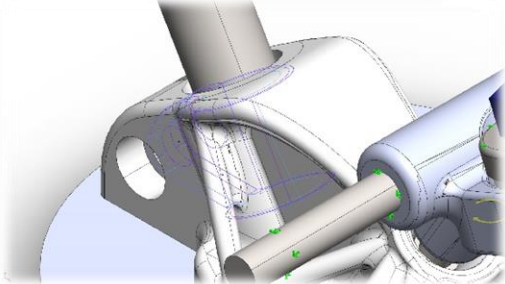
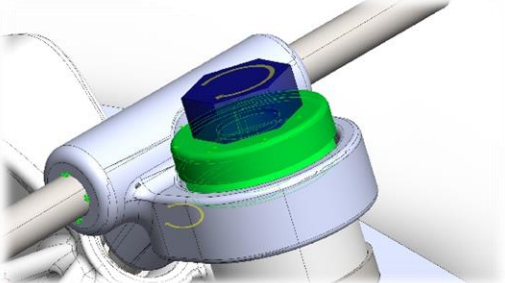
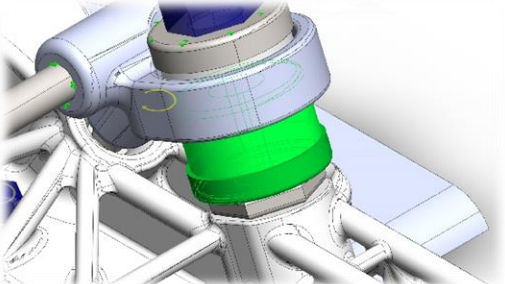
| | |
|---|--|
|  <p>Counterbore with Nut-3</p> | <p>Entities: 2 edge(s) Type: Bolt (Head/Nut diameter) (Counterbore) Connection Type: Distributed Head diameter: 8.000 mm Nut diameter: 8.000 mm Nominal shank diameter: 5.000 mm Material name: Alloy Steel Young's modulus: 2.100e+11 N/m² Poisson's ratio: 0.280 Preload (Torque): 1.000 N.m Friction Factor (K): 0.200 Tight Fit: No</p> |
|  <p>Counterbore with Nut-4</p> | <p>Entities: 2 edge(s) Type: Bolt (Head/Nut diameter) (Counterbore) Connection Type: Distributed Head diameter: 8.000 mm Nut diameter: 8.000 mm Nominal shank diameter: 5.000 mm Material name: Alloy Steel Young's modulus: 2.100e+11 N/m² Poisson's ratio: 0.280 Preload (Torque): 1.000 N.m Friction Factor (K): 0.200 Tight Fit: No</p> |
|  <p>Counterbore with Nut-8</p> | <p>Entities: 2 edge(s) Type: Bolt (Head/Nut diameter) (Counterbore) Connection Type: Distributed Head diameter: 15.000 mm Nut diameter: 15.000 mm Nominal shank diameter: 10.000 mm Material name: Alloy Steel Young's modulus: 2.100e+11 N/m² Poisson's ratio: 0.280 Preload (Torque): 1.000 N.m Friction Factor (K): 0.200 Tight Fit: No</p> |
|  <p>Counterbore with Nut-9</p> | <p>Entities: 2 edge(s) Type: Bolt (Head/Nut diameter) (Counterbore) Connection Type: Distributed Head diameter: 15.000 mm Nut diameter: 15.000 mm Nominal shank diameter: 10.000 mm Material name: Alloy Steel Young's modulus: 2.100e+11 N/m² Poisson's ratio: 0.280 Preload (Torque): 10.197 kgf.cm Friction Factor (K): 0.200 Tight Fit: No</p> |

Table A.6. Contact information for weight, attachment and FIT static numerical studies.

| Contact | Contact Image | Contact Properties |
|------------------------|---|--|
| Local Interaction-1836 |  | Type: Contact interaction pair Entities: 3 face(s) Advanced: Surface to surface |
| Local Interaction-2218 |  | Type: Contact interaction pair Entities: 2 face(s) Advanced: Surface to surface |
| Local Interaction-2219 |  | Type: Bonded interaction pair Entities: 8 face(s) |
| Local Interaction-2220 |  | Type: Bonded interaction pair Entities: 4 face(s) |
| Local Interaction-2222 |  | Type: Contact interaction pair Entities: 14 face(s) Advanced: Surface to surface |

| | | |
|-------------------------------|---|---|
| <p>Local Interaction-2223</p> |  | <p>Type: Contact interaction pair Entities: 12 face(s) Advanced: Surface to surface</p> |
| <p>Local Interaction-2225</p> |  | <p>Type: Contact interaction pair Entities: 4 face(s) Advanced: Surface to surface</p> |
| <p>Local Interaction-2226</p> |  | <p>Type: Contact interaction pair Entities: 4 face(s) Advanced: Surface to surface</p> |
| <p>Local Interaction-2227</p> |  | <p>Type: Bonded interaction pair Entities: 12 face(s)</p> |
| <p>Local Interaction-2240</p> |  | <p>Type: Contact interaction pair Entities: 4 face(s) Advanced: Surface to surface</p> |

| | | |
|--------------------------------|---|--|
| <p>Local Interaction-2241</p> |  | <p>Type: Contact interaction pair Entities: 4 face(s) Advanced: Surface to surface</p> |
| <p>Local Interaction-2247</p> |  | <p>Type: Contact interaction pair Entities: 4 face(s) Advanced: Surface to surface</p> |
| <p>Local Interaction-2248</p> |  | <p>Type: Bonded interaction pair Entities: 22 face(s)</p> |
| <p>Component Interaction-1</p> |  | <p>Type: Contact (Surface to surface) Components: 2 Solid Body (s)</p> |
| <p>Component Interaction-7</p> |  | <p>Type: Contact (Surface to surface) Components: 2 Solid Body (s)</p> |

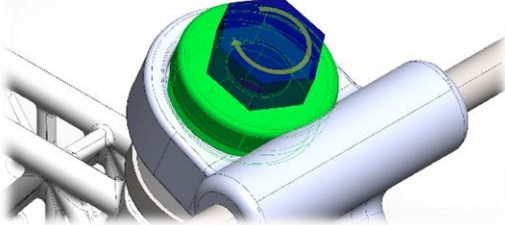
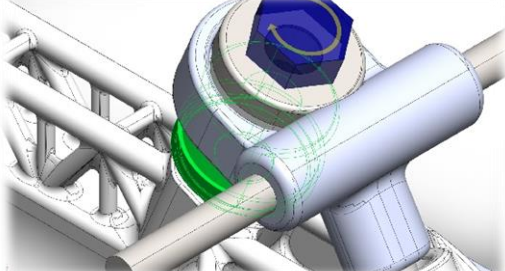
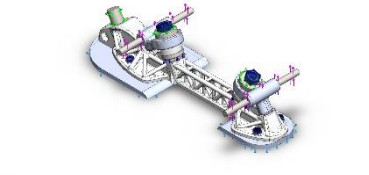
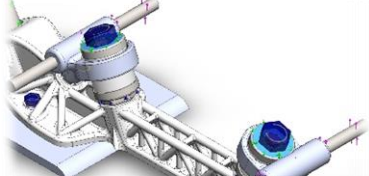
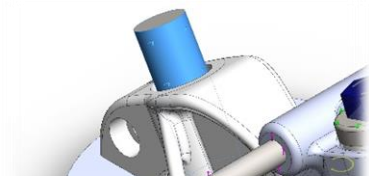
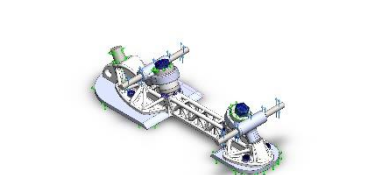
| | | |
|--------------------------------|---|---|
| <p>Component Interaction-8</p> |  | <p>Type: Contact (Surface to surface) Components: 2 Solid Body (s)</p> |
| <p>Component Interaction-9</p> |  | <p>Type: Contact (Surface to surface) Components: 2 Solid Body (s)</p> |

Table A.7. Fixtures; Attachment static numerical study.

| Fixture name | Fixture Image | Fixture Details |
|-------------------------------|---|--|
| <p>Fixed-2</p> |  | <p>Entities: 2 face(s) Type: Fixed Geometry</p> |
| <p>On Flat Faces-1</p> |  | <p>Entities: 2 face(s) Type: On Flat Faces Translation: 0; 0; --- Rotation: ---; ---; --- Units: mm; rad</p> |
| <p>On Cylindrical Faces-1</p> |  | <p>Entities: 1 face(s) Type: On Cylindrical Faces Translation: 0; 0 rad.; 0 Rotation: ---; 0; --- Units: mm; rad</p> |
| <p>Virtual wall-2233</p> |  | <p>Type: Virtual wall Entities: 1 face(s), 1 plane(s) Wall Type: Rigid</p> |

| | | |
|--------------------------|---|--|
| <p>Virtual wall-2235</p> |  | <p>Type: Virtual wall Entities: 1 face(s), 1 plane(s) Wall Type: Rigid</p> |
| <p>Virtual wall-2236</p> |  | <p>Type: Virtual wall Entities: 1 face(s), 1 plane(s) Wall Type: Rigid</p> |
| <p>Virtual wall-2237</p> |  | <p>Type: Virtual wall Entities: 1 face(s), 1 plane(s) Wall Type: Rigid</p> |
| <p>Virtual wall-2238</p> |  | <p>Type: Virtual wall Entities: 1 face(s), 1 plane(s) Wall Type: Rigid</p> |
| <p>Virtual wall-2239</p> |  | <p>Type: Virtual wall Entities: 1 face(s), 1 plane(s) Wall Type: Rigid</p> |
| <p>Virtual wall-2242</p> |  | <p>Type: Virtual wall Entities: 1 face(s), 1 plane(s) Wall Type: Rigid</p> |
| <p>Virtual wall-2243</p> |  | <p>Type: Virtual wall Entities: 1 face(s), 1 plane(s) Wall Type: Rigid</p> |

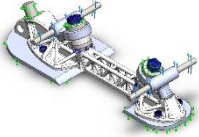

| | | |
|-------------------|---|---|
| Virtual wall-2244 |  | Type: Virtual wall Entities: 1 face(s), 1 plane(s) Wall Type: Rigid |
| Virtual wall-2246 |  | Type: Virtual wall Entities: 1 face(s), 1 plane(s) Wall Type: Rigid |

Table A.8. Loads; Attachment static numerical study.

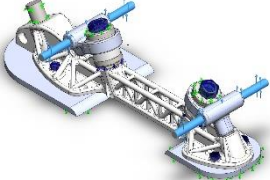
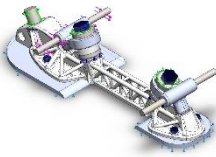
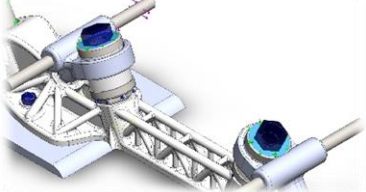
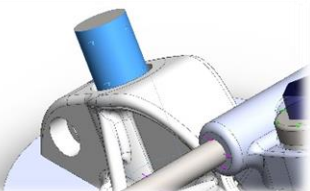
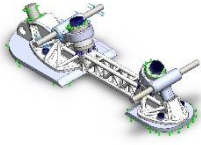
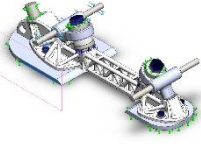
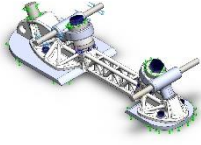
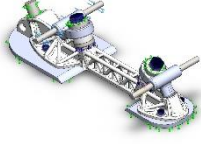
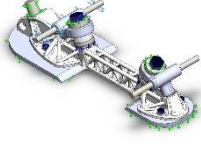
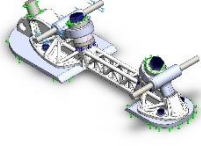
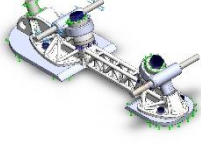
| Load name | Load Image | Load Details |
|-----------|--|--|
| Force-1 |  | Entities: 2 face(s) Reference: Edge< 1 > Type: Apply force Values: ---; ---; - 1 000.000 N Moments: ---; ---; --- N.m |

Table A.9. Fixtures; FIT static numerical study.

| Fixture name | Fixture Image | Fixture Details |
|------------------------|---|---|
| Fixed-2 |  | Entities: 2 face(s) Type: Fixed Geometry |
| On Flat Faces-1 |  | Entities: 2 face(s) Type: On Flat Faces Translation: 0; 0; --- Rotation: ---; ---; --- Units: mm; rad |
| On Cylindrical Faces-1 |  | Entities: 1 face(s) Type: On Cylindrical Faces Translation: 0; 0 rad.; 0 Rotation: ---; 0; --- Units: mm; rad |

| | | |
|-------------------------------|---|---|
| <p>Virtual wall- 2233</p> |  | <p>Type: Entities: Wall Type:</p> <p>Virtual wall 1 face(s), 1 plane(s) Rigid</p> |
| <p>Virtual wall- 2235</p> |  | <p>Type: Entities: Wall Type:</p> <p>Virtual wall 1 face(s), 1 plane(s) Rigid</p> |
| <p>Virtual wall- 2236</p> |  | <p>Type: Entities: Wall Type:</p> <p>Virtual wall 1 face(s), 1 plane(s) Rigid</p> |
| <p>Virtual wall- 2237</p> |  | <p>Type: Entities: Wall Type:</p> <p>Virtual wall 1 face(s), 1 plane(s) Rigid</p> |
| <p>Virtual wall- 2238</p> |  | <p>Type: Entities: Wall Type:</p> <p>Virtual wall 1 face(s), 1 plane(s) Rigid</p> |
| <p>Virtual wall- 2239</p> |  | <p>Type: Entities: Wall Type:</p> <p>Virtual wall 1 face(s), 1 plane(s) Rigid</p> |
| <p>Virtual wall- 2242</p> |  | <p>Type: Entities: Wall Type:</p> <p>Virtual wall 1 face(s), 1 plane(s) Rigid</p> |

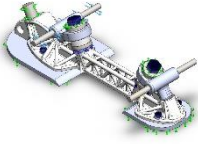
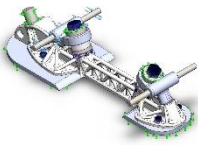
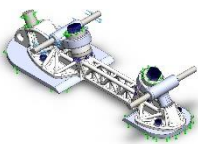
| | | | |
|-------------------|---|----------------------------------|--|
| Virtual wall-2243 |  | Type: Entities: Wall Type: | Virtual wall 1 face(s), 1 plane(s) Rigid |
| Virtual wall-2244 |  | Type: Entities: Wall Type: | Virtual wall 1 face(s), 1 plane(s) Rigid |
| Virtual wall-2246 |  | Type: Entities: Wall Type: | Virtual wall 1 face(s), 1 plane(s) Rigid |

Table A.10. Loads; FIT static numerical study.

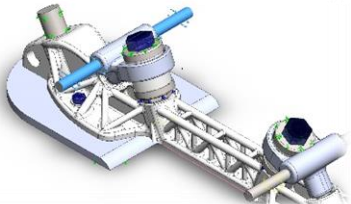
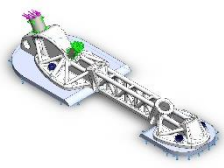
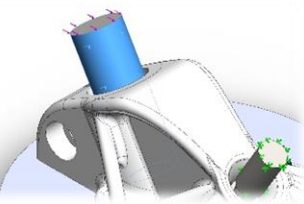
| Load name | Load Image | Load Details |
|-----------|---|--|
| Force-1 |  | Entities: 1 face(s) Reference: Edge< 1 > Type: Apply force Values: ---; ---; --- 118.300 N Moments: ---; ---; --- N.m |

Table A.11. Fixtures; FIB static numerical study.

| Fixture name | Fixture Image | Fixture Details |
|--|---|---|
| Fixed-2 |  | Entities: 2 face(s) Type: Fixed Geometry |
| On Cylindrical Faces-1. Excluded in the corrected study. |  | Entities: 1 face(s) Type: On Cylindrical Faces Translation: 0; 0 rad.; 0 Rotation: ---; 0; --- Units: mm; rad |

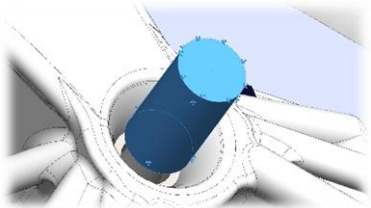
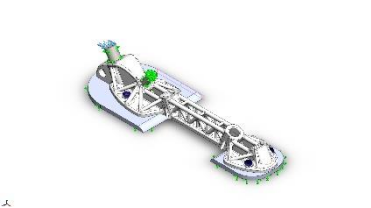
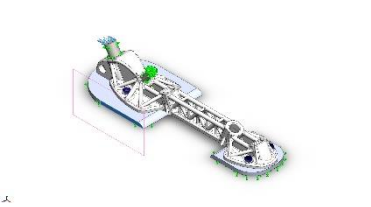
| | | |
|---|---|--|
| <p>Fixed-3. Excluded in the corrected study.</p> |  | <p>Entities: 2 face(s) Type: Fixed Geometry</p> |
| <p>Virtual wall-2233</p> |  | <p>Type: Virtual wall Entities: 1 face(s), 1 plane(s) Wall Type: Rigid</p> |
| <p>Virtual wall-2235</p> |  | <p>Type: Virtual wall Entities: 1 face(s), 1 plane(s) Wall Type: Rigid</p> |

Table A.12. Loads; FIB static numerical study.

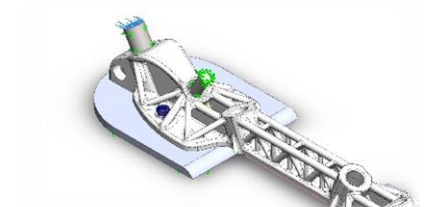
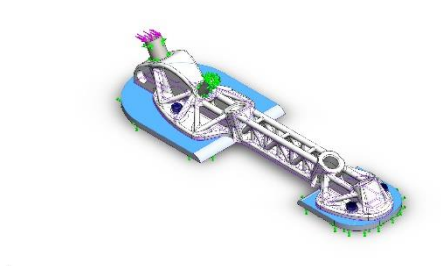
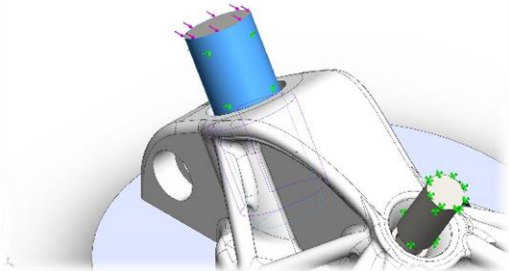
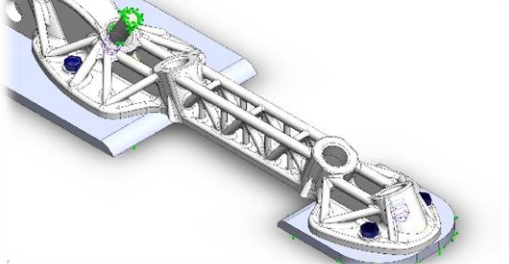
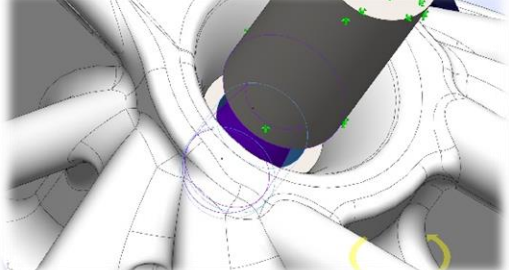
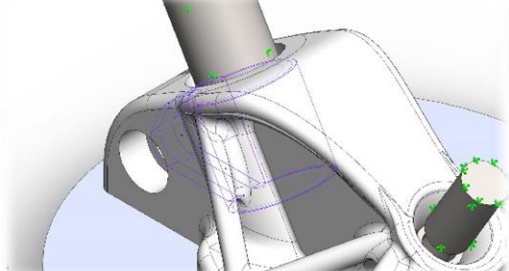
| Load name | Load Image | Load Details |
|----------------|---|--|
| <p>Force-1</p> |  | <p>Entities: 1 face(s) Reference: Edge< 1 > Type: Apply force Values: ---; ---; 118.300 N Moments: ---; ---; --- N.m</p> |

Table A.13. Contact information; FIB static numerical study.

| Contact | Contact Image | Contact Properties |
|-------------------------------|---|--|
| <p>Local Interaction-1836</p> |  | <p>Type: Contact interaction pair Entities: 3 face(s) Advanced: Surface to surface</p> |

| | | |
|---|--|---|
| <p>Local Interaction-2218. Excluded in the corrected study. It was bonded instead.</p> |  | <p>Type: Contact interaction pair Entities: 2 face(s) Advanced: Surface to surface</p> |
| <p>Local Interaction-2227.</p> |  | <p>Type: Bonded interaction pair Entities: 12 face(s)</p> |
| <p>Local Interaction-2240. Excluded in the corrected study.</p> |  | <p>Type: Contact interaction pair Entities: 4 face(s) Advanced: Surface to surface</p> |
| <p>Local Interaction-2248</p> |  | <p>Type: Contact interaction pair Entities: 22 face(s) Advanced: Surface to surface</p> |

APPENDIX B

Table B.1. Mesh convergence for all the numerical studies done for model MD1.4.

| MD1.4 | Nº of Elements | Displacement (mm) | Max. Stress Platform (MPa) | Max. Stress Assembly (MPa) | Max. Element Size | Min. Element Size | Total Nodes | Stress difference (%) | Displacement difference (%) |
|----------------|----------------|-------------------|----------------------------|----------------------------|-----------------------|-----------------------|---------------|-----------------------|-----------------------------|
| Weight-ABS | 60425 | 1.46591 | 22.096 | 224.333 | 28.1470 0 mm | 4.22205 mm | 109198 | - | - |
| | 308346 | 1.60402 | 25.239 | 314.446 | 7.10532 mm | 1.42106 mm | 502586 | 14.22% | 9.42% |
| | 397182 | 1.58440 | 25.391 | 360.845 | 7.10532 mm | 1.27896 mm | 637435 | 0.60% | 1.22% |
| | 476552 | 1.58458 | 25.005 | 400.812 | 7.10532 mm | 1.15106 mm | 757751 | 1.52% | 0.01% |
| | 576383 | 1.58453 | 27.570 | 474.888 | 7.10532 mm | 1.03596 mm | 909241 | 10.26% | 0.00% |
| Weight-CFRP | 48074 | 1.12772 | 89.947 | 263.217 | 28.4213 0 mm | 5.68425 mm | 87337 | - | - |
| | 308346 | 0.99920 | 68.566 | 275.425 | 7.10532 mm | 1.42106 mm | 502586 | 23.77% | 11.40% |
| | 366405 | 0.99346 | 68.917 | 404.774 | 7.10532 mm | 1.31747 mm | 590818 | 0.51% | 0.57% |
| | 541205 | 0.99583 | 67.367 | 449.632 | 7.10532 mm | 1.09249 mm | 854735 | 2.25% | 0.24% |
| Weight-Resin | 48074 | 1.60574 | 18.375 | - | 28.4213 0 mm | 5.68425 mm | 87337 | 0.00% | 0.00% |
| | 308299 | 1.76236 | 21.268 | - | 7.10532 mm | 1.42106 mm | 502521 | 15.74% | 9.75% |
| | 397057 | 1.74064 | 20.642 | - | 7.10532 mm | 1.27896 mm | 637256 | 2.94% | 1.23% |
| | 476424 | 1.73935 | 20.263 | - | 7.10532 mm | 1.15106 mm | 757555 | 1.84% | 0.07% |
| | 576359 | 1.74076 | 19.796 | - | 7.10532 mm | 1.03596 mm | 909201 | 2.30% | 0.08% |
| Attachment-ABS | 46672 | 1.30190 | 16.329 | 165.150 | 38.0623 0 mm | 5.51903 mm | 85347 | - | - |
| | 308346 | 1.41166 | 48.716 | 217.250 | 7.10532 mm | 1.42106 mm | 502586 | 198.34% | 8.43% |
| | 397182 | 1.41384 | 40.768 | 223.678 | 7.10532 mm | 1.27896 mm | 637435 | 16.31% | 0.15% |
| | 496468 | 1.41676 | 41.864 | 233.504 | 7.10532 mm | 1.13685 mm | 787207 | 2.69% | 0.21% |

Table B.2. Continuation of mesh convergence for all the numerical studies done for model MD1.4.

| MD1.4 | N° of Elements | Displacement (mm) | Max. Stress Platform (MPa) | Max. Stress Assembly (MPa) | Max. Element Size | Min. Element Size | Total Nodes | Stress difference (%) | Displacement difference (%) |
|------------------|----------------|-------------------|----------------------------|----------------------------|-----------------------|-----------------------|---------------|-----------------------|-----------------------------|
| Attachment-CFRP | 48074 | 1.35538 | 31.102 | 163.909 | 28.4213 0 mm | 5.68425 mm | 87337 | - | - |
| | 320718 | 1.37548 | 42.251 | 215.872 | 7.10532 mm | 1.39264 mm | 521364 | 35.85% | 1.48% |
| | 397182 | 1.3956 | 43.115 | 221.015 | 7.10532 mm | 1.27896 mm | 637435 | 2.04% | 1.46% |
| | 496468 | 1.39941 | 44.080 | 217.410 | 7.10532 mm | 1.13685 mm | 787207 | 2.24% | 0.27% |
| | 589145 | 1.40065 | 43.856 | 215.394 | 7.10532 mm | 1.02317 mm | 928448 | 0.51% | 0.09% |
| Attachment-Resin | 48074 | 1.84512 | 31.276 | 45.268 | 28.4213 0 mm | 5.68425 mm | 87337 | - | - |
| | 308299 | 1.97778 | 43.999 | 52.978 | 7.10532 mm | 1.42106 mm | 502521 | 17.03% | 7.19% |
| | 397057 | 1.98143 | 42.007 | 53.058 | 7.10532 mm | 1.27896 mm | 637256 | 0.15% | 0.18% |
| | 496414 | 1.98299 | 41.908 | 52.519 | 7.10532 mm | 1.13685 mm | 787118 | 1.02% | 0.08% |
| FIT-ABS | 47995 | 1.33299 | 41.752 | 161.088 | 28.4213 0 mm | 5.68425 mm | 87228 | - | - |
| | 308451 | 1.39765 | 48.884 | 229.014 | 7.10532 mm | 1.42106 mm | 502597 | 17.08% | 4.85% |
| | 445387 | 1.40851 | 23.576 | 219.298 | 7.10532 mm | 1.2 mm | 710402 | 51.77% | 0.78% |
| | 496328 | 1.42268 | 25.665 | 197.104 | 7.10532 mm | 1.13685 mm | 787042 | 8.86% | 1.01% |
| | 589311 | 1.43485 | 25.852 | 207.933 | 7.10532 mm | 1.02317 mm | 928868 | 0.73% | 0.86% |
| FIT-CFRP | 47995 | 1.38414 | 23.960 | 199.485 | 28.4213 0 mm | 5.68425 mm | 87228 | - | - |
| | 308451 | 1.44706 | 25.319 | 277.390 | 7.10532 mm | 1.42106 mm | 502597 | 5.67% | 4.55% |
| | 450494 | 1.47003 | 30.143 | 235.950 | 7.10532 mm | 1.18106 mm | 718328 | 19.05% | 1.59% |
| | 567394 | 1.47628 | 28.851 | 253.943 | 7.10532 mm | 1.06296 mm | 894403 | 4.29% | 0.43% |
| | 594798 | 1.47119 | 30.044 | 251.825 | 7.10532 mm | 1.0118 mm | 937729 | 4.14% | 0.34% |

Table B.3. Continuation of mesh convergence for all the numerical studies done for model MD1.4.

| MD1.4 | Nº of Elements | Displacement (mm) | Max. Stress Platform (MPa) | Max. Stress Assembly (MPa) | Max. Element Size | Min. Element Size | Total Nodes | Stress difference (%) | Displacement difference (%) |
|-----------|----------------|-------------------|----------------------------|----------------------------|-----------------------|-------------------------|---------------|-----------------------|-----------------------------|
| FIT-Resin | 47995 | 1.32285 | 19.755 | 161.319 | 28.4213 0 mm | 5.68425 mm | 87228 | - | - |
| | 308451 | 1.38685 | 20.050 | 216.778 | 7.10532 mm | 1.42106 mm | 502597 | 1.49% | 4.84% |
| | 396928 | 1.40316 | 26.094 | 197.041 | 7.10532 mm | 1.27896 mm | 637135 | 30.14% | 1.18% |
| | 476404 | 1.41026 | 25.850 | 188.234 | 7.10532 mm | 1.15106 mm | 757611 | 0.94% | 0.51% |
| | 577123 | 1.42282 | 27.098 | 195.827 | 7.10532 mm | 1.03596 mm | 910409 | 4.83% | 0.89% |
| FIB-ABS | 39979 | 0.08785 | - | 39.683 | 24.1742 0 mm | 4.83484 mm | 71597 | - | - |
| | 245960 | 0.1329 | - | 104.961 | 6.04355 mm | 1.20871 mm | 399242 | 164.50% | 51.28% |
| | 308053 | 0.13472 | - | 105.005 | 6.04355 mm | 1.08784 mm | 493673 | 0.04% | 1.37% |
| | 379086 | 0.13481 | - | 107.359 | 6.04355 mm | 0.97905 6 mm | 601416 | 2.24% | 0.07% |
| | 475953 | 0.13542 | - | 106.997 | 6.04355 mm | 0.88115 mm | 745733 | 0.34% | 0.45% |
| FIB-CFRP | 39979 | 0.01217 | - | 38.807 | 24.1742 0 mm | 4.83484 mm | 71597 | - | - |
| | 245960 | 0.01852 | - | 103.372 | 6.04355 mm | 1.20871 mm | 399242 | 52.18% | 52.18% |
| | 308053 | 0.01873 | - | 102.321 | 6.04355 mm | 1.08784 mm | 493673 | 1.13% | 1.13% |
| | 379086 | 0.01874 | - | 104.223 | 6.04355 mm | 0.97905 6 mm | 601416 | 0.05% | 0.05% |
| | 475953 | 0.01882 | - | 104.830 | 6.04355 mm | 0.88115 mm | 745733 | 0.43% | 0.43% |
| FIB-Resin | 39979 | 0.13024 | 38.968 | - | 24.1742 mm | 4.83484 mm | 71597 | - | - |
| | 245960 | 0.19790 | - | - | 6.04355 mm | 1.20871 mm | 399242 | 51.95% | 51.95% |
| | 301468 | 0.20050 | - | - | 6.04355 mm | 1.08784 mm | 483650 | 1.31% | 1.31% |
| | 357678 | 0.20073 | - | - | 6.04355 mm | 0.97905 6 mm | 569633 | 0.11% | 0.11% |

Table B.4. Continuation of mesh convergence for all the numerical studies done for model MD1.4.

| MD1.4 | Nº of Elements | Displacement (mm) | Max. Stress Platform (MPa) | Max. Stress Assembly (MPa) | Max. Element Size | Min. Element Size | Total Nodes | Stress difference (%) | Displacement difference (%) |
|---------------------|----------------|-------------------|----------------------------|----------------------------|-------------------|-------------------|---------------|-----------------------|-----------------------------|
| FIB-ABS-CORRECTED | 39720 | 0.61820 | 40.761 | - | 24.08480 mm | 4.81695 mm | 71101 | - | - |
| | 243279 | 0.47334 | 108.631 | - | 6.02119 mm | 1.20424 mm | 394953 | 23.43% | 23.43% |
| | 295126 | 0.47417 | 107.639 | - | 6.02119 mm | 1.09586 mm | 474425 | 0.18% | 0.18% |
| | 367185 | 0.47476 | 108.574 | - | 6.02119 mm | 0.987475 mm | 583023 | 0.12% | 0.12% |
| FIB-CFRP-CORRECTED | 39720 | 0.06009 | 43.172 | - | 24.0848 mm | 4.81695 mm | 71101 | - | - |
| | 243279 | 0.06513 | 107.730 | - | 6.02119 mm | 1.20424 mm | 394953 | 149.54 % | 8.39% |
| | 305155 | 0.06525 | 110.616 | - | 6.02119 mm | 1.08381 mm | 489042 | 2.68% | 0.18% |
| | 371738 | 0.06533 | 112.696 | - | 6.02119 mm | 0.975433 mm | 590663 | 1.88% | 0.12% |
| FIB-Resin-CORRECTED | 39720 | 0.61820 | 40.761 | - | 24.0848 mm | 4.81695 mm | 71101 | - | - |
| | 243279 | 0.66994 | 105.938 | - | 6.02119 mm | 1.20424 mm | 394953 | 8.37% | 8.37% |
| | 305155 | 0.67130 | 104.118 | - | 6.02119 mm | 1.08381 mm | 489042 | 0.20% | 0.20% |
| | 371738 | 0.67219 | 106.233 | - | 6.02119 mm | 0.975433 mm | 590663 | 0.13% | 0.13% |

The Tables B.1 to B.4 contain all the mesh convergence information relating to the numerical studies done in chapter 4. In **bold**, are the studies that converged and subsequent plots were displayed throughout chapter 4. These were all of the model MD1.4.

The convergence tables for the model MD1.3 are displayed *infra*. In this phase, the model was only tested for materials like ABS and CFRP, which was the main objective.

In all these tables, the percentual difference of displacement was the one considered for the convergence criteria. The stress values would sometimes not be adequate due to FEA particularities.

Table B.5. Mesh convergence for all the numerical studies done for model MD1.3.

| MD1.3 | Nº of Elements | Displacement (mm) | Max. Stress Platform (MPa) | Max. Stress Assembly (MPa) | Max. Element Size | Min. Element Size | Total Nodes | Stress difference (%) | Displacement difference (%) |
|----------------|----------------|-------------------|----------------------------|----------------------------|-------------------|-------------------|---------------|-----------------------|-----------------------------|
| Weight-ABS | 48427 | 1.48626 | 31.486 | 286.631 | 27.89050 mm | 5.57809 mm | 87659 | - | - |
| | 94800 | 1.44966 | 33.370 | 286.506 | 14.64250 mm | 2.92850 mm | 164850 | 5.98% | 2.46% |
| | 290878 | 1.66341 | 32.856 | 312.034 | 6.97262 mm | 1.39452 mm | 474096 | 1.54% | 14.74% |
| | 345544 | 1.58698 | 30.033 | 332.424 | 6.97262 mm | 1.25507 mm | 558207 | 8.59% | 4.59% |
| | 482640 | 1.57915 | 29.251 | 347.756 | 4.47307 mm | 1.10000 mm | 765319 | 2.60% | 0.49% |
| | 561980 | 1.57976 | 27.718 | 369.688 | 4.47307 mm | 1.00000 mm | 886811 | 5.24% | 0.04% |
| | 696578 | 1.58361 | 27.291 | 353.076 | 4.02577 mm | 0.90000 mm | 1087473 | 1.54% | 0.24% |
| Weight-CFRP | 58637 | 1.08200 | 83.373 | 184.759 | 27.8905 mm | 4.32302 mm | 105554 | - | - |
| | 326975 | 0.97180 | 69.946 | 450.837 | 6.97262 mm | 1.39452 mm | 527886 | 16.10% | 10.18% |
| | 410763 | 0.97324 | 71.685 | 264.814 | 6.97262 mm | 1.25507 mm | 655971 | 2.49% | 0.15% |
| | 492184 | 1.04431 | 76.275 | 277.974 | 6.97262 mm | 1.12956 mm | 778490 | 6.40% | 7.30% |
| | 598497 | 1.04479 | 76.798 | 282.145 | 5.57809 mm | 1.01661 mm | 939389 | 0.69% | 0.05% |
| Attachment-ABS | 68234 | 1.54660 | 36.782 | 199.487 | 27.89050 mm | 3.83494 mm | 121350 | - | - |
| | 96954 | 1.49632 | 27.249 | 269.250 | 14.2939 mm | 2.85877 mm | 168231 | 25.92% | 3.25% |
| | 314880 | 1.51670 | 40.900 | 223.291 | 6.97262 mm | 1.39452 mm | 509638 | 50.10% | 1.36% |
| | 391045 | 1.51579 | 40.651 | 239.542 | 6.97262 mm | 1.25507 mm | 626073 | 0.61% | 0.06% |
| | 469769 | 1.51724 | 40.826 | 242.261 | 4.47307 mm | 1.12956 mm | 744527 | 0.43% | 0.10% |

Table B.6. Continuation of mesh convergence for all the numerical studies done for model MD1.3.

| MD1.3 | N° of Elements | Displacement (mm) | Max. Stress Platform (MPa) | Max. Stress Assembly (MPa) | Max. Element Size | Min. Element Size | Total Nodes | Stress difference (%) | Displacement difference (%) |
|------------------------|-----------------------|--------------------------|-----------------------------------|-----------------------------------|--------------------------|--------------------------|--------------------|------------------------------|------------------------------------|
| Attachment-CFRP | 48033 | 1.38246 | 34.442 | 154.616 | 27.8905 0 mm | 5.57809 mm | 86890 | - | - |
| | 314881 | 1.52012 | 42.435 | 217.364 | 6.97262 mm | 1.39452 mm | 509639 | 23.21% | 9.96% |
| | 391045 | 1.52736 | 42.093 | 225.140 | 6.97262 mm | 1.25507 mm | 626073 | 0.81% | 0.48% |
| | 462086 | 1.52482 | 42.327 | 216.553 | 5.57809 mm | 1.12956 mm | 733519 | 0.56% | 0.17% |
| FIT-ABS | 47696 | 1.15570 | 14.496 | 170.564 | 27.8905 mm | 5.57809 mm | 86529 | - | - |
| | 292405 | 1.51552 | 13.406 | 214.302 | 6.97262 mm | 1.39452 mm | 475824 | 7.52% | 31.13% |
| | 344877 | 1.56373 | 12.790 | 184.794 | 6.97262 mm | 1.25507 mm | 556905 | 4.59% | 3.18% |
| | 411378 | 1.56698 | 16.550 | 197.278 | 6.27536 mm | 1.12956 mm | 657678 | 29.40% | 0.21% |
| | 503423 | 1.56778 | 16.499 | 196.549 | 4.47307 mm | 1.01661 mm | 798674 | 0.31% | 0.05% |
| FIT-CFRP | 47696 | 1.43043 | 31.000 | 238.201 | 27.8905 mm | 5.57809 mm | 86529 | - | - |
| | 292405 | 1.57598 | 29.293 | 248.069 | 6.97262 mm | 1.39452 mm | 475824 | 5.51% | 10.18% |
| | 345019 | 1.61456 | 30.370 | 242.568 | 6.97262 mm | 1.25507 mm | 557091 | 3.68% | 2.45% |
| | 411936 | 1.61558 | 49.583 | 225.690 | 6.27536 mm | 1.12956 mm | 658494 | 63.26% | 0.06% |
| | 505350 | 1.61162 | 47.177 | 233.304 | 6.97262 mm | 1.01661 mm | 801338 | 4.85% | 0.25% |

Table B.7. Continuation of mesh convergence for all the numerical studies done for model MD1.3.

| MD1.3 | Nº of Elements | Displacement (mm) | Max. Stress Platform (MPa) | Max. Stress Assembly (MPa) | Max. Element Size | Min. Element Size | Total Nodes | Stress difference (%) | Displacement difference (%) |
|----------|----------------|-------------------|----------------------------|----------------------------|-------------------|--------------------|---------------|-----------------------|-----------------------------|
| FIB-ABS | 35136 | 0.06923 | - | 32.069 | 29.08690 mm | 5.81737 mm | 63214 | - | - |
| | 245276 | 0.09196 | - | 48.815 | 5.87680 mm | 1.17536 mm | 394981 | 52.22% | 32.83% |
| | 307661 | 0.08814 | - | 44.452 | 5.87680 mm | 1.05782 mm | 489634 | 8.94% | 4.15% |
| | 373631 | 0.08523 | - | 42.649 | 5.87680 mm | 0.952042 mm | 589480 | 4.06% | 3.30% |
| | 459274 | 0.08229 | - | 40.019 | 5.87680 mm | 0.856838 mm | 716715 | 6.17% | 3.45% |
| | 454971 | 0.08270 | - | 40.386 | 4.70144 mm | 0.856838 mm | 710598 | 0.92% | 0.50% |
| | 528629 | 0.08138 | - | 39.882 | 4.70144 mm | 0.771154 mm | 819359 | 1.25% | 1.60% |
| | 752417 | 0.08241 | - | 40.319 | 4.70144 mm | 0.694039 mm | 1150690 | 1.10% | 1.27% |
| FIB-CFRP | 38842 | 0.00948 | - | 34.664 | 23.50720 mm | 4.70144 mm | 69878 | - | - |
| | 245276 | 0.01276 | - | 46.441 | 5.87680 mm | 1.17536 mm | 394981 | 34.60% | 34.60% |
| | 307959 | 0.01220 | - | 43.602 | 5.87680 mm | 1.05782 mm | 490034 | 4.39% | 4.39% |
| | 463497 | 0.01135 | - | 40.649 | 4.70144 mm | 0.84626 mm | 723735 | 6.97% | 6.97% |
| | 538527 | 0.01099 | - | 37.339 | 4.70144 mm | 0.761634 mm | 833797 | 3.17% | 3.17% |
| | 609172 | 0.01086 | - | 34.022 | 4.70144 mm | 0.68547 mm | 938036 | 1.18% | 1.18% |

APPENDIX C

These were the results considered when advancing to experimental testing. These proved, as explained in chapter 4.4, good enough to proceed but after the experimental testing they were deemed incorrect. In chapter 4.4 the corrected results are to be found.

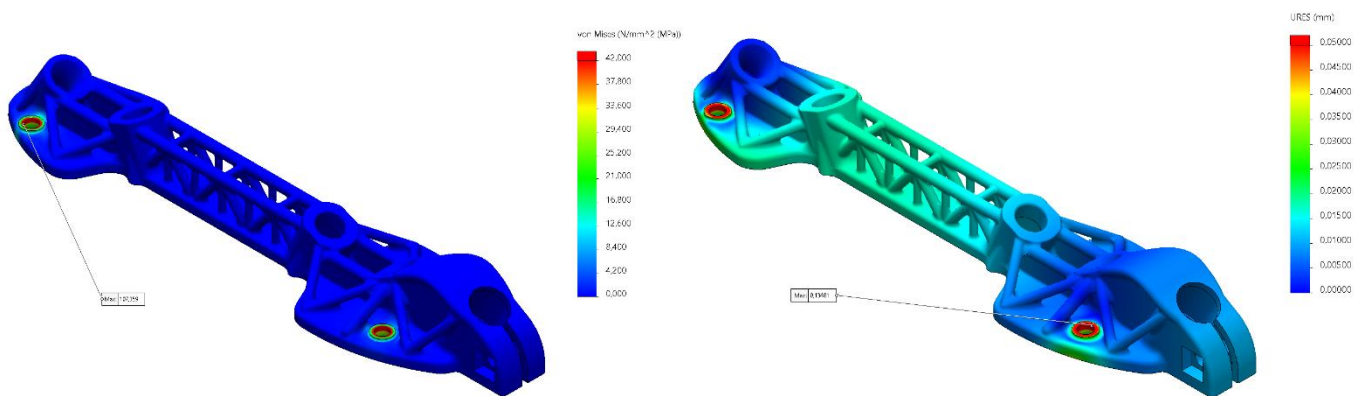


Figure C.1. Wrong FIB static numerical study: Equivalent von Mises Stress plot (left) and resultant displacement (right); ABS.

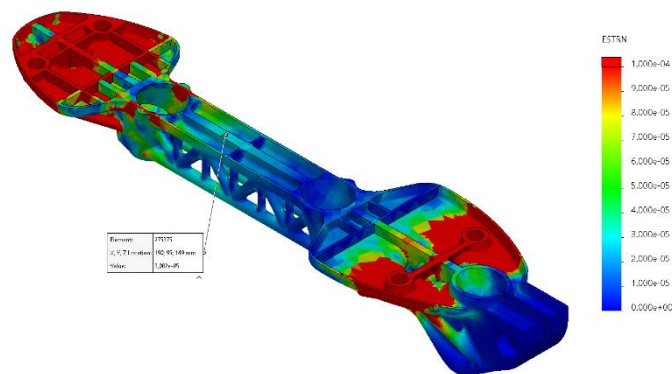


Figure C.2. Wrong FIB static numerical study: Equivalent strain plot; eSun Resin.

Table C.1. Numerical results from the wrong FIB static studies for the 3 different materials.

| | Max. Resultant Displacement platform (mm) | Max. Resultant Displacement Assembly (mm) | Max. Equivalent von Mises Stress Platform (MPa) |
|--------------|--|--|--|
| ABS | 0.13481 | 0.13481 | 107.359 |
| CFRP | 0.01874 | 0.01874 | 104.223 |
| Resin | 0.20050 | 0.20050 | 105.816 |

APPENDIX D

Figure D.1 is the front panel and Figure D.2 is the block diagram for the weight experimental test. This configuration would also be used in the attachment experimental test if the structure did not fail during testing.

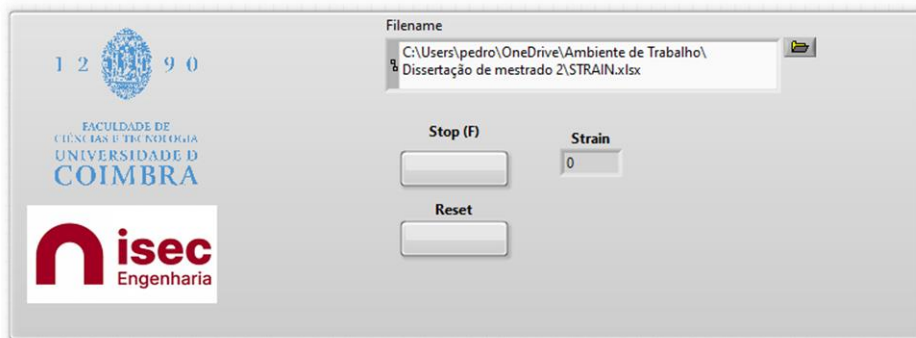


Figure D.1. Front Panel of LabVIEW program for weight testing.

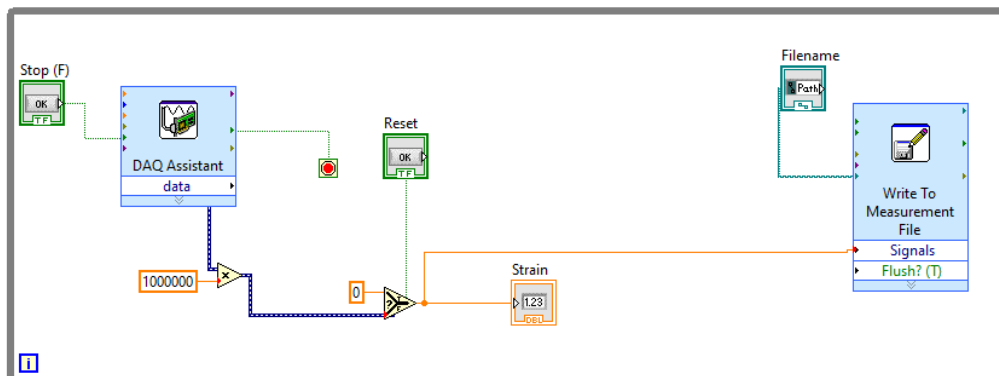


Figure D.2. Block diagram of LabVIEW program for weight testing.

The following two figures are from the FIT and FIB experimental studies. The values in the front panel could not be seen during testing because the computer was closed in the backpack, but still were created to test the program while conceiving it.

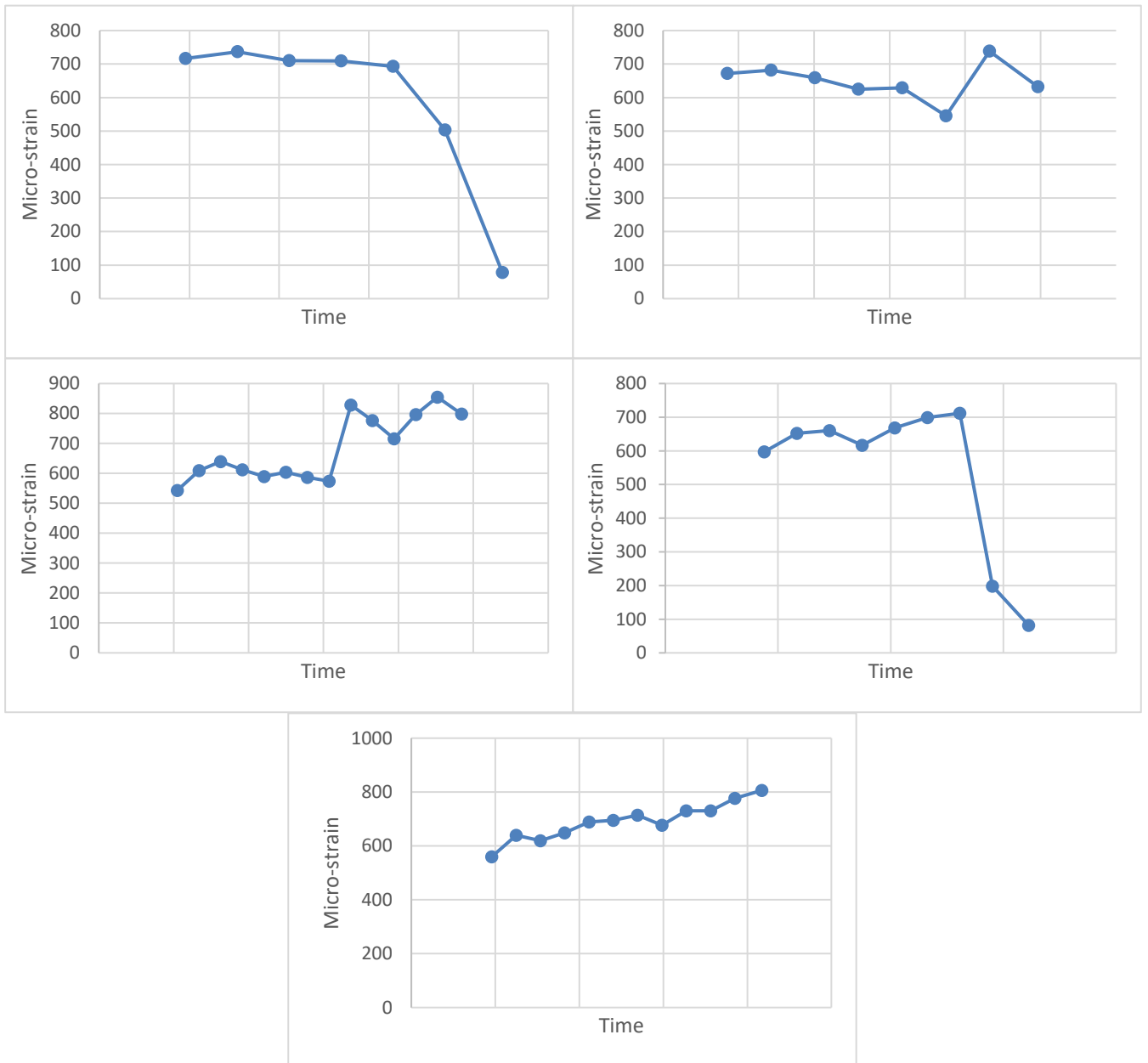


Figure D.5. Graphs of weight testing test runs: first (top left), second (top right), third (middle left), fourth (middle right), fifth (bottom centre).